AN INVESTIGATION OF AN OIL/PACKED BED THERMAL ENERGY STORAGE SYSTEM USING PHASE CHANGE MATERIAL FOR DOMESTIC COOKING

A thesis submitted in fulfillment of the requirements for the degree of Doctor of Philosophy in Physics at the Northwest University, South Africa

by

Shobo Adedamola Babajide

Supervisor

Prof. Ashmore Mawire

December 2016

Declaration

I, Adedamola Babajide Shobo, declare that this thesis entitled: "An Investigation of an Oil/Packed Bed Thermal Energy Storage System Using Phase Change Material for Domestic Cooking" and the work presented in it is my own. I confirm that:

- This work was carried out wholly while I was a candidate for a Doctor of Philosophy degree at Northwest University.
- I have clearly stated where any part of this thesis has been previously submitted for a degree or any other qualification at this University or any other institution.
- I have given sources of quotations from works of others anywhere they are used in this thesis. With the exception of such quotations, this thesis is entirely my own work.
- I have acknowledged all main sources of help during the study.
- I have made clear any contributions from any other person apart from myself in this work.

Signed: _____

Date: _____

Abstract

Feeding is pivotal to human existence and a large amount of energy is utilized globally, each day, for the cooking of food. Sadly, most of the current sources of energy used for most homes have varying degrees of negative impacts on human and environmental health. In developing countries, particularly, the combustion of biomass still forms a major source of energy for domestic cooking applications. About 1.5 million deaths, yearly, are attributed to indoor pollution from to the combustion of biomass that is used for cooking foods in the developing countries. Solar thermal energy is a free, safe and renewable energy resource which may be harnessed into meeting cooking energy needs. However, due to the time-dependency of the availability of solar energy which might not match the periods of demand, it becomes necessary to store the thermal energy during the hours of sunshine for use during periods of insufficient or no solar radiation. Latent heat thermal storage systems provide large thermal energy storage densities by utilizing phase change materials (PCMs). A packed bed of spherically encapsulated erythritol was considered in this research, using sunflower oil as the heat transfer fluid (HTF). A preliminary numerical study indicated that the proposed design will provide good heat storage performance. The experimental study revealed that an aluminum alloy 1050-H14 was chemically compatible with both the PCM and HTF. A separate numerical study indicated that a wall thickness of 1 mm for an aluminum spherical capsule with a diameter of 50 mm will provide mechanical stability when filled with meso-erythritol and heated for thermal energy storage. Experimental tests of thermal stability revealed that meso-erythritol should not be used above 177.0 ^{o}C as it will begin to degrade. The tests of cycling stability revealed meso-erythritol to be chemically stable after several heating and cooling cycles with the solidification enthalpy remaining almost constant. However, the melting temperature is seen to change from about 119 ^{o}C to about 105 ^{o}C due to the fast rate of energy withdrawal from the meso-erythritol sample, forcing it into a metastable state. Very little weight degradation was observed after several heating and cooling cycles. On comparing the thermal stability and thermal cycling results obtained for meso-erythritol with those of acetanilide and an Indium-Tin alloy, meso-erythritol showed comparable performances with the alloy and better performance compared to acetanilide during the heating cycles. However, the performances of meso-erythritol during the cooling cycles were marred by severe supercooling. The lower level of health hazard presented by meso-erythritol as compared to acetanilide and the Indium-Tin alloy still made it attractive to be investigated as the PCM of choice. The charging and discharging performances of meso-

erythritol, acetanilide and the Indium-Tin alloy were investigated simultaneously inside separate spherical aluminum capsules that were fabricated. Meso-erythritol had the highest thermal energy storage density, while acetanilide due to its low density, had the least. However, the large degrees of supercooling exhibited by meso-erythritol impacted negatively on the quality of thermal energy discharged by the PCM as most of the energy was discharged at temperatures below 100 ^{o}C desired for cooking. The Indium-Tin alloy showed the best performance but it was deemed too expensive for use in the proposed packed bed TES system. An oil/packed bed thermal energy storage system was designed and fabricated, with meso-erythritol filled inside 50 mm spherical aluminum spheres as the packed bed while sunflower oil was used as the heat transfer fluid. A secondary storage was included in the system for immediate utilization of thermal energy simultaneously as the packed bed was being charged. Good heat transfer was obtained between the HTF and the encapsulated PCM. High HTF flow rates and high HTF temperatures were observed to result in high rates of thermal energy storage. The rate of thermal energy discharged by the packed bed also increased with an increase in the HTF flow rate. Severe supercooling was exhibited by the encapsulated meso-erythritol which negatively impacted upon the temperature at which the latent heat was discharged. The fabricated thermal storage system can provide hot water for domestic use while storing enough thermal energy for cooking vegetables later.

Acknowledgements

I first want to show gratitude to the Lord Jehovah, the greatest teacher and motivator, from whom all things come.

I am grateful to my supervisor, Prof. Ashmore Mawire, who chose to believe in me and gave me a chance to pursue my dreams. His professional guidance during this research is immeasurable.

I appreciate my parents, Mr. (late) & Mrs. B. A. Shobo, for laying out a solid educational foundation in my life. Dada, I wish you are here to see how much your boy knows now.

I am grateful to the government of South Africa, for investing so much in quality education and research so that I could be part of it.

I am grateful to Prof. Eno Ebenso, the director of the Material Science Innovation and Modeling (MaSIM) research focus area, Faculty of Agriculture, Science and Technology, Northwest University, South Africa. The financial support from MASIM made this research a reality.

I appreciate Prof. Marique Aucamp of the Pharmacy department of the Potchefstroom campus for the induction that I received in thermal cycling techniques on the differential scanning calorimeter. My appreciation also goes to Mr. Thys and Mr. Pieter of the Instrument Makery workshop who fabricated the experimental system.

I am grateful for my colleagues and the staff of the department, Luvo, Getinet, Getachew, Miss Phori, Mr. Nhlapo, Mr. Makgamathe, Dr. Abedigamba, Dr. Bruno, Dr. Abebe, Dr. Dzinavatonga, Dr. Ralph, Dr. Katashaya and Prof. Taole. You all made my tenure very smooth and bearable.

I appreciate all my friends on the Mafikeng campus of the Northwest University, especially Dr. Lukman Olasunkanmi. Conversations with you all made the journey very interesting.

I am grateful to my wife, Oluwatumininu Racheal and my daughter, Aderola Ayanfeoluwa, for sacrificing my presence at home and the regular goodies to allow me to pursue greater knowledge. And my siblings, Yetty, Deola and Shola with their families, thank you for being there.

Table of Contents

List of Figures

List of Tables

CHAPTER ONE: INTRODUCTION

Nomenclature

Symbols	***Description***	m	mass of substance, kg
a_r	fraction of material reacted	Q	quantity of heat, J
c	specific heat capacity, J/kg ^oC	T_f	final temperature
c_{liquid}	specific heat capacity of liquid PCM, J/kg ^oC	T_i	Initial temperature
c_{solid}	specific heat capacity of solid PCM, J/kg ^oC	***Abbreviation***	***Meaning***
dT	change in temperature, ^oC	LHTES	latent heat thermal energy storage
f	melt fraction of PCM	SHTES	sensible heat thermal energy storage
Δh_f	latent heat of fusion, J/kg	TES	thermal energy storage
ΔH	heat of reaction, J	TTES	thermochemical thermal energy storage

1.1. Background of study

For survival and wellbeing, human beings require nourishment from foods and a huge amount of energy is spent daily across the world to meet this need. While some modern means of cooking foods have been embraced largely across the globe, it is estimated that about 38 % of the world's population still rely heavily on the utilization of traditional solid biomass (fuelwood, charcoal, dung, agricultural wastes) for cooking [1]. Gathering of fuelwood for example, has been reported to waste productive time of women and girls in some countries in Africa as well as exposing them to various forms of bodily harm [2]. The use and production of these solid fuels has also been reported to contribute to about 3% of annual carbon dioxide emission and to about 25% of black carbon emission [3]. Sadly, it is projected that about 870,000 people will die every year from health disorders linked to the indoor and outdoor pollution caused by the use of solid biomass for cooking [4]. Forest resources are also degraded with uncontrolled cutting of forest trees for provision of fuelwood and for the production of charcoal. There are underlying issues with the adoption of modern means of cooking as well, for example, about 17% of the global population does not have access to electricity [5]. It is important therefore, to pursue alternative cooking energy solutions that will be safe, environmental-friendly, efficient and from renewable sources.

Solar energy is a free, clean and renewable energy resource with solar radiation values ranging between 775 kWh/m^2 in Lerwick, United Kingdom and 2500 kWh/m^2 in the Sahara desert [6]. Thermal energy from solar energy radiation has been harnessed for cooking

applications for some years now by the development of direct and indirect solar cookers [7]. However, the availability of solar energy is time-dependent and as such utilization for cooking becomes impossible during periods of very low or no solar radiation. Thermal energy storage systems can provide storage of thermal energy from solar radiation for utilization later when required.

1.2. Thermal energy storage (TES) systems

There are three main categories of thermal energy storage systems, based on their modes of thermal energy storage. These are: sensible heat thermal energy storage systems, thermochemical thermal energy storage systems and latent heat thermal energy storage systems.

1.2.1. Sensible heat thermal energy storage (SHTES) systems

In SHTES systems, thermal energy storage is achieved by increasing the temperature of the storage media. The quantity of heat stored (Q) in a particular storage medium depends on the medium's specific heat capacity (c), the change in the temperature of the medium (dT) and the mass of the storage medium (m). This can be expressed mathematically as:

$$Q = \int_{T_i}^{T_f} m\, c dT \tag{1.1}$$

Since SHTES systems only operate based on sensible heating of storage materials, the maximum charging temperature of the systems must always be below the phase transition temperatures of the storage materials utilized. A variety of solid and liquid materials have been utilized as thermal storage materials in SHTES systems [8-9]. Advantages of SHTES systems include low costs and availability of most sensible heat storage materials. Major disadvantages of SHTES systems include temperature variations during heat retrieval and small thermal energy storage densities.

1.2.2. Thermochemical thermal energy storage (TTES) systems

Thermal energy can be stored as heats of reaction absorbed by certain chemical substances in completely reversible chemical reactions [10]. Such reactions can be depicted by equation (1.2) below:

$$A + \Delta H \leftrightharpoons B + C \tag{1.2}$$

where A is the molecule of the original chemical substance, while B and C are the chemical products formed due to the thermochemical reaction. The quantity of heat stored (Q) depends on the mass of the original chemical material (m), the endothermic heat of reaction (ΔH) and the fraction of material reacted (a_r). This can be expressed mathematically as:

$$Q = a_r m \Delta H \tag{1.3}$$

TTES systems possess very large thermal energy storage densities as reaction products can be stored separately at ambient temperature with no heat losses and thus, possibilities of long-term storage. Utilization of TTES systems for thermal energy storage is somewhat complex and presently very expensive. However, research is still ongoing to develop adequate and cheap technologies of achieving thermal energy storage by thermochemical means.

1.2.3. Latent heat thermal energy storage (LHTES) systems

LHTES systems operate on the principle that large amount of thermal energy is absorbed by some materials during their phase transitions (melting and vaporization). These phase change materials (PCMs) also release thermal energy back during phase reversal transitions. The solid-liquid phase transitions of PCMs are preferred to liquid-gas transitions due to large volume changes and the development of high pressures that occur with transitions from the liquid to the gas phase. Also for most PCMs, the enthalpy associated with the solid-liquid transition is larger than that associated with the liquid-gas transition [9]. The quantity of heat stored by the LHTES system is made up of sensible heat stored from an initial temperature (T_i) to the melting temperature (T_m), the latent heat of fusion (Δh_f) and the sensible heat stored from the melting temperature to the final temperature (T_f) of the PCM. This can be expressed mathematically as:

$$Q = \int_{T_i}^{T_m} m\, c_{liquid}\, dT + mf\Delta h_f + \int_{T_m}^{T_f} mc_{solid}\, dT \tag{1.4}$$

where m is the mass of the PCM, c_{liquid} and c_{solid} are the specific heat capacity of liquid and solid PCM respectively, and f is the melted fraction of the PCM.

LHTES systems possess larger thermal energy densities than sensible heat thermal energy storage systems and the nearly-isothermal behaviour of PCMs during phase transition makes them attractive for temperature-controlled applications.

1.3. Phase change materials

A phase change material may be defined as a material that will store or release a large quantity of heat when it changes its phase at certain temperatures. Fig. 1.1 shows a schematic of a temperature-enthalpy curve for an ideal phase change material. The ideal PCM takes in the latent heat of fusion (Δh_f) as it melts and releases the same when it solidifies. The ideal PCM also takes in the latent heat of vaporization (Δh_v) when it vaporizes and releases the same quantity of heat when the process is reversed in condensation. These processes occur isothermally for an ideal PCM but in reality they have been observed to occur over a narrow temperature range. For most materials, large volume changes accompany the liquid-gas transitions which will make the systems complex [10]. Therefore, the solid-liquid transitions of PCMs are mostly utilized in LHTES systems.

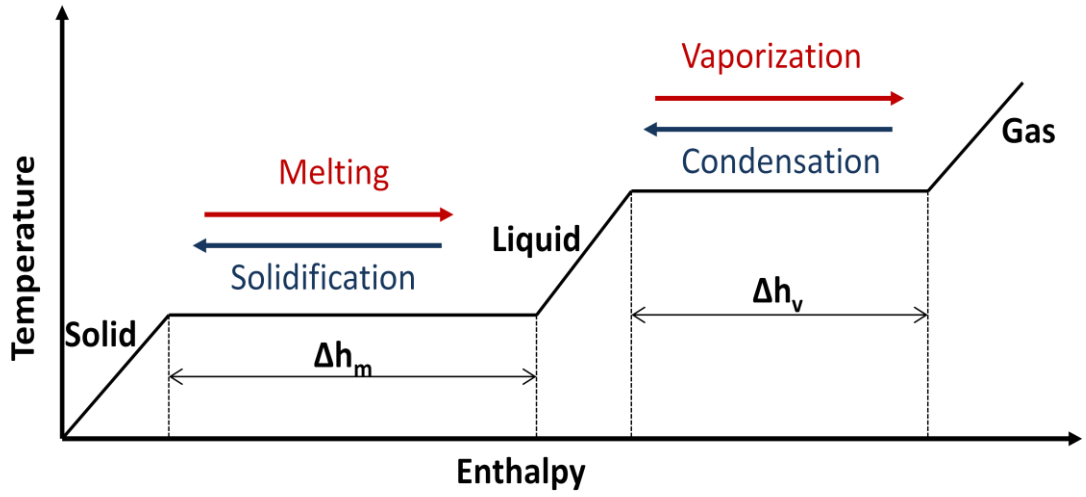

Fig. 1.1. A schematic temperature-enthalpy curve for an ideal PCM.

1.3.1. Classification of phase change materials

Phase change materials are classified into the following groups:

(a) Organic PCMs which include paraffins and non-paraffin compounds like fatty acids.

(b) Inorganic PCMs which include salts, salt hydrates and metallics.

(c) Eutetic PCMs are minimum-melting compositions of two or more chemical components, each of which melt and solidify congruently. These include organic-organic, inorganic-inorganic and organic-inorganic chemical compositions [8, 11].

1.3.2. Desirable properties of phase change material

Apart from the fact that the PCM to be utilized in a LHTES system should have its transition temperature around the proposed operational temperature, the following are the desirable thermophysical, kinetic, chemical and economic properties expected:

(a) High latent heat of transition,
(b) High mass density,
(c) High specific heat capacity,
(d) High thermal conductivity,
(e) Congruent melting,
(f) Small volume change during phase transition,
(g) Little or no supercooling,
(h) Chemical stability over several heating and cooling cycles,
(i) Chemical compatibility with containment material,
(j) Safe, that is, non-toxic, non-flammable and non-explosive,
(k) Cost effective,
(l) Available in large quantities.

1.4. Solar cookers

Solar cookers have been described as heat exchangers that are designed to utilize solar thermal energy in cooking processes [12]. Direct solar cookers make use of direct solar radiation to cook food but due to exposure of users to solar radiation as well, they have not been widely accepted. Moreover, they cannot be used at night or periods with very cloudy skies and they have been reported to prolong the cooking time due to low temperatures attained in the cookers [13]. Direct solar cookers include the box type of cookers as well as the concentrating type of cookers. For the case of indirect solar cookers, the cooking unit and the solar collection unit are physically separated and a heat-transferring medium is used to transfer heat from the solar collector to the cooking unit [7]. With indirect solar cookers, cooking may be done in the convenience of a kitchen as with the case of many conventional cooking practices. Again the use of indirect solar cookers to cook food will also be restricted to periods when there is sunshine. It is therefore essential to integrate a form of thermal energy storage system with the design of an indirect solar cooker for the provision of thermal energy for cooking when solar energy supply is unavailable or inadequate.

1.4.1. Indirect solar cookers with thermal energy storage

Mussard et al. [14] presented a comparative experimental study of two types of solar cookers namely; an SK 14 solar cooker which is a direct solar cooker and a prototype of a parabolic trough cooker which was integrated with a TES unit. A thermal fluid, Duratherm 630, was used to transfer thermal energy from the absorbing unit to the storage unit. The storage unit was a steel cylinder filled with the HTF and eight tubes containing a $NaNO_3$-KNO_3 binary mixture (PCM). Boiling and frying were done with the two cookers and they concluded with an optimized cooking surface on the prototype, it was possible for the solar cooker with storage to have a comparable performance to that of a conventional direct solar cooker.

Sharma et al. [15] investigated the performance of a prototype solar cooker which consisted of an evacuated tube solar collector (ETSC) and a cooking unit that was incorporated with a PCM thermal energy storage. The cooking/storage unit consisted of two hollow concentric cylinders with inner diameters of 304 mm and 441 mm respectively. The space between the cylinders was then filled with 45 kg of erythritol (PCM). Water was used to transfer heat from the collector to the cooking/storage unit .They reported cooking of food twice in a day; at noon when solar radiation was available and in the evening when the thermal energy stored during the day was then used for cooking. Additionally, they reported that the evening cooking was faster than the noon cooking. However, a low heat transfer rate was observed to and from the PCM thus a more efficient heat exchanger which would enhance the rate of heat transfer was essential.

Hussein et al. [12] developed a novel indirect solar cooker with outdoor elliptical cross sectional area heat pipes with flat plate collector and an indoor cooking unit which was integrated with a PCM storage. The solar radiation incident on the collector was enhanced by using two plane reflectors while water vapour served as the HTF. The cooking unit consisted of two vapour-tight pots with capacities of 3 litres and 4 litres respectively. The pots were placed inside a helical condensing coil which was embedded in the inner box of the cooking/storage unit. The space between the pots and the inner walls of the box was filled with magnesium nitrate hexanitrate ($Mg(NO_3)_2 \cdot 6H_2O$) as the PCM for thermal energy storage and glass wool to improve the thermal conductivity of the PCM. They reported that the cooker was able to cook two meals (noon and evening) and also that the remaining stored thermal energy was enough to cook breakfast the next morning. The stored thermal energy in

the cooker was also sufficient to be used for heating or cooking meals hot at night and cooking the breakfast of the next day.

1.5. Problem statement

Domestic heating demands are the dominant end-use of energy in the residential sector and a large percentage of people in the developing countries still rely on the burning of biomass to meet these needs. These practices have been associated with various negative impacts on public and environmental health. Since the solar thermal energy resource presents a tremendous potential for the provision of a clean and a renewable means of meeting domestic heating demands, there is the need to provide a means of storage of this time-dependent energy resource for use during periods of low or no solar radiation.

1.6. Research Objectives

The main aim of this thesis is to design and construct a laboratory-scale oil/packed bed TES system with encapsulated phase change material for cooking application and investigate its thermal performances during charging and discharging cycles. A packed bed type of heat exchanger has been reported to provide good heat transfer between the HTF and the thermal storage material in a TES.

The specific objectives of the thesis are:

1. To conduct preliminary numerical studies of a packed bed latent heat thermal energy storage, using a simple one-dimensional mathematical model validated with experimental results.
2. To encapsulate the PCM using a suitable material and in a desirable geometry.
3. To compare the thermal stability and cycling stability of some PCM candidates with melting temperatures between 100 ^{o}C and 120 ^{o}C.
4. To compare the thermal performances of the encapsulated PCM candidates in order to select a suitable PCM.
5. To design, construct and investigate the performance of a laboratory-scale oil/packed bed TES during charging and discharging cycles.

1.6. Outline of the thesis

Chapter One: This chapter gives a background of the study and introduces terms and concepts that will be encountered in the subsequent chapters. The objectives of this research work are also clearly stated out also in this chapter.

Chapter Two: A preliminary numerical study of a packed bed of an encapsulated erythritol, using sunflower oil as the heat transfer fluid, is carried out in this chapter. This is done by using a simple one-dimensional model and the influences of the HTF flow velocity and the HTF inlet temperature into the bed during charging are investigated.

Chapter Three: The encapsulation of erythritol in aluminum capsule is investigated in this chapter. The aluminum alloy is first investigated to be chemically compatible with both meso-erythritol and sunflower oil. The mechanical stability of the spherical capsule is then investigated with a number of wall thicknesses by carrying out some numerical studies. A sample capsule is then fabricated and filled with meso-erythritol. The sample is then subjected to heating to verify the mechanical stability.

Chapter Four: This chapter presents the experimental investigation of the thermal and chemical stability of meso-erythritol along with acetanilide and an Indium-Tin alloy, whose melting points are comparable with that of meso-erythritol. The results are compared for a possible domestic cooking application. The three PCMs are also compared in terms of their health hazards.

Chapter Five: The charging and discharging performances of acetanilide, meso-erythritol and an Indium-Tin alloy, inside similar spherical aluminum capsules, is investigated in this chapter. The results for the three encapsulated PCMs are compared. This will give some insight into the behaviour of an individual capsule of meso-erythritol in the packed bed thermal storage system while also exploring the use of acetanilide and the Indium-Tin alloy.

Chapter Six: This chapter describes the design and fabrication of the oil/packed bed TES system. The performances of the system are investigated during charging and discharging cycles and the results are presented in this chapter.

Chapter Seven: This chapter presents the conclusions drawn from the research carried out based on the previous chapters. Recommendations are also made for future research studies.

References

[1] IEA 2015. World Energy Outlook 2015. Executive summary. International Energy Agency, Paris. Available at: https://www.iea.org/Textbase/npsum/ WEO2015SUM. pdf (accessed 21/08/16).

[2] Lambe F, Jüriso M, Wanjiru H, Senyagwa J. Bringing clean, safe, affordable cooking energy to households across Africa: an agenda for action. Prepared by the Stockholm Environment Institute, Stockholm and Nairobi, for the New Climate Economy. Available at: http://newclimateeconomy.report/misc/working-papers (accessed 21/08/16).

[3] Putti VR, Tsan M, Mehta S, Kammila S. The state of the global clean and improved cooking sector. Technical report # 007/15, Energy Sector assistance program. The World Bank. Available at: http://openknowledge.worldbank. org/bitstream/handle/ 10986/ 21878/96499.pdf (accessed 21/08/16).

[4] Rysankova D, Putti VR, Hyseni B, Kammila S, Kappen JF. Lean and Improved Cooking in Sub-Saharan Africa: A Lanscape Report. Report No. 98664. Africa Clean Cooking Solutions Initiative. The World Bank, Washington DC. Available at: http://documents.worldbank.org/curated/en/2015/07/24853349/clean-improved-cooking-subsaharan-africa-landscape-report (accessed 21/08/16).

[5] IEA 2015. Electricity Access Database. International Energy Agency, Paris. Available at: http://www.worldenergyoutlook.org/resources/energydevelopment/ energyaccess database/ (accessed 21/08/16).

[6] Faninger G. The potential of solar thermal technologies in a sustainable energy future. Results from 32 years of International R&D co-operation. Solar heating and cooling programme. International Energy Agency. Available at: www.iea-shc.org.

[7] Muthusivagami RM, Velraj R, Sethumadhavan R. Solar cookers with and without storage - A review. Renewable and Sustainable Energy Reviews 2010; 14: 691-701.

[8] Sharma A, Tyagi VV, Chen CR, Buddhi D. Review on thermal energy storage with phase change materials and applications. Renewable and Sustainable Energy Reviews 2009; 13:318-45.

[9] Fernandes D, Pitie F, Cáceres G, Baeyens J. Thermal energy storage: "How previous findings determine current research priorities". Energy 2012; 39:246-57.

[10] Regin AF, Solanki SC, Saini JS. Heat transfer characteristics of thermal energy storage system using PCM capsules: A review. Renewable and Sustainable Energy Reviews 2008; 12: 2438-58.

[11] Abhat A. Low temperature latent heat thermal energy storage: Heat storage materials. Solar Energy 1983; 30(4): 313-32.

[12] Hussein HMS, El-Ghetany HH, Nada SA. Experimental investigation of novel indirect solar cooker with indoor PCM thermal storage and cooking unit. Energy Conversion and Management 20 08; 49:2237-46.

[13] Tesfay AH, Kahsay MB, Nydal OJ. Solar powered heat storage for baking Injera in Ethiopia. Energy Procedia 2014; 57: 1603-12.

[14] Maxime M, Gueno A., Nydal OJ. Experimental study of solar cooking using heat storage in comparison with direct heating. Solar Energy 2013; 98: 375-83.

[15] Sharma SD, Iwata T, Kitano H, Sagara K. Thermal performance of a solar cooker based on an evacuated tube solar collector with a PCM storage unit. Solar Energy 2005; 78: 416-26.

CHAPTER TWO: PREMILIMINARY NUMERICAL STUDY

2.1. An Overview

As mentioned in chapter one, latent heat thermal storage systems can provide large thermal energy densities for the storage of solar thermal energy during the periods of sunshine to be utilized for applications like cooking during non-sunshine periods. Erythritol had been suggested by a number of studies to be a good phase change material due to its large latent heat of fusion and its melting temperature (~118 - 122 ^{o}C) which makes it an ideal PCM candidate for cooking applications. Due to the low thermal conductivity of erythritol, an efficient heat transfer enhancement in the storage thermal storage tank is essential for greater charging and discharging efficiencies. Literature revealed that there have been experimental studies on some other forms of heat enhancement techniques for erythritol in thermal storages but there is no experimental study yet on a packed bed of spherically encapsulated erythritol. The mathematical modeling and simulation of the proposed physical system is valuable for the design of such system. The performances of such systems with certain parameters may be predicted to some degree of correctness while avoiding the wastage of material resources during the design and construction. Thus in order to have an idea of the thermal performances of a packed bed of erythritol, using sunflower oil as the heat transfer fluid, mathematical modeling and simulation of the proposed system will be helpful.

A simple one-dimensional mathematical model, which was validated with experimental results, was used to study the charging performances of the proposed thermal storage system with respect to changes in the HTF flow velocity and HTF inlet temperature. This research was presented at the Third South African Solar Energy Conference, SASEC 2015, which was held from 11th to 13th May, 2015 at the Kruger National Park, South Africa. The full paper is presented in this chapter as research paper 1.

2.2. Research Paper 1:

Numerical investigation of a packed bed thermal energy storage system for solar cooking using encapsulated phase change material

Shobo A. B.*, Mawire A.

*Department of Physics and Electronics, North West University, Mafikeng Campus, Private Bag X2046, Mmabatho 2745, South Africa.

E-mail: adetumirola@gmail.com ashmore.mawire@nwu.ac.za

Abstract

A numerical model for a packed bed thermal energy storage (TES) system using phase change material (PCM) is presented. The storage system is to be utilized for a solar cooking application. Sunflower oil is the heat transfer fluid (HTF) during charging cycles. The packed bed TES consists of spherical capsules filled with erythritol, as the phase change material. The model uses dual-phase mathematical heat transfer equations while the phase change phenomena inside the PCM capsules is analyzed by using the effective heat capacity method. Results from the model are validated with experimental results from literature. Numerical and experimental results are reasonably comparable. The effects of the inlet temperature and the flow rate of the HTF on the temperature profiles of the packed bed are presented.

Nomenclature

Symbols	***Unit***	***Description***	***Subscipts***	
ε	[-]	Porosity/Void fraction	f	fluid/HTF
ρ	[kg/m^3]	Density	S	PCM
c	[J/kg ^{0}C]	Specific heat capacity	m1	solid-solid transition
υ_f	[m/s]	Velocity of HTF	m2	solid-liquid transition
λ	[W/m ^{0}C]	Thermal conductivity	s1	solid PCM
T	[^{0}C]	Temperature	s2	liquid PCM
h_f	[W/m^3 ^{0}C]	Volumetric heat transfer coefficient	ini	initial
r	[m]	Radius of PCM sphere		
Re	[-]	Reynolds number		
Pr	[-]	Prandtl number		
μ_f	[kg/m s]	Dynamic viscosity of HTF		
y	[m]	Axial distance		
d_p	[m]	Diameter of PCM sphere		
γ_{th}	[J/kg]	Latent heat		

2.3. Introduction

For livelihood, humans need food and the cooking of food is done on a daily basis. Thus, a huge amount of energy is expended daily for cooking purposes [1]. According to the World Health Organisation (WHO), about 2.5 billion people in developing countries rely on biomass for cooking and about 1.5 million deaths in developing countries can be attributed to indoor pollution caused by the combustion of biomass due to the emission of carbon monoxide, hydrocarbons and particulate matter [2]. This heavy dependence on biomass for cooking needs may also lead to serious environmental degradation as the trees in forests could be depleted for the provision of fuelwood and charcoal.

Solar energy possesses the highest theoretical potential of about $120,000$ TW, of the earth's renewable energy resources [3]. Solar cookers are safe, practical, potentially low-cost and they have public and environmental health benefits particularly in developing countries [4]. Technically, cooking involves heating an amount of food to the boiling point of water and keeping the food at that boiling temperature for a desired period of time [5].

Direct solar cookers, which utilize direct or reflected solar radiation for solar cooking, have been in existence for years. These include solar panel cookers, solar box cookers and solar parabolic cookers [6]. They have the disadvantages of usefulness only during periods of good solar radiation, exposure of operators to the solar radiation and that cooking can only be done outdoors [7]. Indirect solar cookers utilize the heat transferred from a solar collector to the cooking unit by means of a heat transfer fluid (HTF) [5].

However, the supply of solar energy is time-dependent, as such, a discrepancy may arise between solar energy supply and demand. Thermal energy storage (TES) systems may cater for this time-discrepancy by storing solar thermal energy during sunshine hours for use later [8, 9]. TES systems can be classified as active or passive. The former can be direct or indirect. In the direct type, the storage medium is also the heat transfer fluid, whereas in the indirect type, a second fluid is used for storing the heat. In passive TES systems, a solid material is used as the storage medium (packed bed) while the HTF passes through the storage medium only during the charging and discharging phases [10].

Packed bed configurations have shown excellent heat transfer characteristics by providing a large surface area for heat exchange [11]. The spherical geometry of encapsulation of PCM is preferred because it presents a larger area of the encapsulated PCM for heat transfer than

other geometries of encapsulation. It also makes the storage tank to have a greater packing density [12].

A latent heat thermal energy storage (LHTES) system operates on the principle that large amount of heat (latent heat of fusion) is stored in/released from a phase change material (PCM) as it changes its phase. The solid-liquid phase-change transformation is usually utilized for this purpose. The LHTES system is particularly attractive for domestic cooking applications due its high thermal energy storage density and its isothermal behaviour during the heat retrieval process [13]. Various studies recommended that a LHTES system with an operational temperature higher than 100 ℃ will achieve faster cooking and longer storage time [9, 14-15].

Erythritol is a natural occurring sugar alcohol present in various fruits and fermented foods. It is produced industrially by glucose fermentation. It has a solid-liquid phase change temperature of about 117 ℃, with a latent heat of 344 kJ/kg. It is widely used in the food industry as a low-calorie sweetener and also as an excipient in pharmaceutical formulations. It is cheap and readily available and can be encapsulated for use as phase change material in a TES system [16-18].

Sunflower oil is widely used for industrial and domestic cooking in South Africa. It is locally manufactured in South Africa and reasonably priced at about R 12 (~USD 1.2) per litre. The choice of sunflower oil as the HTF borders on the following: (i) it is cheap, readily available and can be easily produced by extracting the oil from sunflower seeds, (ii) it is edible and non-toxic (iii) its characteristics are comparable to other thermal oils used for domestic heat storage applications as reported in literature [19-20] and (iv) it has a flash point around 250 ℃, a temperature that is much higher than the operating temperature of the proposed TES.

Karthikeyan et al. [13] conducted a numerical investigation of a packed bed TES unit filled with spherically encapsulated PCM by comparing results from three mathematical models. The first model, a continuous solid phase model, considered all the PCM at the same height in the storage unit as being at the same temperature at a particular time. This model neglected axial thermal conduction. The second model included axial conduction in both the HTF and the PCM. The third model however, was a conduction-based, enthalpy model which considered thermal gradients inside the PCM capsules. The third model showed a closer agreement with experimental results than the first two models. Peng et al. [21] analyzed the

behaviour of a packed bed LHTES system using concentric-dispersion equations and the phase change phenomena of the PCM in the capsules by the effective heat capacity method.

This paper presents a numerical investigation of the transient behaviour of a packed bed LHTES system, using encapsulated erythritol as the PCM and sunflower oil as the HTF. The aim is to investigate the TES system for domestic cooking needs, using a dual-phase mathematical model.

2.4. A solar cooking unit integrated with a LHTES system

Fig. 2.1 shows a schematic diagram of a indirect solar cooking unit integrated with a single, packed bed, TES tank. The cold HTF is pumped into the solar collector to be heated up and then back into the packed bed through the top of the tank during the charging cycle. As the HTF flows down through the PCM spheres, heat is transferred from the HTF to the PCM. The process is continued until the PCM spheres attain the inlet temperature of the HTF. During the discharging cycle, the hot HTF flows from the top of the TES tank into the cooking unit where it exchanges heat with the food to be cooked while the cold HTF is pumped back into the TES tank through the bottom.

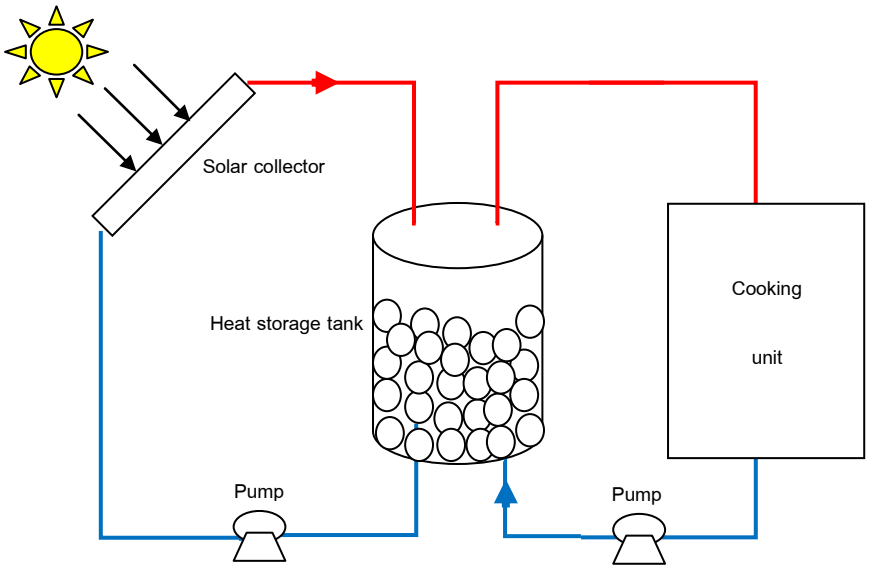

Fig. 2.1. The Schematic diagram of a solar cooker with a thermal storage.

2.5. Mathematical model

A schematic diagram of the packed bed LHTES system, consisting of a perfectly insulated vertical cylinder of length, *H*, diameter, *D*, with inlet and outlet manifolds at top and bottom ends, is shown in Fig. 2.2. The encapsulated spherical PCM spheres are randomly packed in

the tank with porosity, *e*, through which the HTF flows. The HTF and the PCM are assumed to be initially at the same temperature.

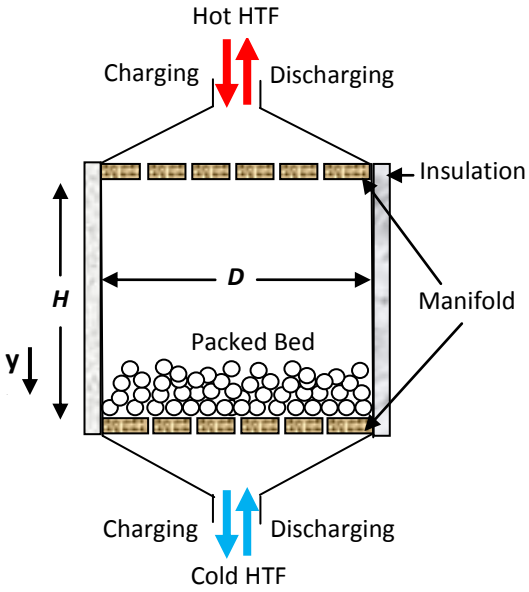

Fig. 2.2. Schematic diagram of the packed bed LHTES system.

The mathematical model used in this work is similar to that used by [21], except that the radial dispersion in the PCM spheres was not considered.

The following assumptions were made in the formulation of the mathematical model used:

1) The tank is perfectly insulated with the HTF flowing from the top when charging and from bottom when discharging.
2) The flow is axial and incompressible.
3) The temperature of the HTF is considered constant at entry into the storage tank.
4) The thermal resistance of the encapsulation material is neglected.
5) Radiant heat transfer in the storage is neglected.
6) The thermo-physical properties of the HTF are considered constant and calculated at an average temperature $T_{av} = (T_{in} + T_{out})/2$.
7) The PCM spheres are identical.
8) There is no internal heat generation in the bed.

The governing equations for the mathematical model for the HTF and PCM are respectively:

$$\varepsilon\rho_f c_f \frac{\partial T_f}{\partial t} + \varepsilon v_f \rho_f c_f \frac{\partial T_f}{\partial y} = \varepsilon\lambda_f \frac{\partial^2 T_f}{\partial y^2} - h_f\left(T_f - T_s\right) \tag{2.1}$$

$$(1-\varepsilon)\rho_s c_s \frac{\partial T_s}{\partial t} = (1-\varepsilon)\lambda_s \frac{\partial^2 T_s}{\partial y^2} + h_f\left(T_f - T_s\right) \tag{2.2}$$

The Reynolds number is calculated as:

$$Re = \frac{\rho_s d_p \varepsilon v_f}{\mu_f} \tag{2.3}$$

The Prandtl number is calculated using:

$$Pr = \frac{c_f \mu_f}{\lambda_f} \tag{2.4}$$

The volumetric heat transfer coefficient from [22] is calculated as:

$$h_f = \frac{6(1-e)\left[2 + 1.1Re^{0.6}Pr^{1/3}\right]\lambda_f}{d_p^2} \tag{2.5}$$

2.5.1. Phase change

The phase change within the encapsulated PCM is accounted for by the apparent heat capacity method. The PCM undergoes three stages during charging and discharging, namely: solid stage, solid-liquid phase change and liquid stage.

(a) During the solid stage, $T_s < T_{m1}$

$$c_s = c_{s1};\ \rho_s = \rho_{s1};\ \lambda_s = \lambda_{s1} \tag{2.6}$$

(b) During solid-liquid phase change, $T_{m1} < T_s < T_{m2}$

$$c_s = \frac{c_{s1} + c_{s2}}{2} + \frac{\gamma_{th}}{T_{m2} - T_{m1}};\ \rho_s = \frac{\rho_{s1} + \rho_{s2}}{2};\ \lambda_s = \frac{\lambda_{s1} + \lambda_{s2}}{2} \tag{2.7}$$

(c) During the liquid stage, $T_p > T_{m2}$

$$c_s = c_{s2};\ \rho_s = \rho_{s2};\ \lambda_s = \lambda_{s2} \tag{2.8}$$

2.5.2. Initial and boundary conditions

At time $t = 0$,

$T_f = T_s = T_{ini} \qquad for\ 0 \le y \le H$

At time $t > 0$,

$T_f(0,t) = 70;\ \frac{dT_s}{dy} = 0 \qquad$ for y = 0

$\frac{dT_f}{dy} = 0;\ \frac{dT_s}{dy} = 0 \qquad$ for y = H

2.5.3. Method of solution

The two coupled, parabolic equations (eqn, (2.1) and (2.2)), were solved simultaneously for the new values of the temperatures of HTF and PCM at increasing time steps. A finite difference method was implemented by using the Matlab's pdepe solver [23].

2.5.4. Model validation

The dual-phase heat transfer model was validated using experimental data of Nallusamy et al. [24]. The temperature profile for the PCM at x/H=0.25 was compared to that obtained from the model during a charging cycle. The result is presented in Fig. 2.3. There are some appreciable deviations from the experimental result, at some points, which may be attributed to (i) the effect of the encapsulation material, (ii) the radial thermal dispersion in the PCM spheres and (iii) heat losses from the walls, which was not accounted for in the model used for the simulation. Results obtained from the model showed acceptable agreement with the experimental results. The prediction of the model will suffice for the purpose of this study.

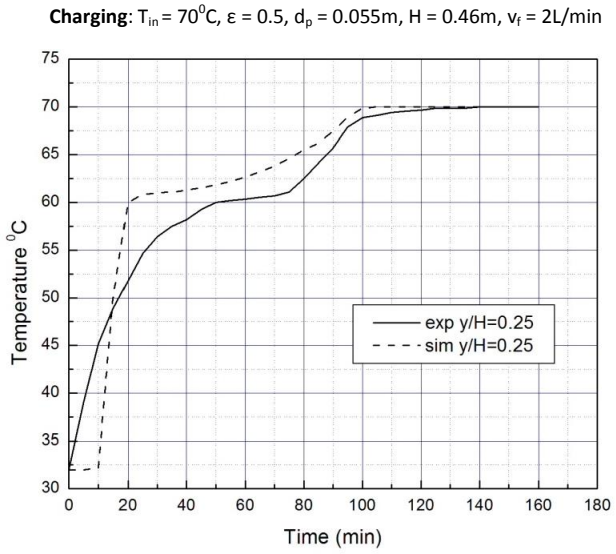

Fig. 2.3. A comparison between the numerical simulation results and experimental data for the temperature profile of the packed bed system.

2.5.5. Quantity of heat stored

The quantity of heat, Q, stored in an elemental volume of the PCM is calculated by:

$$Q = \rho_{s1} c_{s1} (1 - \varepsilon) V_{elem} (T_{m1} - T_{ini}) \quad (9)$$

for the sensible heat from initial temperature (T_{ini}) to the commencement of phase change, where V_{elem} is the volume of the element of PCM at a height in the storage tank.

$$Q = \rho_{s1} (1 - \varepsilon) V_{elem} \gamma_{th} \quad (10)$$

for phase change.

$$Q = \rho_{s2} c_{s2} (1 - \varepsilon) V_{elem} (T_{final} - T_{m2}) \quad (11)$$

for the sensible heating from end of phase change to final temperature (T_{final}) of the PCM in the element.

2.6. Results and discussion

2.6.1. Effect of HTF inlet temperature on charge time

For the purpose of simulation, the TES tank used is as depicted in Fig. 2.2, with a height of 0.46 m and a radius of 0.18 m. Spherically encapsulated erythritol PCM balls of radius 0.0275 m were randomly packed in the tank with a porosity of 0.5.

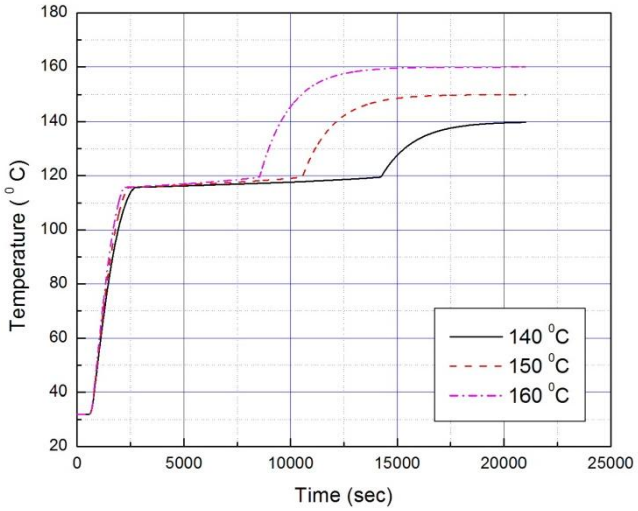

Fig. 2.4. Variation of charging time for the TES system at y/H = 0.5 with HTF flow velocity of 1 L/min.

Fig. 2.4 shows the effect of varying the inlet temperature of sunflower oil (HTF) at a flow velocity of 1 L/min, on the charging time. With an increase in the HTF inlet temperature from 140 ^{0}C to 150 ^{0}C, the charging time for the TES unit (at y/H = 0.5) reduced by about 12.5 %. Fig. 2.5 shows the effect of variation of the inlet temperature on the charging time for the TES at 2 L/min. The increment of inlet temperature from 150 ^{0}C to 160 ^{0}C also saw a 12.5 % reduction in the charging time for a flow velocity of 1 L/min. For a flow velocity of 2 L/min, the charging time reduced by 13.33 % for a temperature increase from 140 ^{0}C to 150 ^{0}C and 7.69 % for a temperature increase from 150 ^{0}C to 160 ^{0}C. The rate of heat transfer is increased by an increase in the temperature of the HTF due to the increase in the thermal gradient between the HTF and PCM. Therefore, an increase in the inlet temperature of the sunflower oil will reduce the charging time of the TES unit.

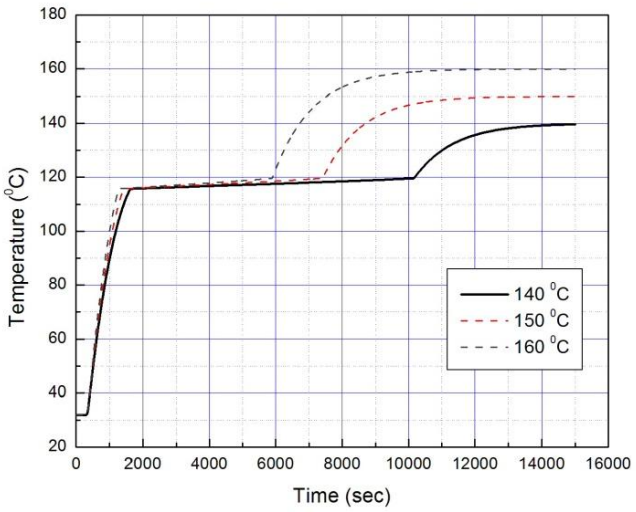

Fig. 2.5. Variation of charging time for the TES system at y/H = 0.5 with HTF flow velocity of 2 L/min.

2.6.2. Effect of HTF flow velocity on the charging time

Fig. 2.6 shows the variation in the charging time for varying flow rates at 140 °C. Fig. 2.7 also shows the variations in the charging time at the middle of the TES system for varying flow rates at 150 °C. With an increase in the HTF flow velocity from 1 L/min to 2 L/min, the charge time reduced by about 7.56 % and an increase of the flow velocity from 2 L/min to 3 L/min brought a 3.67 % reduction in the charging time of the TES system at y/H = 0.5.

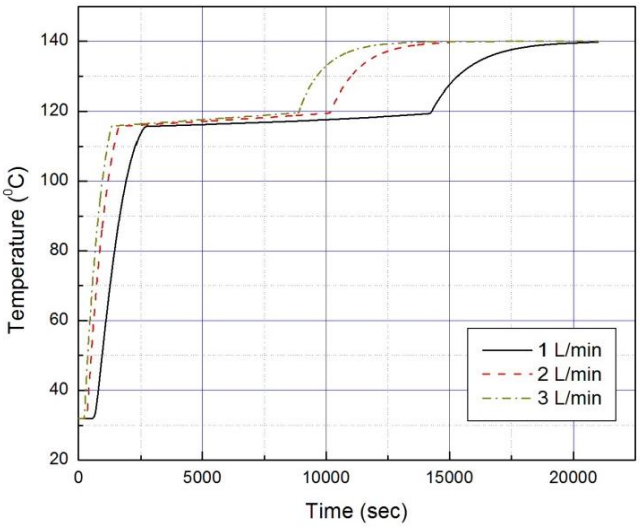

Fig. 2.6. Variation of charging time at y/H = 0.5 with varying flow rates at an inlet temperature of 140 °C.

An increase in the flow velocity of sunflower oil through the packed bed will reduce the charging time. This is because an increase in the HTF flow velocity through the bed will cause an increase in the Reynolds number which will invariably increase the heat transfer coefficient of the HTF to the bed.

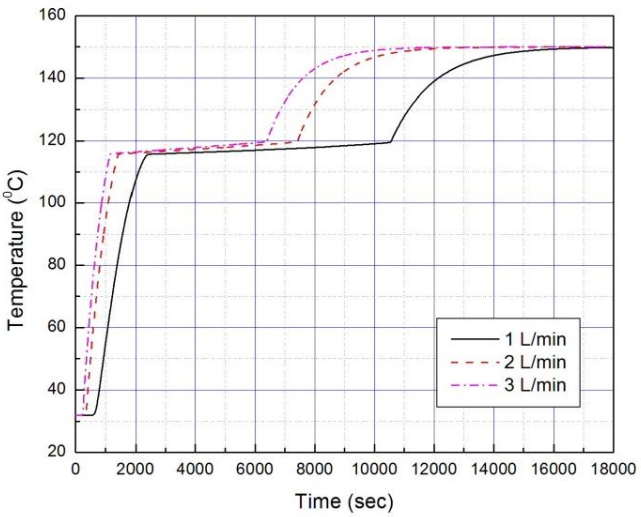

Fig. 2.7. Variation of charging time at y/H = 0.5 with varying flow rates at an inlet temperature of 150 °C.

2.6.3. Sensitivity analysis

From Fig. 2.8, while keeping the flow rate constant, an increase in the HTF inlet temperature form 140 °C to 160 °C, shows an increasing trend in the quantity of heat stored. This is due to the fact more thermal energy is available for storage at higher temperatures of the HTF.

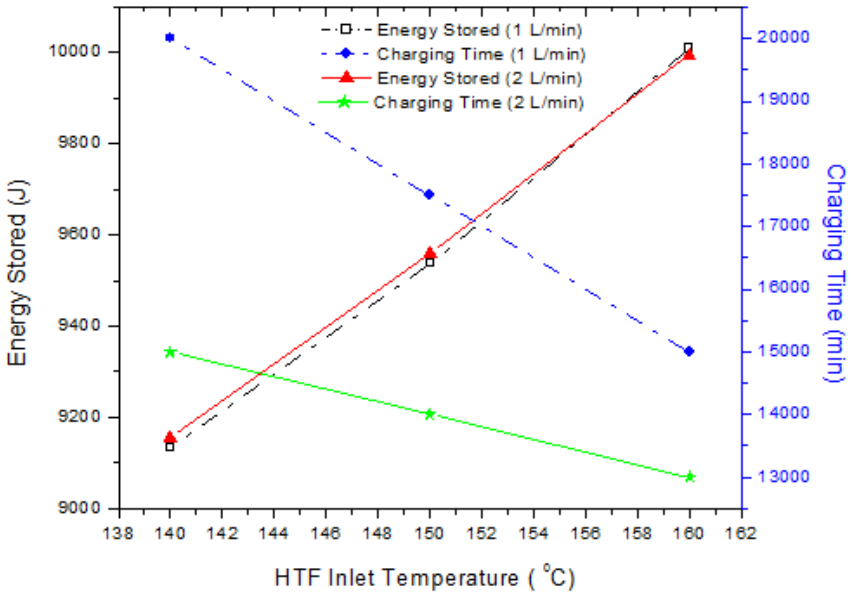

Fig. 2.8. Variation of energy stored and charging time with HTF flow rate at y/H = 0.5.

There was no significant difference in the quantity of heat stored in the PCM with flow rates of 1 L/min and 2 L/min because the quantity of heat stored is not dependent on the flow rate. The charging time shows a decreasing trend with an increase in the HTF inlet temperature in both flow rates

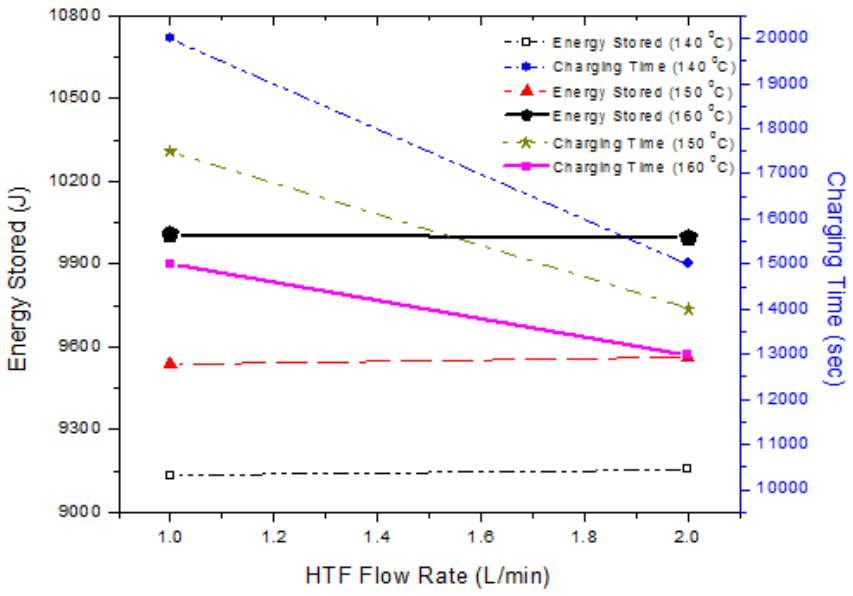

Fig. 2.9. Variation of energy stored and charging time with HTF flow rate at y/H = 0.5.

as an account of greater rate of heat transfer, caused by the larger thermal gradients. From Fig. 2.9, it is observed that there was very slight increase in the quantity of energy stored with a constant temperature of HTF at 140 ^{o}C, 150 ^{o}C and 160 ^{o}C with increasing flow rate. The charging time shows a more noticeable decreasing trend with increasing flow rate, due to the greater rate of heat transfer influenced by an increase in the Reynolds number.

2.7. Conclusion

The dual-phase model presented has been used to predict the performance of a packed bed TES unit, employing encapsulated erythritol as a packed bed and sunflower oil as the HTF. Results are given only for the charging cycles as a similar behaviour is expected, in the reverse pattern for discharging, within the assumptions employed in the study. An increase in the inlet temperature of the oil into the packed bed has shown to significantly decrease the charging time of the TES unit and also to decrease the maximum charging temperature. However, an increase in the operating temperature of erythritol will increase the risk of thermal degradation after several charging and discharging cycles. Thus, there is a trade-off between higher inlet temperature (consequently, lower charging time) and the possible durability (efficiency) of the TES unit over a period of time. An increase in the flow velocity also brought about a decrease in the charging time of the TES unit which, of course, will mean more pumping power which can increase the cost of the unit. The HTF inlet temperature has significant impact on both the charging time and quantity of heat stored in the TES system. The flow rate though has significant impact on the charging time, but does

not have significant impact on the quantity of heat stored in the TES system. Higher HTF inlet temperature means shorter charging times while more energy is available in the TES system for cooking. A higher flow rate implies that a lower duration for charging the TES system. The results are useful to identify the optimal operational and design parameters of the packed bed TES system for practical operations.

References

[1] International Energy Agency. Energy for Cooking in Developing Countries. In: World Energy Outlook 2006. OECD Publishing.

[2] Smith KR, Haigler E. Co-benefits of climate mitigation and health protection in energy systems: scoping methods. Annu. Rev. Publ. Health 2008; 29: 11-25.

[3] United States Department of Energy. Basic research needs for solar energy utilization. In: Report on the Basic Energy Sciences Workshop on Solar Energy Utilization, September 2005.

[4] Gayapershad R, Dladla ST, Brooks MJ. Preliminary results from a performance evaluation study of commercial solar cookers. Poster presentation at World Conference of Physics and Sustainable Development, October 31-November 2, 2005.

[5] Sedighi M, Zakariapour M. A review of direct and indirect solar cookers. Sus. Energy 2014; 2(2): 44-51.

[6] Cuce E, Cuce PM. A comprehensive review on solar cookers. Appl. Energy 2013; 102: 1399-421.

[7] Kimambo CZM. Development and performance testing of solar cookers. J.Energy in S. Africa 2007; 18 (3): 41-51.

[8] Wu S, Fang G. Thermal performance simulations of a packed bed cool thermal energy storage system using u-tetradecane as phase change material. Int. J. of Therm. Sci. 2011; 49: 1752-62.

[9] Mussard M, Nydal OJ. Charging of a heat storage coupled with a low-cost small-scale solar parabolic trough for cooking purposes. Sol. Energy 2013; 95: 144-54.

[10] Cassetta M, Cau G, Puddu P, Serra F. Numerical investigation of a packed bed thermal energy storage system with different heat transfer fluids. Energy Procedia 2014; 45: 598-607.

[11] Bindra H, Bueno P, Morris F, Shinnar R. Thermal analysis and exergy evaluation of packed bed thermal storage systems. Appl. Therm. Eng. 2013; 52: 255-63.

[12] Xia L, Zhang P, Wang RZ. Numerical heat transfer analysis of the packed bed latent heat storage system based on effective packed bed model. Energy 2010; 35: 2022-32.

[13] Karthikeyan S, Solomon GR, Kumaresan V, Velraj R. Parametric studies on packed bed storage unit filled with PCM encapsulated spherical containers for low temperature solar air heating application. Energy Convers. Manage. 2014; 78: 74-80.

[14] Lecuona A, Nogueira JI, Vereda C, Ventas R. Solar cooking figures of merit. Extension to heat storage. Mater. process energy: communicating current research and technological developments 2013; 1: 134-41.

[15] Sharma SD, Buddhi D, Sawhney RL, Sharma A. Design, development and performance evaluation of a latent heat storage unit for evening cooking in a solar cooker. Energy Convers. Manage. 2000; 41: 1497-508.

[16] Ohmori S, Ohno Y, Makino T, Kashihara T. Characteristics of erythritol and formulation of a novel coating with erythritol termed thin-layer sugarless coating. Int. J. Pharm. 2004; 278: 447–57.

[17] Endo K, Amikawa S, Matsumoto A, Sahashi N, Onoue S 2005. Erythritol-based dry powder of glucagon for pulmonary administration. Int. J. Pharm. 2005; 290: 63–71.

[18] Gonnissen Y, Remon JP, Vervaet C. Development of directly compressible powders via co-spray drying. Eur. J. Pharm. Biopharm. 2007; 67: 220–6.

[19] Mawire A, McPherson M, Heetkamp RRJ. Thermal performance of a small oil-in-glass tube thermal energy storage system during charging. Energy 2009; 34: 838-49.

[20] Mawire A, Phori A, Taole S. Performance comparison of thermal energy storage oils for solar cookers during charging. Appl. Therm. Eng. 2014; 73 (1): 1321-9.

[21] Peng H, Dong H, Ling X. Thermal investigation of PCM-based high temperature thermal energy storage in packed bed. Energy Convers. Manage. 2014; 81: 420-7.

[22] Incopera, F.P., Dewitt, D.P., Bergman, T.L., Lavine, A.S. Fundamentals of heat and mass transfer. 6th ed. USA: SOS Free Stock; 2007.

[23] Matlab. The MathWorks Inc., R2012a. Natick, Massuchusettes.

[24] Nallusamy N, Velraj R. Numerical and experimental investigation on a combined sensible and latent heat storage unit with solar water heating system. J. Sol. Energy-T ASME 2009; 131: 1-8.

CHAPTER THREE: ENCAPSULATION OF PCM

3.1 An overview

In order to achieve a packed bed configuration intended for this research work, it is important to enclose erythritol, the phase change material, in a suitable containment of desirable geometry. The spherical geometry of encapsulation was highlighted in paper 1 (Chapter Two) to present a large area of the PCM for heat transfer while also giving the cylindrical thermal storage tank a large packing density, thus, a large thermal energy storage density. From the numerical study presented in chapter two, the packed bed of spherically encapsulated erythritol showed very good thermal energy storage and discharging characteristics. The importance of the chemical compatibility of the capsule material for a PCM was highlighted in chapter one. In this chapter, the use of aluminum spherical capsules for the containment of erythritol in the proposed packed bed thermal energy storage is investigated. This study includes the chemical compatibility of an aluminum alloy (1050-H14) with sunflower oil, the heat transfer fluid, and with erythritol, the PCM. The mechanical stability of the proposed spherical capsule with various wall thicknesses was also investigated in order to determine how thick the spherical capsule should be for the desired capsule diameter.

The research work carried out for the investigation of the encapsulation of erythritol and the results thereof are contained in the paper presented at the 24th conference of the domestic use of energy, which was held at the Cape Peninsula University of Technology, Cape Town, South Africa from March 29th to 31st, 2016. The full research paper is hereby presented as research paper 2.

3.2. Research Paper 2:

Investigation of aluminum encapsulation of a PCM for domestic cooking

Shobo A. B.*, Mawire A.

*Department of Physics and Electronics, North West University, Mafikeng Campus, Private Bag X2046, Mmabatho 2745, South Africa.

E-mail: adetumirola@gmail.com ashmore.mawire@nwu.ac.za

Abstract

This paper considers spherical macroencapsulation of erythritol as a phase change material (PCM), using an aluminum alloy (1050-H14), for use in a packed bed latent heat thermal energy storage system which is intended for domestic cooking. The strength of the capsule's wall thickness to withstand air pressure in the capsule is investigated numerically for capsules with a radius of 50 mm. The aluminum alloy shows a perfect chemical compatibility with erythritol and with sunflower oil, which is the heat transfer fluid. Results show an improvement of the thermal conductivity of erythritol with increasing capsule wall thickness (0.5 mm, 1.0 mm, 1.5 mm and 2.0 mm) which is evident in the charging times. The average charging rate reduced with increasing capsule wall thickness. The strength of the capsule increased with an increase in the capsule wall thickness, though the energy storage density reduced with an increase in the capsule wall thickness. Results indicate that an aluminum sphere with a radius of 50 mm and with a wall thickness of 1.0 mm will provide an optimal thermal performance for the encapsulation of erythritol in the proposed thermal energy storage system.

***Index Terms*— Aluminum, Erythritol, Macroencapsulation, Sunflower Oil, Thermal energy storage.**

3.3. Introduction

Solar thermal energy is a renewable and environmentally-friendly form of energy, capable of meeting domestic energy demands for example, cooking needs [1]. The discrepancies that may exist between solar energy supply and demand may be catered for, by latent heat thermal energy storage systems. This is as a result of the high energy storage densities they posses, induced by large latent heat of transition of phase change materials particularly during the solid-liquid transition [2]. The isothermal behavior of phase change materials during the phase transition is particularly attractive for cooking since cooking of foods is mostly done at an almost uniform rate of heat transfer [3].

In dual phase thermal energy storage (TES) systems, a heat transfer fluid (HTF) transports thermal energy from a heat capture unit to the phase change material in a heat storage unit during the charging cycle. During the discharging cycle, the heat transfer fluid transports thermal energy from the phase change material in the storage unit to the heat utilization unit. In order to avoid mixing of the phase change material and the heat transfer fluid, which may lead to some chemical reactions (depending on the choice of the two), a form of containment is needed for the PCM in the thermal energy storage tank. Bulk packaging of phase change materials in thermal energy storage tanks can unduly lengthen the charging and discharging times of the system. This is due to the low thermal conductivity values of most phase change materials. Smaller containments or capsules present a larger surface area of the phase change materials for heat transfer in the storage tanks. This counters the drawbacks of low thermal conductivity of the phase change materials [4].

The order of the dimension of encapsulation of phase change materials form the basis of their classification into: macroencapsulation (above 1mm), microencapsulation (0 - 1000 μm) and nanoencapsulation (0 - 1000 nm). The heat transfer rate between the HTF and the PCM is higher in both the microcapsules and the nanocapsules than in the macrocapsules due to larger surface area to volume ratios. Microencapsulation and nanoencapsulation of phase change materials are, however, very complex procedures due to the small sizes involved. Microencapsulation and nanoencapsulation of phase change materials are very complex procedures requiring specialized equipment which may increase the total cost of a thermal energy storage system [5].

Macroencapsulation of PCM is easier to achieve and may be done in various geometries including spherical, tubular, cylindrical and rectangular geometries. Materials used in literature for macroencapsulation include metals, plastics, ceramics and rubbers. To determine the choice of encapsulation material for use in a thermal energy storage system, the geometry and dimensions of the capsule, some factors have to be put into consideration [6]:.

1) Both the PCM and the HTF should be chemically non-reactive with the encapsulation material,

2) The encapsulation material should be impermeable to both the HTF and the melted PCM for the range of the operating temperatures of the system,

3) The capsule should be designed in such a way as to be able to accommodate the mechanical stresses that will develop due to volumetric changes accompanying the phase change transition of the PCM [4, 5]. It is necessary to leave an air void space when filling the

capsule in order to allow for volume expansion of the PCM when heated. Internal pressure is generated as the PCM melts and expands, compressing the air which is also already being heated [5]. The mechanical strength of the capsule is determined principally by its core-to-shell ratio. A high core-to-shell ratio might make the encapsulating shell too thin to withstand mechanical stresses which will develop during the volume expansion of the PCM. However with the core-to-shell ratio being too low, the shell becomes too thick and thus a reduction of the PCM content of the capsule [7].

The spherical geometry of encapsulation has been shown to provide a better packing fraction in a cylindrical thermal energy storage tank while presenting a good heat transfer contact area between the PCM and the heat transfer fluid [8]. The phase change material to be utilized for a particular TES system should be chosen such that its phase transition temperature is about the proposed operating temperature of the system [4]. For cooking applications, the PCM should have a phase transition temperature greater than 100 ^{o}C so as to bring the water content of the food to boil and vaporize [9].

This study investigates the suitability of encapsulating erythritol in an aluminum spherical capsule, for use in a packed bed latent heat thermal energy storage system. This system is designed for food cooking applications by the Solar Thermal Energy Research group at Northwest University. The proposed system will utilize sunflower oil as the HTF and have a maximum charging temperature of 140 ^{o}C. The strength of the capsule to withstand the stress due to the air pressure in the capsule is considered. Aluminum alloys have found a wide range of domestic and industrial applications. This is due to the fact that aluminum is abundant; the densities of its commercially available alloys are low (allowing them to be worked easily); aluminum is also reported to be very resistant to corrosion; and aluminum alloys have high thermal conductivity values [10, 11]. Studies have reported that erythritol, a naturally occurring sugar alcohol present in many fruits, is an ideal candidate for use as a PCM. Its phase transition temperature (117 ^{o}C - 123 ^{o}C) also makes it attractive for cooking applications [12, 13]. Sunflower oil has also been shown to possess good heat transfer characteristics, comparable with some commercially available HTFs [14, 15]. Both the PCM and the HTF are food-grade materials; they thus pose no threat of contamination for domestic use [16]. The transient heat transfer behaviour of the designed encapsulated phase change material is also investigated.

Nomenclature

Roman letter	*Description*	*Greek letter*	*Description*
C	constant in equation (8)	β	coefficient of thermal expansion, [/K]
F	melt fraction of PCM	γ_{th}	latent heat, [J/kg]
d	diameter, [m]	λ	thermal conductivity, [W/m K]
g	gravitational acceleration, [m/s^2]	μ	dynamic viscosity, [kg/m s]
h	convective heat transfer coefficient, [W/m^2 K]	υ_{HTF}	heat transfer fluid's velocity, [m/s]
k	thermal conductivity, [W/m K]	ρ	density, [kg/m^3]
n	constant in equation 8		
p_{air}	air pressure inside capsule, [Pa]	***Subscript***	***Meaning***
p_e	yield pressure of capsule, [Pa]	Al	Aluminum
Pr	Prandtl number, [-]	p,eff	effective parameter during phase change
r	radius, [m]	f	final
r_i	internal radius of capsule, [m]	i	initial
r_o	outside radius of capsule, [m]	Liquid	liquid phase of PCM
Ra	Rayleigh number, [-]	p/PCM	phase change material
Re	Reynolds number, [-]	Solid	solid phase of PCM
T_{m1}	temperature at commencement of melting, [K]	Abbreviations	
T_{m2}	temperature at the end of melting, [K]	EPCM	encapsulated phase change material
V	volume, [m^3]	HTF	heat transfer fluid
Y	yield stress of Aluminum, [Pa]	LHTES	latent heat thermal energy storage
%V	fractional volume	PCM	phase change material
		TES	thermal energy storage

3.4. Materials and methods

The spherical capsule is to be made from commercial grade aluminum alloy (1050-H14). The properties of the aluminum alloy are given in Table 3.1. A sample of 99 % pure meso-erythritol was purchased from J & K Scientific Ltd., Beijing, China and a branded sunflower oil was purchased from the open market in South Africa. The properties of meso-erythritol are given in Table 3.2.

Table 3.1. Properties of aluminum alloy 1050-H14.

PROPERTY	*VALUE*
Coefficient of expansion [b]	2.3 x 10^{-5} /K
Density [a]	2705 kg/m^3
Elongation at break point [b]	7 %
Melting point [a] (solidus)	646 ^oC
(liquidus)	657 ^oC
Poisson's ratio [a]	0.33
Shear Modulus [b]	26.0 GPa
Shear strength [b]	83.0 Mpa
Specific heat capacity [a]	900 J/kg K
Tensile strength (proof) [a]	145 MPa
Tensile strength (ultimate) [a]	160 MPa
Thermal conductivity [a]	227 W/m K
Thermal diffusivity [b]	9.5 x 10^{-5} m^2/s

[a] and [b] were taken from [17] and [18] respectively

Table 3.2. Thermophysical properties of meso-erythritol.

PROPERTY	PHASE	VALUE
Density (kg/m^3)	Solid (20 ^oC)	1480[a]
	Liquid (140 ^oC)	1300[a]
Specific heat capacity (J/kg K)	Solid	1383[a]
	Liquid	2765[a]
Thermal conductivity (W/m K)	Solid (20 ^oC)	0.733[a]
	Liquid (140 ^oC)	0.326[a]
Latent heat (J/kg K)		339,800[a]
T_{m1}(^oC)		117[b]
T_{m2}(^oC)		123[b]

[a] and [b] were taken from references [19] and [20] respectively

3.4.1. Test of compatibility of materials

Two rectangular pieces measuring 15 mm × 13 mm × 1mm, were cut from the aluminum sheet purchased. The pieces were weighed separately, using an electronic weighing balance with a precision of ± 0.0001g. The surface morphologies of the two pieces were studied and photographs taken, using an electron scanning microscope (Microtrac SEMTRAC mini, SM 3000) at a magnification of x70. One of the pieces was put in a glass sample bottle which was then filled with erythritol such that the piece was completely immersed. The cover of the

sample bottle was perforated with a needle to allow for the expansion of air. The second aluminum piece was put in a beaker of sunflower oil alongside the sample bottle. Heat was applied to the beaker by a stirring hotplate with continuous stirring. A thermometer was immersed in the oil to monitor the temperature. Once the temperature of the oil attained 140 ^{o}C, it was maintained at about this temperature for 6 hrs by manually adjusting the temperature of the hotplate via the temperature knob. The pieces were then quickly removed, washed carefully and dried. They were reweighed and their surface morphologies observed again using the electron microscope.

3.4.2. Analysis of elastic deformation of encapsulation

Erythritol has been reported to undergo a volume increase of about 10 % from the solid to the liquid phase [13]. For purpose of this study, the spherical capsule was assumed to be filled to 85 % of its volume with erythritol to accommodate the volume increase with an increase in the temperature. With an assumption that the spherical shell does not expand at all (the volume expansion of the shell is much less than that of the PCM), the pressure of the air in the capsule at any temperature, T, may be determined from the combined gas equation and given as [7]:

$$p_{air,f} = p_{air,i} \times \frac{1 - \%V_{PCM}}{\left[1 - \left(\%V_{PCM}\left(\frac{\rho_{PCM,i}}{\rho_{PCM,f}}\right)\right)\right]} \times \frac{T}{T_i} \tag{3.1}$$

where $p_{air,f}$, $p_{air,i}$ are the final air pressure at temperature T and the initial air temperature in the sphere respectively, $\%V_{PCM}$ is the fraction of the capsule's volume filled by the PCM, $\rho_{PCM,i}$, $\rho_{PCM,f}$ are the densities of the PCM at the initial and final temperatures inside the sphere respectively.

At a critical internal pressure, p_e, the capsule will begin to yield. This yield pressure is given by [20] as:

$$p_e = \frac{2Y}{3}\left(1 - \frac{{r_i}^3}{{r_o}^3}\right) \tag{3.2}$$

3.4.3. Mathematical modeling of the thermal performance of the encapsulated PCM

The mathematical model used to simulate the transient heat transfer in the encapsulated PCM considers radial heat transfer in the sphere and is given as:

$$\frac{\partial T_p}{\partial t} = \frac{\lambda_p}{\rho_s c_s}\left(\frac{\partial^2 T_p}{\partial r^2} + \frac{2}{r}\frac{\partial T_p}{\partial r}\right) \tag{3.3}$$

where T_p, λ_p, ρ_p, c_p are the temperature, thermal conductivity, density and specific heat capacity of the encapsulated PCM.

The capsule size required to give the desired void fraction for the design specification of the proposed TES unit is of a radius of 50 mm. Since the encapsulated phase change material is considered for use in a packed bed thermal energy storage system, the HTF is assumed to be flowing over the sphere with a uniform velocity and temperature. The HTF flow was assumed to be incompressible with a velocity of 0.001 m/s and at a temperature of 140 ^{o}C. The effect of the air void in the capsule was not considered by this study.

The boundary conditions are:

$$\lambda_{Al}\frac{\partial T_p}{\partial r} = h_p\left(T_{HTF} - T_{p,r=r_o}\right) \quad at\ r = r_o;\ and \quad \frac{\partial T_p}{\partial r} = 0 \quad at\ r = 0 \tag{3.4}$$

where λ_{Al} is the thermal conductivity of the aluminum capsule, T_{HTF} is the HTF's temperature and h_p is the heat transfer coefficient, given by [21] as:

$$h_p = \frac{\lambda_{Al}}{d_p}\left[2 + 1.1\left(Re^{0.6}Pr^{\frac{1}{3}}\right)\right] \tag{3.5}$$

The Reynolds number is calculated from:

$$Re = \frac{\rho_{HTF} v_{HTF} d_p}{\mu_{HTF}} \tag{3.6}$$

and the Prandtl number is calculated from:

$$Pr = \frac{c_{HTF}\mu_{HTF}}{\lambda_{HTF}} \tag{3.7}$$

The mathematical model was solved, for temperatures at each radial node, at new time steps using an implicit-time marching, finite difference method. The simulation was done by writing a MATLAB code.

As the PCM melts, the solid PCM sinks to the bottom of the capsule while the liquid PCM, being less dense, rises. Buoyancy-driven convection thus becomes a dominant means of heat transfer in the PCM as it melts and this will be accounted for by introducing the effective thermal conductivity ($\lambda_{p,eff}$) which is given by [21]:

$$\lambda_{p,eff} = \lambda_{PCM,Liquid} C Ra^n \tag{3.8}$$

where C and n are constants with values of 0.18 and 0.25 respectively.

The Rayleigh number is given by:

$$Ra = \frac{g\beta\Delta T L^3 \rho_p c_p}{\lambda_p} \tag{3.9}$$

where g is the magnitude of the gravitational acceleration, β is the coefficient of thermal expansion of the PCM, ΔT is the difference between temperature away from the surface of PCM and the temperature at the surface of the PCM, L is the characteristic length, ρ_p is the density of liquid PCM, c_p is the specific heat capacity of liquid PCM and λ_p is the thermal conductivity of liquid PCM. The thermal conductivity of the PCM during phase change is then given by:

$$\lambda_p = F\lambda_{p,eff} + (1-F)\lambda_{PCM,Solid} \tag{3.10}$$

where F is the melt fraction of the PCM and it is given by:

$$F = \begin{cases} 0 & if\ T_p < T_{m1} \\ \dfrac{T_p - T_{m1}}{T_{m2} - T_{m1}} & if\ T_{m1} \le T_p \le T_{m2} \\ 1 & if\ T_p > T_{m2} \end{cases} \tag{3.11}$$

The density of the PCM is computed by:

$$\rho_p = F\rho_{PCM,Liquid} + (1-F)p_{PCM,Solid} \tag{3.12}$$

The phase transition process of the PCM was approached using the apparent heat capacity method (equations 3.12 to 3.15).

$$c_{PCM} = c_{PCM,Solid}; \qquad for\ T_p < T_{m1} \tag{3.13}$$

$$c_p = \left[\frac{c_{PCM,Solid} + c_{PCM,Liquid}}{2} + \frac{\gamma_{th}}{T_{m2} - T_{m1}}\right]; \qquad for\ T_{m1} < T_p \le T_{m2} \tag{3.14}$$

$$c_p = c_{PCM,Liquid}; \qquad for\ T_p < T_{m1} \tag{3.15}$$

The simulation was executed until the temperature at the center of the encapsulated PCM was equal to the temperature of the HTF. The number of nodes (Nr) along the radius was 51while a time step (Δt) of 0.1 seconds was used. All the radial nodes were assumed to be initially at the same temperature of 20 ^{o}C. The temperature of the air in the void at any time was taken to be an average of the temperature at all the nodes in the core of the capsule.

3.5. Results and discussion

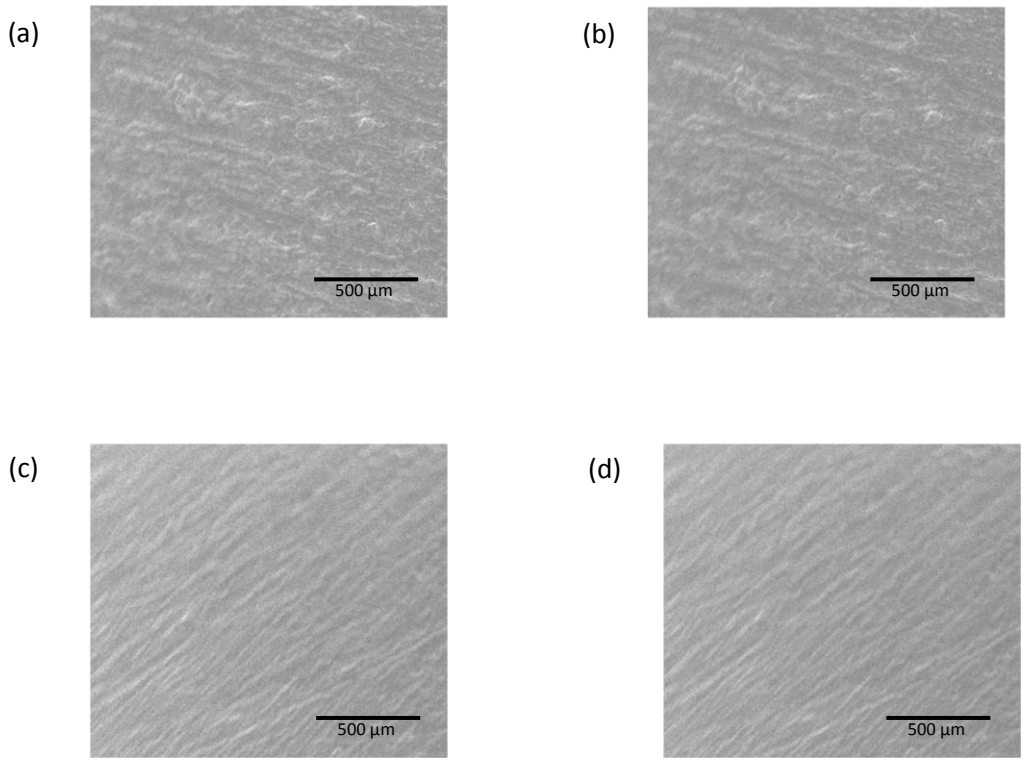

Fig. 3.1. Photographs of the surface of the aluminium sample put in (a) Erythritol before heating, (b) Erythritol after heating, (c) Sunflower Oil before heating, and (d) Sunflower Oil after heating.

Both aluminium pieces heated in erythritol and sunflower oil respectively show no mass loss when reweighed. Also, there was no visible variation in their surface morphologies after been heated (Fig. 3.1).

Table 3.3. Effects of encapsulation thickness on various parameters at the same HTF flow velocity (0.001 m/s).

Diameter of spherical capsule	Thickness of capsule wall	Core-to-Shell ratio	Charging time (min)	Average Charging rate (J/s)	Energy Density (MJ/m^3)	Yield pressure p_e (MPa)	Air pressure at 140 ^oC (MPa)
50 mm	No shell	-	255.0	3.131	731.97	-	-
	0.5 mm	49:1	253.0	2.970	688.93	5.685	7.0288
	1.0 mm	24:1	250.0	2.826	647.60	11.142	7.0287
	1.5 mm	15.7:1	247.0	2.685	607.96	16.377	7.0287
	2.0 mm	11.5:1	244.0	2.548	569.98	21.393	7.0287

The thickness of the aluminium encapsulation is directly proportional to the core-to-coating ratio as evident in Table 3.3. As the thickness of the capsule wall increases, less space will be available for the PCM to occupy thus a reduction in the amount of energy stored in the PCM.

The energy density of the PCM varies inversely as the thickness of encapsulation; this can also be seen on Table 3.3.

The average charging rate as well as the charging time of the PCM was also observed to decrease with the capsule wall thickness. This was as a result of decreasing volume of PCM with increasing encapsulation thickness and thus, less time was required by PCM contents to charge up. For a thickness of 0.5 mm, the air pressure was greater than the yield pressure of the encapsulation, thus it is undesirable because the capsule will rupture. Other thicknesses considered showed lower air pressure compared with the yield pressure value for each case. There was no significant difference in air pressure in the capsules for encapsulation thicknesses of 1.0 mm, 1.5 mm and 2.0 mm. Fig. 3.2 shows the temperature histories at the center of the erythritol spheres with radii of 50 mm radius with various capsule thicknesses and the erythritol sphere with no encapsulation, from the simulation during the charging period. There was no significant difference in the thermal responses at the centers of all the encapsulated erythritol and that without encapsulation from the beginning of charging. However, noticeable differences in the thermal performances can be observed towards the end of the phase change process. The erythritol sphere with no encapsulation took the longest time to complete phase change and consequently the longest charging time. It can be seen on Table 3.3 and Fig. 3.2 that the charging time for the erythritol capsules reduced progressively with increasing thickness of encapsulation as compared with that without encapsulation.

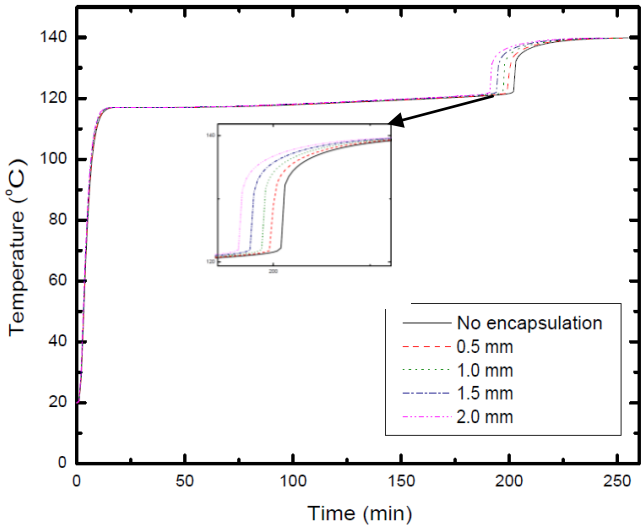

Fig.3.2. Temperature histories at the centers of erythritol sphere of diameter 50 mm without encapsulation and Erythritol spheres with various capsule thicknesses during charging.

This is as a result of improvement of the thermal conductivity of erythritol by the aluminum capsule, though this comes at a cost of reduction in the energy storage density of the PCM (as shown on Table 3.3). The yield pressure shows an increase with increasing shell thickness

thus, the strength of the capsule increases with the thickness of the encapsulation material. There is a decline in the average charging rate with increasing capsule wall thickness as a consequence of the reduced amount of the PCM available for energy storage.

3.6. Conclusions

Aluminum shows very good compatibility with erythritol and sunflower oil thus, it may be used as an encapsulation material for erythritol in the proposed TES system for domestic cooking. An aluminum spherical capsule of thickness 0.5 mm and radius of 50 mm filled to 85 % of its volume by erythritol will not be appropriate as the air pressure that will develop inside the capsule at 140 ^{o}C will be greater than the yield pressure of the capsule. The capsule will rupture and the PCM will spill, mixing with the HTF. However, spherical aluminum capsules of thicknesses 1.0 mm, 1.5 mm and 2.0 mm are capable of withstanding the internal air pressures that will develop in them for a temperature range of 20 ^{o}C to 140 ^{o}C.

The aluminum encapsulation enhanced the thermal conductivity of erythritol with increasing thickness but at a compromise of a reduction in the total energy stored by erythritol. Therefore, the thickness of encapsulation of a PCM should be kept as low as reasonably possible for maximum energy storage efficiency.

The encapsulation of erythritol with an aluminum spherical capsule of radius 50 mm and shell thickness 1.0 mm will give the optimal performance in terms of the charging rate and the energy storage density.

The authors have fabricated an aluminum spherical capsule with a radius of 50 mm and with a wall thickness of 1.0 mm. The capsule was then filled to 85 % of its volume with erythritol and then heated while immersed in a bath of sunflower oil. The capsule showed no signs of leakage or fracture. Further experimental tests will be carried out to compare the thermal performance of the encapsulated erythritol with results obtained from this study. Also, the durability of the fabricated spherical aluminum capsules will be investigated by subjecting the encapsulated erythritol to several charging and discharging cycles.

References

[1] Okello D, Nydal OJ Banda EJK. Experimental investigation of thermal de-stratification in rock bed TES systems for high temperature applications. Energ. Convers. Manage. 2014; 86: 125-31.

[2] Aadmi M, Karkri M, Hammouti ME. Heat transfer characteristics of thermal energy storage for PCM (phase change material) melting in horizontal tube: Numerical and experimental investigations. Energy 2015; 85: 339-52.

[3] Muthusivagami RM, Velraj R Sethumadhavan R. Solar cookers with and without thermal storage-A review. Renew. Sust. Energ. Rev. 2010; 14: 691-701.

[4] Regin AF, Solanski SC Saini JS. Heat transfer characteristics of thermal energy storage system using PCM capsules: A review. Renew. Sust. Energ. Rev. 2008; 12: 2438-58.

[5] Alam TE, Dhau JS, Goswami DY Stefanakos E. Macroencapsulation and characterization of phase change materials for latent heat energy storage systems. Appl. Energ. 2015; 154: 92-101

[6] Salunkhe PB, Shembekar PS. A review on effect of phase change material encapsulation on the thermal performance of a system. Renew. Sust. Energ. Rev. 2012; 16: 5603-16.

[7] Blaney JJ, Neti S, Misiolek WZ, Oztekin A. Containment capsule stresses for encapsulated phase change materials. Appl. Therm. Eng. 2012; 50: 555-61.

[8] Xia L, Zhang P, Wang RZ. Numerical heat transfer analysis of the packed bed latent heat storage system based on an effective packed bed model. Energy 2010; 35(5): 2022-32.

[9] Sharma SD, Buddhi D, Sawney RL, Sharma A. Design, development and performance evaluation of a latent heat storage unit for evening cooking in a solar cooker. Energ. Convers. Manage. 2000; 41: 1497-508.

[10] Sanders RE. Technology Innovation in Aluminum Products. JOM 2001; 53(2): 21-25.

[11] Njoku CN, Onyelucheya OE. Response Surface Optimization of the Inhibition Efficiency of Gongronema latifolium as an Inhibitor for Aluminum Corrosion in HCl Solutions. International Journal of Materials and Chemistry 2015; 5(1): 4-13.

[12] Sharma SD, Iwata T, Kitano H, Sagara K. Thermal performance of a solar cooker based on an evacuated tube solar collector with a PCM storage unit. Sol. Energy 2005; 78(3): 416-426.

[13] Kakiuchi H, Yamazaki M, Yabe M, Chihara S, Terunuma Y, Sakata Y, Usami T. "A study of Erythritol as phase change material," in IEA Annex 10-PCMs and chemical reactions for thermal energy storage, second workshop, Sofia, Bulgaria, Nov. 11-13, 1998.

[14] Mawire A McPherson M. Experimental characterisation of a thermal storage system using temperature and power controlled charging. Renew. Energ. 2008; 33: 682-93.

[15] Mawire A, McPherson M, van der Heetkamp RRJ. Thermal performance of a small oil-in-glass tube thermal energy storage system during charging. Energy 2009; 34: 838-49.

[16] Mawire A. Performance of Sunflower Oil as a sensible heat storage medium for domestic applications. Journal of Energy Storage 2016; 5: 1-9.

[17] http://www.matweb.com/search/QuickText.aspx?SearchText=1050-H14

[18] http://www.makeitfrom.com/material-properties/1050-H14-Aluminum/

[19] Agyenim F, Rhodes M, Knight I. "The use of phase change material (PCM) to improve the coefficient of performance of a chiller for meeting domestic cooling in Wales," presented at the 2nd PALENC Conference and 28th AIVC Conference on Building Low Energy Cooling and Advanced Ventilation Technologies in the 21st Century, Crete island, Greece, Sept. 27-29, 2007.

[20] Chakrabarty J. "Further solutions of elastoplastic problems," in Theory of Plastics, 3rd ed., Burlington: Elsevier Butterworth-Heinemann, 2006; Ch. 5: 323-418.

[21] Adine HA,. E. Qarnia. (2008). Numerical analysis of the thermal behavior of a shell-and-tube heat storage unit using phase change materials. Appl. Math. Model., vol. 33, pp. 2132 -2144.

[22] Wakao N, Kaguei S, Funazkri T. Effect of Fluid Dispersion Coefficients on Particle-to-Fluid Heat Transfer Coefficients in Packed Beds. Chem. Eng. Sci. 1979; 34(3):

CHAPTER FOUR: THERMAL STABILITY TESTS OF PCM CANDIDATES

4.1. An Overview

For a particular phase change material, it is essential to determine the maximum temperature it can endure without degrading before utilizing it for thermal energy storage. The operational temperatures of the proposed thermal energy storage system must be lower than the temperature at which the desired PCM will degrade. It is equally important that the thermophysical properties of the desired PCM remain stable for several heating and cooling cycles to facilitate the predictability of the thermal energy storage system in which the PCM is used.

This chapter contains the experimental investigation of the suitability of erythritol, alongside two other PCMs with comparable melting points, as PCMs for a thermal energy storage system designed for a domestic cooking application. Factors considered in the study are thermal stability, cycling stability and health hazard of the PCMs. This research work is contained in research paper 3, which has been submitted for publication in the Renewable Energy journal and it is presently under review.

Elsevier Editorial System(tm) for Renewable Energy

Manuscript Draft

Manuscript Number: RENE-D-16-02432

Title: RAPID THERMAL CYCLING OF THREE PHASE CHANGE MATERIALS (PCMs) FOR COOKING APPLICATIONS

Article Type: Research Paper

Keywords: Phase change materials; thermal stability; cycling stability; acetanilide; meso-erythritol; In48Sn.

Corresponding Author: Mr. ADEDAMOLA BABAJIDE SHOBO, M.Sc.

Corresponding Author's Institution: NORTHWEST UNIVERSITY

First Author: ADEDAMOLA BABAJIDE SHOBO, M.Sc.

Order of Authors: ADEDAMOLA BABAJIDE SHOBO, M.Sc.; ASHMORE MAWIRE, PhD; MARIQUE AUCAMP, PhD

4.2. Research Paper 3:

Rapid thermal cycling of three phase change materials (PCMs) for cooking applications

Shobo A.B.[a] **Mawire A.**[a] **Aucamp M.**[b]

[a] Department of Physics and Electronics, Northwest University (Mafikeng Campus), Private Bag X2046, Mmabatho 2735, South Africa.

[b] Faculty of Health Sciences, Center of Excellence for Pharmaceutical Sciences, Northwest University (Potchefstroom Campus), Private Bag X6001, Potchefstroom 2520, South Africa.

Highlights

- Rapid thermal cycling of acetanilide, meso-erythritol and In-48Sn investigated as PCMs for cooking applications.
- Thermal stability, cycling stability, chemical stability and health hazard of PCMs investigated.
- Acetanilide and meso-erythritol supercooled below temperatures desired for cooking applications.
- Rapid degradation of acetanilide with thermal cycles.
- In-48Sn showed very good promise as a PCM for cooking applications under high rates of heating and cooling.

Abstract

The performances of acetanilide, meso-erythritol and In-48Sn as phase change materials (PCMs) for cooking applications have been investigated under rapid heating and solidification cycles. Thermal stability tests of the PCMs were investigated and also cycling stability with high heating and cooling rates, using simultaneous differential scanning calorimetry (DSC) and thermogravimetric analysis (TGA). Chemical stability of the PCMs after 20 rapid heating and solidification cycles were investigated by infrared spectroscopy. Degrees of health hazard associated with the PCMs were also investigated based on the National Fire Protection Association (NFPA) system. In-48Sn showed greatest thermal stability up to 289.7 ^{o}C with meso-erythritol showing stability up to 177.0 ^{o}C, while acetanilide is thermally stable up to 133.3 ^{o}C. Thermal properties of acetanilide remained within stable limits with rapid thermal cycles but rapid weight degradation was observed. Two forms of meso-erythritol were exhibited with different melting points. The solidification temperature of meso-erythritol also showed considerable variations while the enthalpy of solidification remained reasonably stable. Acetanilide and meso-erythritol exhibited

subcooling below 100 ^{o}C making them undesirable for cooking applications under rapid heating and cooling cycles. The melting temperature, the solidification temperature and enthalpy of melting for In-48Sn are stable over the rapid thermal cycles. With the solidification temperature of In-48Sn above 100 ^{o}C throughout the thermal cycles, it proved to be a promising PCM for cooking applications under rapid heating and cooling cycles. Residues of the PCMs after thermal cycling showed no structural changes as compared with the fresh samples. The health hazards related to the PCMs are all within acceptable limits, though care needs to be taken not to allow acetanilide and In-48Sn into foods.

Keywords: Phase change materials (PCM), thermal stability, cycling stability, acetanilide, meso-erythritol, In48Sn.

4.3. Introduction

The application of phase change materials (PCMs) in latent heat thermal storage systems for the storage of solar thermal energy and waste heat for various temperature applications have been widely explored in the past few years. PCMs in latent heat thermal storage systems have advantages of large energy storage densities due to the large amounts of thermal energy that can be stored and retrieved during their phase change transitions. The solid-liquid phase change transitions of PCMs are particularly of interest due to their great efficiencies and larger enthalpies associated with these transitions [1]. The isothermal/near-isothermal behaviour of PCMs during heat storage or heat retrieval processes is also attractive for some temperature-controlled applications. Therefore, for a particular application, the melting and the solidification temperatures of the PCM to be utilized are of paramount importance. Due to the possibility of the existence of many PCM candidates with phase transition temperatures about the desired temperature application, many other properties need to be considered for the choice of the suitable PCM. These properties include: density, specific heat capacity, latent heat of fusion, thermal conductivity, degree of supercooling, thermal stability, cycling stability, toxicity, degree of health hazard, compatibility with containment material, abundance and cost [2-3].

Studies have recommended that PCMs with melting temperatures higher than 100 ^{o}C should be used in heat storages for efficient cooking applications [4-5]. It is therefore important for cooking applications that the PCM's solidification temperature be higher than 100 ^{o}C. Since cooking of food is a daily routine, the PCM utilized in a thermal storage for this purpose should also exhibit good thermal cycling stability. Particular attention also needs to be paid to

the degree of the health hazard posed by the PCM used in thermal storage systems for cooking applications [3]. The materials considered for this study have been considered due to the fact that their melting temperatures are above 100 ^{o}C.

Acetanilide has been identified by a number of studies as a PCM for latent thermal energy storage systems for temperature applications between 110 ^{o}C and 120 ^{o}C [2, 6-7]. Acetanilide has been utilized as a PCM for heat storage for cooking applications in some published studies [8-9]. El-Sebaii et al. [10] presented a study involving fast thermal cycling of acetanilide for 500 cycles. Results showed that the melting temperature and latent heat of fusion decreased after 500 cycles. They concluded that acetanilide showed good thermal stability and is thus a promising PCM for the storage of solar thermal energy for indoor cooking. The study by El-Sabaii and Al-Agel [11] reported 15 ^{o}C supercooling of acetanilide during 1000 cycles of acetanilide.

Erythritol has also been identified by several studies as a PCM for latent heat thermal energy storage systems for temperature applications between 110 ^{o}C and 120 ^{o}C [12-17]. Sharma et al. [18] utilized erythritol as a heat storage material in a heat storage designed for a cooking application. The study by Kaizawa et al. [13] reported that erythritol began to decompose at 160 ^{o}C and as such its maximum charging temperature for heat storage should be less than 160 ^{o}C. Shukla et al. [19] presented an accelerated thermal cycling test of erythritol and results indicated no degradation of erythritol during 75 thermal cycles while the degree supercooling of 15 ^{o}C was observed.

In-48Sn is an alloy of indium and tin with a composition of 52 % Indium and 48 % tin by weight. It is commonly used as a low melting temperature solder in electronic circuit construction. The only application of the alloy as a PCM for heat storage, found in literature, is for heat dissipation in an encapsulation for an electronic module in the invention of Myers et al. [20]. There is no literature presenting the thermal and cycling stability of this alloy for use as a PCM.

The objective of this paper is to investigate the performances of acetanilide, meso-erythritol and In-48Sn as PCMs for cooking applications under rapid heating and cooling conditions.

4.4. Materials and methods

4.4.1. Materials

The materials investigated in this research are commercial grade acetanilide (purity 98%) purchased from Alfa Aeser GmbH & Co.KG, Germany [21]. Commercial grade meso-erythritol (purity 99.92%) was purchased from J&K scientific, China [22] and the commercial grade In-48Sn ingot (purity 99.9%) was purchased from The Indium corporation of America, U.S.A [23]. The melting temperature and density of the acetanilide sample as indicated by the manufacturer is 113 - 116 ^{o}C and 1210 kg/m^{3} respectively. The meso-erythritol sample is indicated by the manufacturer to have a melting temperature range of 118 ^{o}C - 122 ^{o}C and the density of erythritol is 1480 kg/m^{3} at 20 ^{o}C and 1300 kg/m^{3} at 140 ^{o}C as reported in literature [16]. The In-48Sn alloy is indicated by the manufacturer to have a melting temperature of 118 ^{o}C and a density of 7300 kg/m^{3}.

4.4.2. Methods

Tests of thermal and cycling stability were conducted on the SDT Q600 simultaneous thermal analyzer (TA instrument, Delaware, USA), which is a dual purpose thermogravimetric analyzer (TGA) and a differential scanning calorimeter (DSC). It thus measures simultaneously weight changes and heat flow in a material with respect to temperature and time, under a controlled atmosphere. Thermal stability tests of the PCMs were done with a heating rate of 10 ^{o}C/min in open, 90 µl alumina pans under a 50 ml/min flow of nitrogen. For the test of cycling stability, each PCM sample was subjected to 20 rapid heating/cooling rates at 20 ^{o}C/min from a temperature below their observed solidification temperature to a temperature below their observed decomposition temperature. The cycling tests were conducted with each PCM sample in 90 µl alumina pans, under a 20 ml/min flow of nitrogen.

The chemical stability of each of the PCM was investigated by comparing infrared spectra obtained before and after the thermal cycling. The spectra were recorded on a Cary 670 FTIR spectrometer (Agilent Technologies, California, USA) from 600 to 4000 cm^{-1}. Spectral acquisitions were done using Essential FTIR v.3.50.083 (Operant LLC, USA).

The degree of health hazard of each material is obtained from the material datasheet provided by the manufacturer of each of the material tested.

4.5. Results and discussions

4.5.1. Thermal stability tests

Fig. 4.1 (a) - (c) shows the DSC-TGA thermograms obtained for acetanilide, meso-erythritol and In-48Sn at a heating rate of 10 ^{o}C/min. Decomposition of acetanilide was observed to commence at about 133.3 ^{o}C which is taken as the point where the curve for the first derivative of weight with temperature begins to rise (Fig. 4.1(a)). This indicates that the maximum charging temperature for acetanilide as a PCM for thermal storage should be below 133.3 ^{o}C. Decomposition of meso-erythritol is observed at about 177.0 ^{o}C (Fig. 4.1 (b)); therefore the maximum charging temperature of meso-erythritol should be kept below 177.0 ^{o}C. There is an initial weight loss in the In-48Sn sample from the start of heating which is thought to be due to some volatile impurities in the sample.

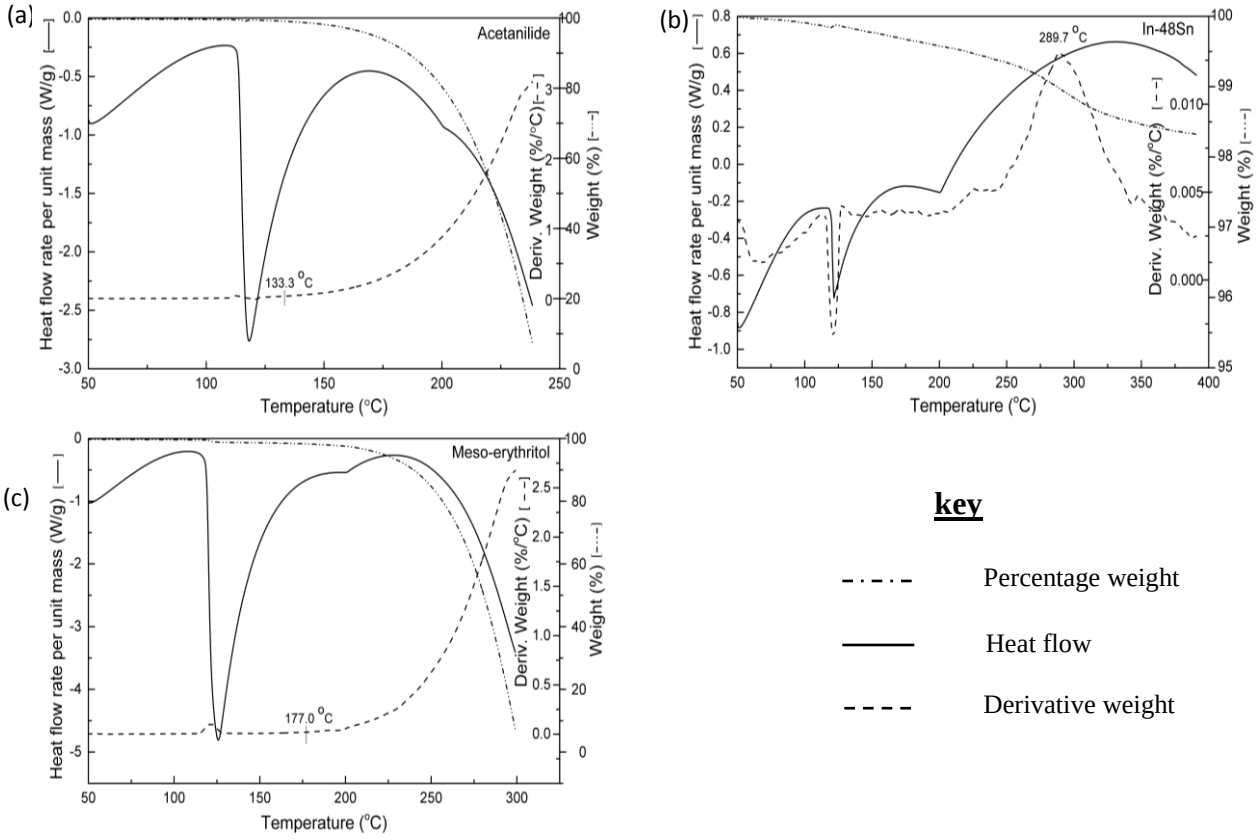

Fig. 4.1. TGA-DSC thermograms of (a) acetanilide, (b) meso-erythritol and (c) In-48Sn at a heating rate of 10 ^{o}C/min.

However, decomposition of In-48Sn is noticed at about 289.7 ^{o}C, where the first derivative of the weight with respect to temperature shows a peak. For effectiveness, the maximum charging temperature of In-48Sn should be kept below 289.7 ^{o}C. In-48Sn shows very little decomposition of about 1.67 % at about 389.0 ^{o}C while acetanilide and meso-erythritol show

decomposition of 92.64 % and 92.58 % at 238.3 ^{o}C and 299.0 ^{o}C respectively. In-48Sn therefore shows the greatest thermal stability followed by meso-erythritol and lastly acetanilide.

4.5.2. Thermal cycling tests - DSC

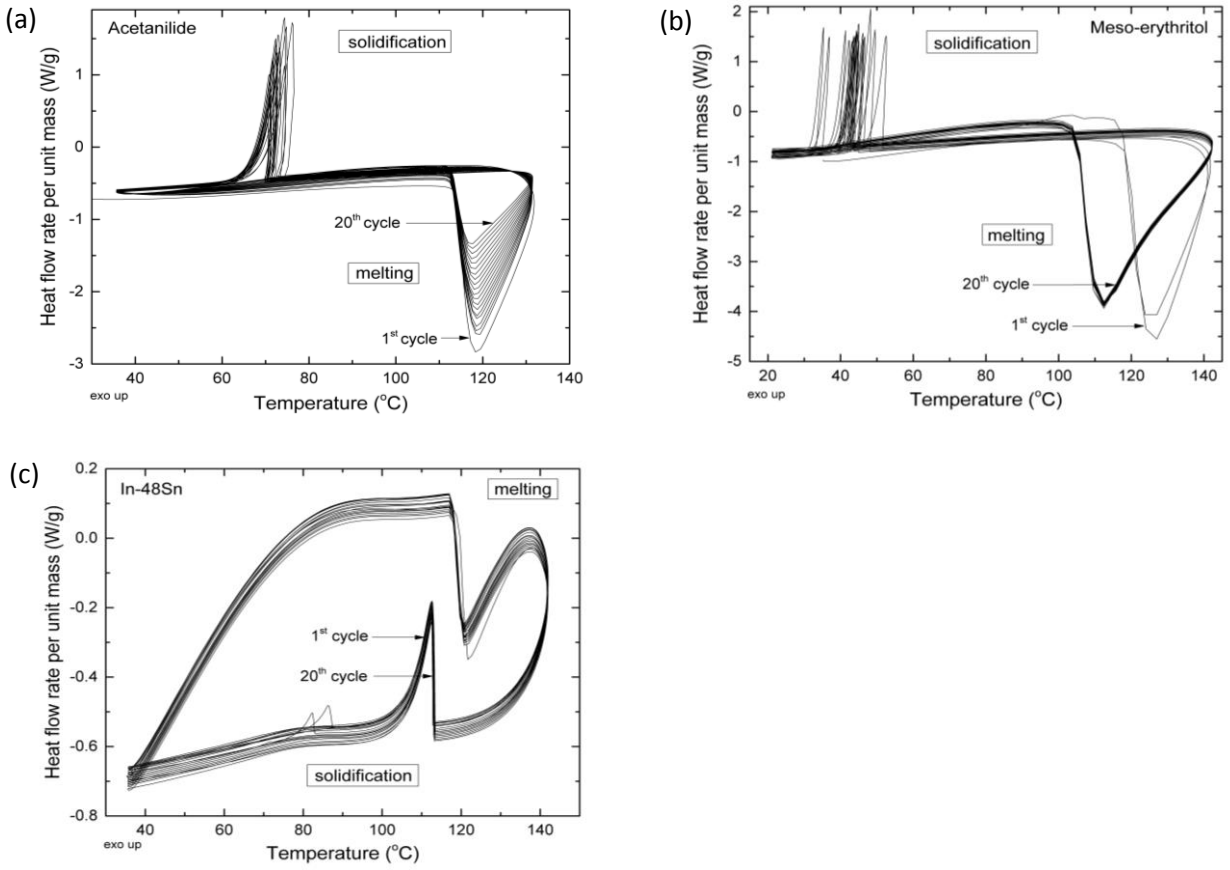

Fig. 4.2. DSC thermograms of (a) acetanilide, (b) meso-erythritol and (c) In-48Sn alloy for 20 heating and solidification cycles at heating/cooling rates of 20 ^{o}C/min.

The DSC heat flow thermograms obtained for the cycling stability tests for acetanilide, meso-erythritol and In-48Sn at heating/cooling rates of 20 ^{o}C/min respectively, are shown in Fig.4.2 (a) - (c). Acetanilide was thermally cycled between 35 ^{o}C and 130 ^{o}C, meso-erythritol between 20 ^{o}C and 140 ^{o}C and In-48Sn between 35 ^{o}C and 140 ^{o}C. The solidification enthalpies of the PCMs for each cycle were obtained by numerical integration of the area under the solidification peak of the weight-corrected heatflow thermograms, using the TA instruments' Universal analysis 2000 software. The melting temperatures (T_m), solidification temperatures (T_s) and solidification enthalpies (ΔH_s) obtained for each of the PCM at each thermal cycle are recorded on Tables 4.1 - 4.3.

Table 4.1. Melting range, solidification range and enthalpy of solidification of acetanilide obtained for each thermal cycle on the DSC.

Cycle No.	T_m (^oC)	T_s (^oC)	ΔH_s (J/g)	Cycle No.	T_m (^oC)	T_s (^oC)	ΔH_s (J/g)
1	113.86 - 118.40	72.79 - 74.39	141.1	**11**	112.97 - 118.30	73.11 - 74.45	142.3
2	112.99 - 118.38	74.50 - 76.31	142.7	**12**	112.97 - 118.19	69.60 - 70.91	139.0
3	112.97 - 118.83	72.90 - 74.81	141.3	**13**	112.95 - 118.19	71.20 - 72.34	140.7
4	112.97 - 118.61	71.20 - 73.05	142.0	**14**	112.95 - 117.87	71.09 - 72.15	140.9
5	112.97 - 118.83	70.56 - 72.36	140.3	**15**	112.96 - 117.76	70.24 - 71.26	140.0
6	112.96 - 118.61	70.77 - 72.48	140.8	**16**	112.93 - 117.98	69.92 - 70.87	140.0
7	112.97 - 118.61	71.73 - 73.35	140.9	**17**	112.97 - 117.66	70.13 - 71.08	139.1
8	112.99 - 118.51	71.20 - 72.71	140.3	**18**	112.93 - 117.66	70.24 - 71.08	138.9
9	112.98 - 118.51	70.24 - 71.69	140.2	**19**	112.94 - 117.44	69.70 - 70.45	139.5
10	112.97 - 118.19	70.56 - 71.86	140.0	**20**	112.93 - 117.12	70.34 - 71.08	140.6

From Table 4.1, the melting onset for acetanilide showed little deviations of between -0.93 ^oC and -0.87 ^oC for subsequent thermal cycles from that observed in cycle 1. The peak melting temperature varied with between -0.43 ^oC and +1.28 ^oC from the value of 118.40 ^oC in cycle 1. The solidification onset for subsequent cycles deviate between -3.19 ^oC and +1.71 ^oC from a value of 72.79 ^oC in cycle 1 while the peak solidification temperature deviated between -3.94 ^oC and +1.92 ^oC from the value in cycle 1. The enthalpy of solidification of acetanilide show deviations between -2.2 J/g and +1.6 J/g from that obtained in cycle 1. The degree of supercooling exhibited by acetanilide is between 43.88 ^oC and 48.59 ^oC through the 20 heating and solidification cycles. The variations of the melting temperature, the solidification temperature and the enthalpy of solidification are minimal and can also be observed on the DSC thermogram (Fig. 4.2 (a)). These variations present no definite trend and therefore are unpredictable within the limits of the thermal cycles. It can therefore be concluded that these thermophysical properties of acetanilide remain within stable limits over several thermal cycles. The same conclusion was reached by El-Sabaii et al. [10].

Table 4.2 shows the values obtained for the melting temperature range, solidification temperature range and solidification enthalpy for meso-erythritol during the heating and solidification cycles. It was observed that melting temperature range made a very big leap from 119.18 ^oC - 125.73 ^oC in the first cycle to 105.05 ^oC - 112.80 ^oC in the second cycle and remained around the same range until the seventeenth cycle when it became 117.81 - 125.10 ^oC. For the eighteenth cycle the melting temperature range again was 105.38 ^oC - 111.68 ^oC

with almost similar results for the remaining cycles. Rapid cooling of erythritol has been reported by Jesus et al. [24], to result in its amorphous form which is metastable with a melting temperature of about 104 ^{o}C. This was reported to be due to an amorphous solid erythritol obtained from melt, bypassing a solid-solid transition when heated again. Once in the metastable state in the second cycle, very little variations in the melting onset of between +0.09 ^{o}C and +0.34 ^{o}C are observed until it slipped briefly into its stable state in cycle 17.

Table 4.2. Melting range, solidification range and enthalpy of solidification of meso-erythritol obtained for each thermal cycle on the DSC.

Cycle No.	T_m (^{o}C)	T_s (^{o}C)	ΔH_s (J/g)	Cycle No.	T_m (^{o}C)	T_s (^{o}C)	ΔH_s (J/g)
1	119.18 - 125.73	32.98 - 35.36	213.1	**11**	105.37 - 111.90	43.43 - 44.87	218.9
2	105.05 - 112.80	34.85 - 36.91	216.5	**12**	105.34 - 111.85	42.18 - 43.64	217.2
3	105.14 - 112.67	40.69 - 42.35	219.8	**13**	105.37 - 111.93	39.70 - 41.42	212.0
4	105.21- 112.55	42.56 - 44.16	221.8	**14**	105.36 - 111.93	41.81 - 43.20	214.9
5	105.28 - 112.30	44.55 - 46.18	223.6	**15**	105.39 - 111.93	51.38 - 52.55	228.1
6	105.31 - 112.18	46.41 - 48.41	224.4	**16**	105.39 - 111.68	43.68 - 45.03	216.8
7	105.36 - 112.05	42.93 - 44.45	220.4	**17**	117.81 - 125.10	48.03 - 49.55	223.0
8	105.32 - 112.05	42.43 - 43.98	218.0	**18**	105.38 - 111.68	44.79 - 46.33	218.3
9	105.34 - 112.18	45.29 - 46.64	221.2	**19**	105.37 - 111.93	36.84 - 37.85	208.4
10	105.35 - 112.18	43.05 - 45.02	219.0	**20**	105.36 - 111.80	46.16 - 47.29	221.3

Likewise, little variations in the melting peaks of between -1 ^{o}C and -0.75 ^{o}C were observed in the metastable state from cycle 2 with the exception of cycle 17. The variation of the solidification onset and peak from the cycle 1 to cycle 2 is not as large as that noticeable with the melting temperature. Variations of +1.87 ^{o}C and +1.55 ^{o}C were observed in the solidification onset and peak from cycle 1 and cycle 2 respectively. The solidification onset then oscillates with variations between +1.99 ^{o}C and +16.53 ^{o}C about the value at cycle 2 for subsequent cycles. A similar pattern was observed with the peak melting temperature as well, with variation of +1.55 ^{o}C from cycle 1 to cycle 2 and variations between +0.94 ^{o}C and +15.64 ^{o}C about the value at cycle 2 for subsequent cycles. These variations in the solidification temperature range are responsible for the scattered solidification peaks noticeable on the DSC thermogram (Fig. 4.2 (b)). Meso-erythritol exhibits large degrees of supercooling between 92.75 ^{o}C and 60.55 ^{o}C as observed during the 20 heating and solidification cycles. Variations in the solidification enthalpy are between -4.7 J/g and +15

J/g. There is no clear effect of the switch between the stable state to the metastable state on the solidification enthalpy.

Table 4.3. Melting range, solidification range and enthalpy of solidification of In-48Sn obtained for each thermal cycle on the DSC.

Cycle No.	T_m (^oC)	T_s (^oC)	ΔH_s (J/g)	Cycle No.	T_m (^oC)	T_s (^oC)	ΔH_s (J/g)
1	117.65 - 121.74	112.98 - 112.47	22.8	**11**	117.27 - 120.77	113.28 - 112.77	21.3
2	117.27 - 120.26	112.80 - 112.46	21.5	**12**	117.40 - 120.75	113.12 - 112.63	21.3
3	117.15 - 120.31	112.92 - 112.58	21.6	**13**	117.02 - 120.77	113.43 - 112.85	21.1
4	117.27 - 120.28	112.92 - 112.68	21.4	**14**	117.27 - 120.91	113.08 - 112.58	21.0
5	117.27 - 120.29	112.92 - 112.60	22.1	**15**	117.27 - 120.92	113.24 - 112.67	20.9
6	117.40 - 120.48	113.42 - 112.87	21.1	**16**	117.15 - 120.90	113.10 - 112.53	21.4
7	117.40 - 120.46	113.29 - 112.89	21.3	**17**	117.27 - 120.93	113.16 - 112.61	21.3
8	117.40 - 120.62	113.29 - 112.88	21.3	**18**	117.40 - 120.96	113.07 - 112.56	21.3
9	118.05 - 120.60	113.42 - 112.85	21.4	**19**	117.40 - 120.77	113.17 - 112.65	21.2
10	117.40 - 120.63	113.32 - 112.83	21.2	**20**	117.40 - 120.78	113.07 - 112.54	21.2

Table 4.3 shows the values obtained for the melting temperature range, solidification temperature range and solidification enthalpy for In-48Sn during the heating and solidification cycles. Deviations between -0.63 ^oC and +0.4 ^oC are observed on the onset of melting in the subsequent cycles from that in cycle 1. The melting peaks varied between -1.48 ^oC and -0.81 ^oC in subsequent cycles from the value observed in cycle 1. The solidification onset in subsequent cycles deviated between -0.18 ^oC and +0.45 ^oC from the value observed in cycle 1. The solidification peaks deviated between -0.01 ^oC and +0.42 ^oC in subsequent cycles from that observed in cycle 1. The degree of supercooling exhibited by In-48Sn in all the cycles varies between 7.06 ^oC and 8.76 ^oC. Deviation of the value of the enthalpy of solidification for In-48Sn in subsequent cycles compared to that in cycle 1 is between -2.0 J/g and -0.7 J/g. It can be observed that the melting temperature range, solidification temperature range and solidification enthalpy of In-48Sn are very stable over several heating/solidification cycles.

4.5.3. Thermal cycling tests - TGA

Table 4.4 shows the results obtained from simultaneous TGA with the thermal cycling of acetanilide, meso-erythritol and In-48Sn. Though the maximum heating temperature for each PCM was kept below its earlier observed decomposition temperature, acetanilide showed an

Table 4.4. Percentage of initial weight of acetanilide, meso-erythritol and In-48Sn left after each thermal cycle.

Cycle No.	Acetanilide % weight	Erythritol % weight	In-48Sn % weight
1	96.57	98.63	99.66
2	93.66	98.46	99.57
3	90.64	98.34	99.51
4	87.76	98.14	99.46
5	85.07	97.99	99.41
6	82.03	97.83	99.37
7	79.20	97.62	99.37
8	76.09	97.46	99.31
9	73.20	97.29	99.27
10	70.30	97.29	99.23
11	67.31	96.96	99.19
12	64.39	96.75	99.15
13	61.45	96.54	99.12
14	58.50	96.32	99.10
15	55.56	96.11	99.08
16	52.69	95.93	99.06
17	49.78	95.75	99.04
18	46.91	95.58	99.03
19	44.03	95.44	99.02
20	41.17	95.28	99.01

almost constant rapid rate of degrading per cycle. After 20 cycles, only 41.17 % of the original weight of the acetanilide sample was left. Meso-erythritol showed a slower rate of degrading per cycle, with 95.28 % of the original weight of the sample left after 20 thermal cycles. The best performance was shown by In-48Sn with 99.01 % of its original weight remaining after the thermal cycles.

4.5.4. Chemical stability

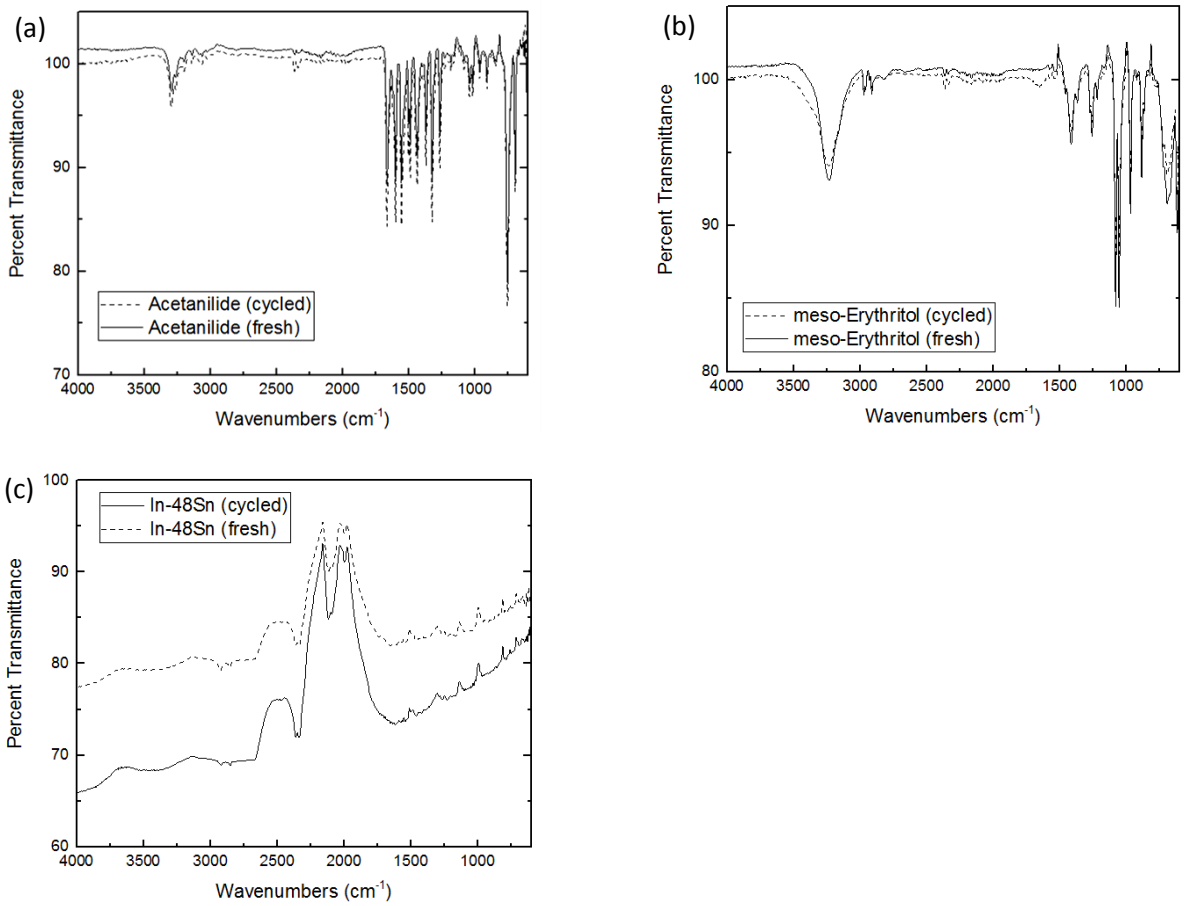

Fig. 4.3. Infrared spectra obtained for fresh and cycled samples of (a) acetanilide, (b) meso-erythritol and (c) In-48Sn.

In order to investigate the chemical stabilities of the PCMs in this study, the FT-IR spectra of three PCMs were obtained prior to and after the 20 thermal cycles. Fig. 4.3 (a) - (c) shows the infrared spectra obtained for the fresh and the residue of each PCM after the thermal cycles. The infrared spectrum obtained before thermal cycling show similar peak profiles with that obtained from the fresh sample for each of the PCM. This is an indication that the residue of each PCM, after thermal cycling, possesses the same chemical structure as original material. It should be pointed out that the metastability exhibited by meso-erythritol was not observable from the spectra obtained from the meso-erythritol residue as it might have gone into its stable crystalline form due to the time lag in transferring the residue from the DSC equipment to the FT-IR equipment.

4.5.5. Health hazard

Table 4.5. NFPA health hazard ratings for acetanilide, meso-erythritol and In-48Sn.

PCM	Health hazard (NFPA)
Acetanilide	2 [22]
Meso-erythritol	1 [23]
In-48Sn	2 [24]

Table 4.5 shows the health hazard ratings for acetanilide, meso-eryrhtritol and In-48Sn according to the National Fire Protection Association (NFPA) rating system. The NFPA 704 blue diamond is a standard system for identification of health hazards of materials for emergency response. The grading is from 0 to 4, where 0 indicates substances that present very minimal hazards to health and 4, substances that could cause severe hazard or death with short exposure. Acetanilide and In-48Sn possess ratings of 2 which indicates a risk of incapacitation or residual injury during long exposure without any medical attention. Meso-erythritol, however, presents a low rating of 1 which indicates risk of irritation upon exposure with only minor injuries sustainable even if no medical attention is sought. Health hazard values for the three materials are low and are within acceptable limits for use as PCMs.

4.6. Conclusions

In-48Sn showed greater thermal stability than both acetanilide and meso-erythritol and will be useful in storing sensible heat up to about 289.68 ^{o}C. Though acetanilide and meso-erythritol had large enthalpies of solidification, they exhibited supercooling to temperatures below 100 ^{o}C, therefore they will be undesirable for cooking applications under the conditions of this study. Moreover, very rapid degradation of acetanilide occurred progressively with thermal cycles. Meso-erythritol also exhibited a transition into a metastable form with a lower melting temperature than its stable form, though this change of form showed no evident effect on the enthalpy of solidification. In-48Sn showed very good cycling stability with very little variations in its melting temperature, solidification temperature and solidification enthalpy. The alloy also showed very low degrees of supercooling of between 7.06 ^{o}C and 8.76 ^{o}C and solidification temperatures throughout all the cycles were above 100 ^{o}C. In-48Sn thus is a promising PCM for cooking applications under high rates of heating and cooling. Though In-48Sn possesses a low value of enthalpy of fusion and solidification, it has a large density which will give it a considerable thermal mass. Its thermophysical properties showed very good stability during thermal cycling even at high

rates of heating and cooling. Acetanilide, meso-erythritol and In-48Sn show very good chemical stability after rapid thermal cycles. The degrees of health hazard of the three materials are within acceptable limits.

Acknowledgements

The authors wish to acknowledge the support provided by the Material Science Innovation and Modeling (MaSIM) research focus area, Faculty of Agriculture, Science and Technology, Northwest University, South Africa. The authors also wish to acknowledge the National Research Foundation, South Africa, through the Research Development Grants for Y-rated Researchers (RDYR-Grant number: 95574) and the Incentive Funding for Rated Researchers (IFRR-Grant number: 90638) schemes.

References

[1] Fernandes D, Pitie F, Caceres G, Baeyens J. Thermal energy storage: "How previous findings determine current research priorities". Energy 2012; 39: 246-57.

[2] Sharma A, Tygi VV, Chen CR, Buddhi D. Review on thermal energy storage with phase change materials and application. Renew. Sust. Energ. Rev. 2009; 13: 318-45.

[3] Miro L, Barreneche C, Ferrer G, Sole A, Martorell I. Health hazard, cycling and thermal stability as key parameters when selecting a suitable phase change material (PCM). Thermochim. Acta 627-629 (2016) 39-47.

[4] Sharma SD, Buddhi D, Sawhney RL, Sharma A. Design, development and performance evaluation of a latent heat storage unit for evening cooking in a solar cooker. Energ. Convers. Manage. 2000; 41(14): 1497-508.

[5] Domanski R, El-Sebaii AA, Jaworski M. Cooking during off-sunshine hours using PCMs as storage media. Energy 1995; 20(7): 607-16.

[6] Kenisarin M, Mahkamov K. Solar energy storage using phase change materials. Renew. Sust. Energ. Rev. 2007; 11: 1913-65.

[7] Sharma SD, Sagara K. Latent heat storage materials and systems: A review. Int. J. Green Energy 2005; 2: 1-56.

[8] Saini P, Sharma V, Singh C. Performance evaluation of thermal storage unit based on parabolic dish collector for indoor cooking application. J. Acad. Indus. Res. 2014; 3(7): 304-10.

[9] Choudhari KS, Shende MD. Solar cooker using PCM material. J. Basic Appl. Eng. Res. 2015; 2(17): 1449-53.

[10] El-Sebaii AA, Al-Amir S, Al-Marzouki FM, Faidah AS, Al-Ghamdi AA, Al-Heniti S. Fast thermal cycling of acetanilide and magnesium chloride hexahydrate for indoor solar cooking. Energ. Convers. Manage. 2009; 50: 3104-11.

[11] El-Sabaii AA, Al-Agel F. Fast thermal cycling of acetanilide as a storage material for solar energy applications. ASME. J. Sol. Energy Eng. 2012; 135(2).

[12] Gunasekara SN, Pan R, Chiu JN, Martin V. Polyols as phase change materials for low-grade excess heat storage. Energy Procedia 2014; 61: 664-9.

[13] Kaizawa A, Marouka N, Kawai A, Kamano H, Jozuka T, Senda T, Akiyama T. Thermophysical and heat transfer properties of phase change material candidate for waste heat transportation system. Heat Mass Transfer 2008; 44: 763-9.

[14] Agyenim F, Rhodes M, Knight I. The use of phase change material (PCM) to improve the coefficient of performance of a chiller for meeting domestic cooling in Wales, In: Proceedings of 2nd PALENC conference and 28th AIVC conference on building low energy cooling and advanced technologies in the 21st century, Crete Island, Greece, 2007.

[15] Puupponen S, Mikkola V, Ala-Nissila T, Seppala A. Novel microstructured polyol-polystrene composite for seasonal heat storage. Appl. Energy 2016; 172: 96-106.

[16] Nomura T, Tsubota M, Oya T, Okinaka N, Akiyama T. Heat release performance of direct-contact heat exchanger with erythritol as phase change material. Appl. Therm. Eng. 2013; 61: 28-35.

[17] Kakiuchi H, Yamazaki M, Yabe M, Chihara S, Terunuma Y, Sakata Y, Usami T. A study of Erythritol as phase change material, In: Chemical Engineering and Technology, Royal Institute of Technology. IEA Annex 10-PCMs and chemical reactions for thermal energy storage, second workshop, Sofia, Bulgaria, 1998.

[18] Sharma SD, Iwata T, Kitano H, Sagara K. Thermal performance of a solar cooker based on an evacuated tube solar collector with a PCM storage unit. Sol. Energy 2005; 78: 416-26.

[19] Shukla A, Buddhi D, Sharma SD, Sagara K. Accelerated thermal cycle test of erythritol for latent heat storage application. In: Proceedings of the EM4 Indore workshop IEA ECES IA annex 17, Indore, India, 2003.

[20] Myers B, Chaudhuri AK, Burns JH. Thermally-capacitive phase change encapsulant for electronic devices, US Patent; US20030157342; 2003.

[21] https://www.alfa.com/en/content/msds/USA/A14361.pdf (accessed 11.08.16).

[22] http://www.jk-scientific.com/Product/ProductDetails/4241?categoryid=793 (accessed 11.08.16).

[23] http://www.indium.com/technical-documents/safety-data-sheets/european/ (accessed 12.08.16).

[24] Jesus AJL, Nunes SCC, Silva MR, Beja AM, Redinha JS. Erythritol: Crystal growth from melt, Int. J. Pharm. 2010; 388: 129-135.

CHAPTER FIVE: COMPARISON OF THREE ENCAPSULATED PCMS

5.1. An Overview

In order to understand the packed bed thermal energy storage system, an understanding of the behaviour of an individual capsule of erythritol during the charging and the discharging cycles will provide a useful insight. Therefore in this chapter, the performances of a single capsule of erythritol is considered during charging and discharging cycles, investigating the influences of the HTF flow rate and the HTF temperature. A comparison is also made with similar capsules of acetanilide and an Indium-Tin alloy subjected to the same conditions. The research carried out in this chapter is contained in the attached research paper 5 which has been submitted to the Applied Thermal Engineering journal and it is currently under review.

Manuscript Details

Manuscript number	ATE_2016_1105
Title	EXPERIMENTAL COMPARISON OF THE THERMAL PERFORMANCES OF ACETANILIDE, MESO-ERYTHRITOL AND AN In-Sn ALLOY IN SIMILAR SPHERICAL CAPSULES
Article type	Research Paper

Abstract

The thermal performances of acetanilide, meso-erythritol and an In-Sn alloy, as phase change materials (PCM) for medium temperature applications, inside separate, spherical aluminum capsules is investigated. The average of the radial temperatures in the capsules is used for analyses during the charging and discharging experiments. The influences of the HTF flow rate and temperature during the simultaneous charging of the encapsulated PCMs are investigated. Meso-erythritol shows the greatest charging rates at all HTF flow rates and HTF temperatures considered, followed by the In-Sn alloy and lastly by acetanilide. The influence of HTF flow rate during simultaneous discharge of the encapsulated PCMs is also investigated. Large subcooling exhibited by acetanilide and meso-erythritol greatly reduces the quantity of thermal energy that is useful for the intended application. The In-Sn alloy, due to the very little subcooling it exhibits, discharges the highest quantities of useful thermal energy at all the flow rates.

Keywords	Acetanilide; Indium-Tin; meso-erythritol; spherical encapsulation; phase change material.

Corresponding Author	ADEDAMOLA SHOBO

5.2. Research Paper 4:

Experimental comparison of the thermal performances of acetanilide, meso-erythritol and an In-Sn alloy in similar spherical capsules

A. B. Shobo*, A. Mawire

Department of Physics and Electronics, Northwest University, Private Bag X2046, Mmabatho 2745, South Africa

Abstract

The thermal performances of acetanilide, meso-erythritol and an In-Sn alloy, as phase change materials (PCM) for medium temperature applications, inside separate, spherical aluminum capsules is investigated. The average of the radial temperatures in the capsules is used for analyses during the charging and discharging experiments. The influences of the HTF flow rate and temperature during the simultaneous charging of the encapsulated PCMs are investigated. Meso-erythritol shows the greatest charging rates at all HTF flow rates and HTF temperatures considered, followed by the In-Sn alloy and lastly by acetanilide. The influence of HTF flow rate during simultaneous discharge of the encapsulated PCMs is also investigated. Large subcooling exhibited by acetanilide and meso-erythritol greatly reduces the quantity of thermal energy that is useful for the intended application. The In-Sn alloy, due to the very little subcooling it exhibits, discharges the highest quantities of useful thermal energy at all the flow rates.

Keywords: Acetanilide, Indium-Tin, meso-erythritol, spherical encapsulation, phase change material

5.3. Introduction

Latent heat storage systems have been reported to have an appeal of large thermal energy storage densities and are particularly useful for temperature-controlled heating/cooling. This comes as a result of a large amount of thermal energy stored and released in the form of latent heat during the solid-liquid phase transition of phase change materials (PCMs) [1]. The melting and solidification temperatures of PCMs govern the operating principle of latent heat storage systems [2]. As there may be more than one PCM with phase change temperatures in the required range, other properties of the PCM to consider are the values of specific heat, latent heat, density and thermal conductivity, congruency of melting, exhibition of sub-

cooling, chemical stability, compatibility with the containment material, abundance and cost [3].Various studies have identified the major drawbacks of most PCMs as their low thermal conductivities, exhibition of sub-cooling and phase segregation [4]. Low thermal conductivity of a PCM will lengthen the charging and the discharging times of a latent heat storage system thus, reducing the overall efficiency of the storage system in which it is utilized. The sub-cooling phenomenon may reduce the latent heat efficiency of the system as the PCM cools to a temperature lower than its melting point and then the temperature increases by some degrees as the PCM starts to solidify, releasing latent heat in the process [5]. Severe sub-cooling of a PCM may therefore hinder its use for temperature-controlled heating. Segregation may also become a problem with PCMs composed of several components as they may not re-combine during the solidification cycle.

Packed bed configurations of latent heat storage systems provide good heat exchange pathways by providing large surface-to-volume ratios for heat exchange between the heat transfer fluid (HTF) and the encapsulated phase change material (EPCM). Apart from the enhancement of thermal conductivity provided by the encapsulation of PCMs, it is also reported to reduce the problem of segregation [4, 6]. Macro-encapsulation of PCMs in spherical containers for packed bed storage systems in particular, has been reported to give a better packing density and thus higher thermal energy storage capacities in thermal storage tanks than other geometries of encapsulation [7]. Moreover, Wei et al. [8] reported that spherical encapsulation gave a better heat transfer performance than plate, cylindrical and tubular encapsulations.

The overall thermal performance of a packed bed heat storage system will apparently be largely influenced by the behaviour of individual constituent EPCMs. Hence, an understanding of the thermal performance of a PCM in an individual capsule of a desired geometry will provide a good prediction of the thermal performance of the thermal storage system in which it is to be utilized. A number of studies have been carried out in order to understand better the thermal behaviour of PCMs in single spherical capsules. ElGhnam et al. [9] reported an experimental study of the freezing and melting of water inside a spherical capsule. Tan et al. [10] presented an experimental and computational study of constrained melting of paraffin wax n-octadecane inside a spherical capsule. Akiyama et al. [11] investigated both numerically and experimentally, the charging and discharging characteristics of some inorganic salts and metals as PCMs for thermal storage with an operational temperature range of 500 K to 1100 K in single spherical capsules. Amin et al.

[12] developed a mathematical relation for the effective thermal conductivity of water in a single spherical capsule.

Erythritol, a sugar alcohol, has been identified and utilized as a PCM for heat storage in a number of studies [13-15]. Acetanilide, also an organic compound, has also been identified and used as a PCM candidate for heat storage applications [16-19].

Risueño et al. [20] suggested the use of metals and metal alloys as PCMs to increase the thermal performances of thermal energy storage systems due to their high density and high thermal conductivity values. The In-Sn alloy considered for this study is a metallic alloy of Indium and Tin with a composition of 51.73 % of Indium and 48.27 % of Tin, commonly used as a lead-free solder. The only application of this alloy as a PCM, found in literature, is for heat dissipation in an encapsulation for an electronic module in the invention of Myers et al. [21].

For a particular range of temperature applications, a careful choice of the PCM is necessary from a wide range of potential PCM candidates with comparable phase change temperatures. The PCMs considered in this study have solid-liquid transition temperatures in the range of 110 - 120 ^{o}C, useful for medium temperature applications. The objective of this study is to compare the charging and discharging characteristics of acetanilide, erythritol and the In-Sn alloy in similar but separate spherical capsules for possible applications in packed bed thermal energy storage systems for medium temperatures. This is with a view to help with the choice of a PCM candidate for use in a packed bed thermal storage system for medium temperature applications.

Nomenclature

c_L	Specific heat capacity of liquid PCM	PCM	Phase change material
c_S	Specific heat capacity of solid PCM	Q_{cum}	Cumulative heat stored in EPCM
EPCM	Encapsulated phase change material	$Q_{cum,dis}$	Cumulative heat discharged from EPCM
f	Melt fraction	T_{av}	Average radial temperature of EPCM
f_s	Solid fraction	T_{ini}	Initial average radial temperature of EPCM
H	Enthalpy of melting	T_{Hot}	Initial average elevated radial temperature of EPCM
HTF	Heat transfer fluid	T_{m1}	Melting onset temperature of PCM
In-Sn	Indium-Tin	T_{m2}	Melting peak temperature of PCM
m_{PCM}	Mass of PCM		

5.4. Materials and experimental methods

5.4.1. Materials

The commercial grade meso-erythritol with a purity of 99 % used in this study was purchased from J & K Scientific, China [22]. The sample of acetanilide with a purity of 98 % used in this study was purchased from Alfa Aesar GmbH & Co. KG, Karlsruhe, Germany [23]. An ingot of the In-Sn alloy (composition: 51.73% In, 48.27% Sn) used in this study was purchased from the Indium Corporation, United States of America [24]. The HTF used is sunflower oil, which was reported by Mawire et al. [25] to give a comparable thermal performance to some commercially available thermal fluids. Aluminum was considered as the capsule material due to its good thermal conductivity, high resistance to corrosion and easy workability during fabrication [26]. A differential scanning calorimeter (SDT Q600, TA Instruments) was used to determine the melting temperatures and melting enthalpies of the three PCMs. The heating rate used was 10 ^{o}C/min while a constant nitrogen flow of 50 ml/min was applied during the measurement. Fig. 5.1 (a) - (c) shows the DSC thermograms obtained for acetanilide, meso-erythritol and the In-Sn alloy respectively. The melting of acetanilide occurred at temperatures between 113.3 - 116.2 ^{o}C with a melting enthalpy of 139.7 J/g, meso-erythritol melted between 118.4 - 122.0 ^{o}C with a melting enthalpy of 310.6 J/g and the In-Sn alloy melted at temperatures between 118.6 - 119.7 ^{o}C with a melting enthalpy of 24.7 J/g. The measured values of the melting temperatures and melting enthalpies obtained from the thermograms, for the three PCMs, as well as some other thermophysical properties are listed on Table 5.1. The specific heat capacities of acetanilide and meso-erythritol were obtained from literature while that of the In-Sn alloy was measured using a differential scanning calorimeter (DSC 204 F1 Phoenix, NETZSCH). The density of the In-Sn alloy at room temperature was obtained by a buoyancy method while densities at other temperatures were obtained from the thermal expansion measurements which were obtained by using a push-rod dilatometer (DIL 402C, NETZSCH). The values of the densities for acetanilide and erythritol were obtained from literature as referenced in Table 5.1.

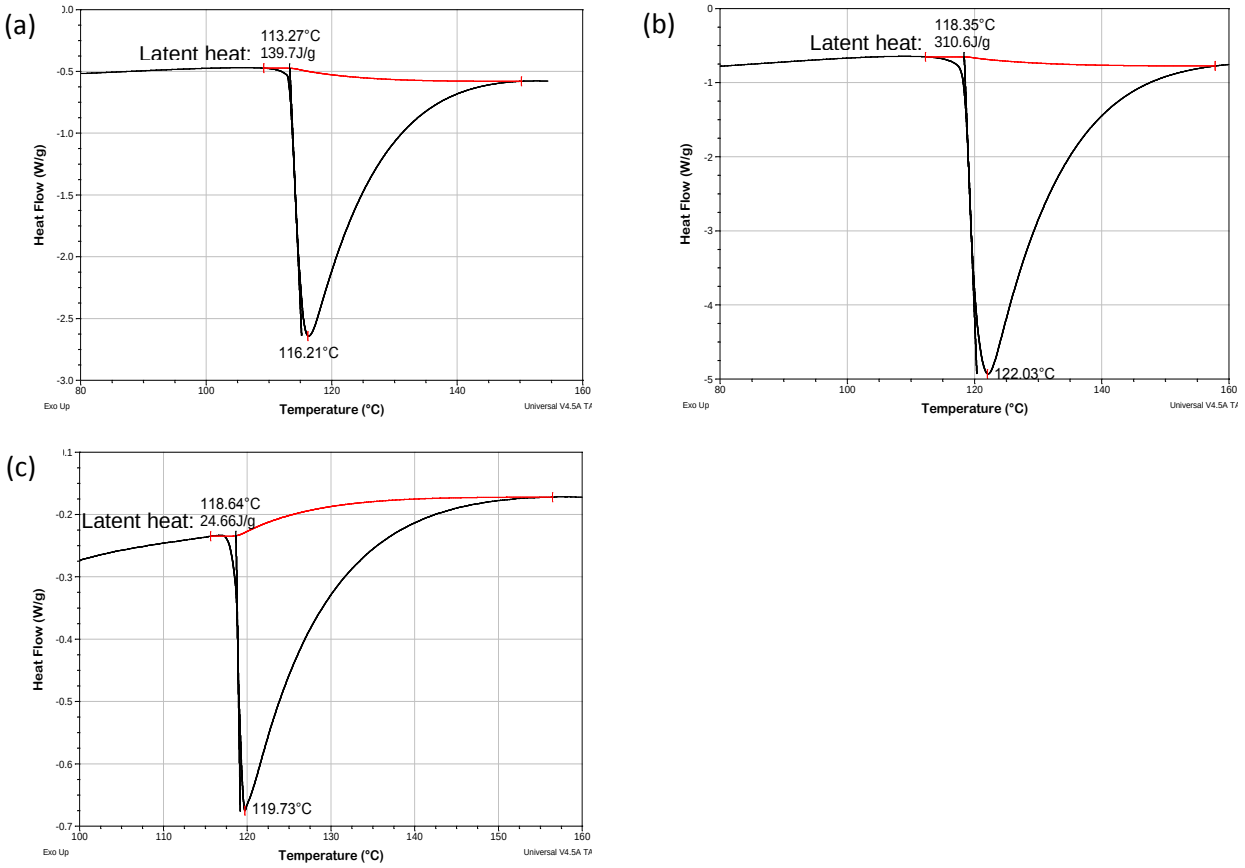

Fig 5.1. DSC thermograms obtained for (a) acetanilide, (b) meso-erythritol and (c) the In-Sn alloy.

Table 5.1. Some thermophysical properties of acetanilide, meso-erythritol and the In-Sn alloy.

Property	**Phase change material**		
	Acetanilide	**Erythritol**	**In-Sn alloy**
Melting temperature (^{o}C)	113.3 - 116.2	118.4 - 122.0	118.6 - 119.7
Specific heat capacity (kJ/kg K)	2.0 [27]	1.38 (20 ^{o}C), 2.76 (140 ^{o}C) [28]	0.229 (20 ^{o}C), 0.416 (120 ^{o}C)
Melting enthalpy (kJ/kg)	139.7	310.6	24.66
Density (kg/m^{3})	1210 [29]	1480 (20 ^{o}C), 1300 (140 ^{o}C) [28]	7270 (20 ^{o}C), 7080 (130 ^{o}C)
Thermal conductivity (W/m K)	0.13 (120 ^{o}C) [30]	2.64 (20 ^{o}C), 1.17 (140 ^{o}C) [28]	40.92 (30 ^{o}C), 62.02 (120 ^{o}C)

5.4.2. Experimental methods

Fig. 5.2 shows a schematic of the experimental set-up consisting of a vertical, cylindrical heat storage tank, a circulation pump (GPA series sliding vane magnetic drive pump, Green-pumps, Padova, Italy) with the frequency controlled by a VLT Micro drive FC 51 (Danfoss A/S, Graasten, Denmark. Maximum error = 0.8 % of full scale), an electric heating unit fitted with a TZN4S temperature controller (Autonics, Illinois, USA. Display accuracy = ± 0.3 %),

a M133P pulse type positive displacement flow meter (MacNaught Pty. Ltd., Sydney, Australia), heat exchanger compartments (temperature control and discharging unit), a data acquisition unit (Agilent 34970A, Keysight Technologies, USA) and a personal computer. The insulated, stainless steel, cylindrical storage tank (a) with a diameter of 12.8 cm is filled with sunflower oil which is pumped around the entire flow line by the circulating pump (b). The volumetric flow rate of the HTF is controlled by the adjusting the frequency of the pump via the microdrive (c) connected to the pump (b).

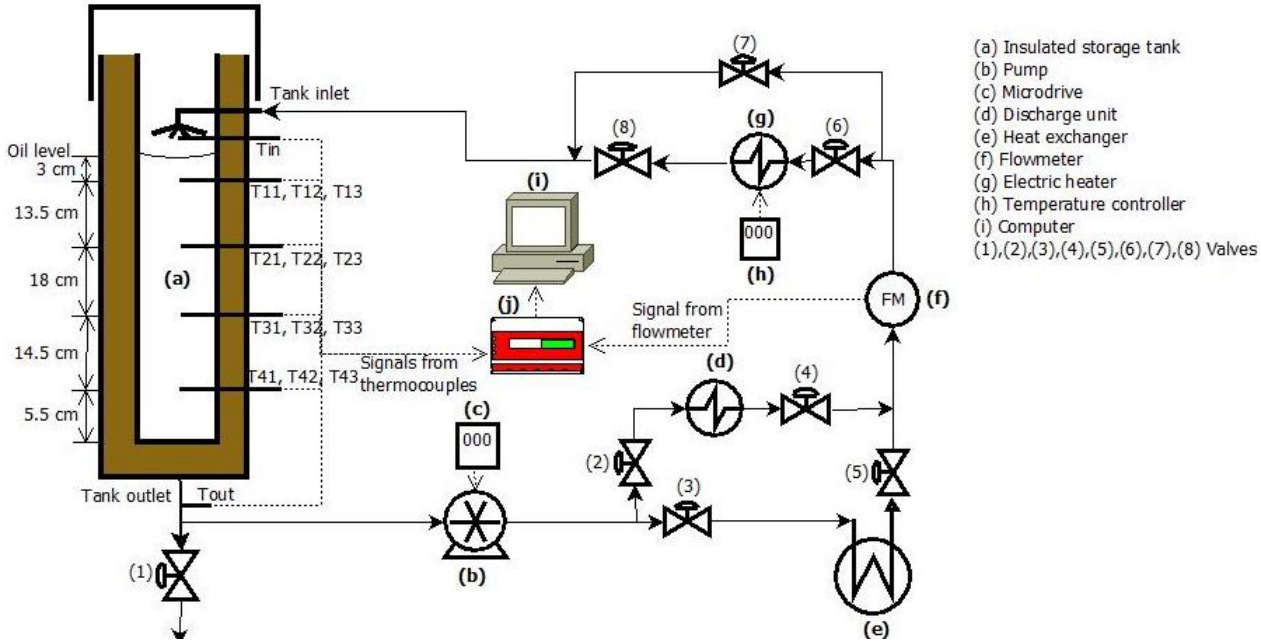

Fig. 5.2. The schematic of the heat storage system utilized for the experiment.

Three K-type thermocouples each at different radial nodes (1.3 cm, 3.8 cm and 6 cm) are at four axial distances in the storage tank as shown in Fig. 5.2. The average temperature measured by the three thermocouples at each level is taken as the HTF temperature at that level. The direction of flow of the HTF is from the top to the bottom of the tank during both charging and discharging cycles. During charging cycles, valves (1), (2), (4) and (7) are closed while valves (3), (5), (6) and (8) are opened. During discharging cycles, valves (1), (3), (5), (6) and (8) are closed while valves (2), (4) and (7) are opened.

Fig. 5.3 (a) shows a photograph of one of the three aluminum spherical capsules fabricated by soldering two hemispheres. One of the half-sphere has a hole punched to accommodate a stainless steel O-ring which is threaded on the inside surface for a screw cap. One K-type thermocouple (T1) is soldered such that it makes good contact with the outside surface of the

sphere. Five other K-type thermocouples (T2, T3, T4, T5, T6) were then inserted through holes punched on the sphere sides and soldered firmly such that their tips lie at different radial distances along a horizontal plane through the center of the sphere as shown in Fig. 5.3(b). The aluminum spheres had diameters of 50 mm and their wall thicknesses were 1 mm. Melted samples of acetanilide, meso-erythritol and the In-Sn alloy were each poured into separate capsules. The molten contents of the capsules were then allowed to cool down to about 20 ^{o}C under a stream of dry air. A stainless steel screw cap with a rubber washer was used to secure the mouth of each capsule. The capsules were then lowered gently into the storage tank and suspended individually with a thread, just below the level of the thermocouples T21, T22 and T23.

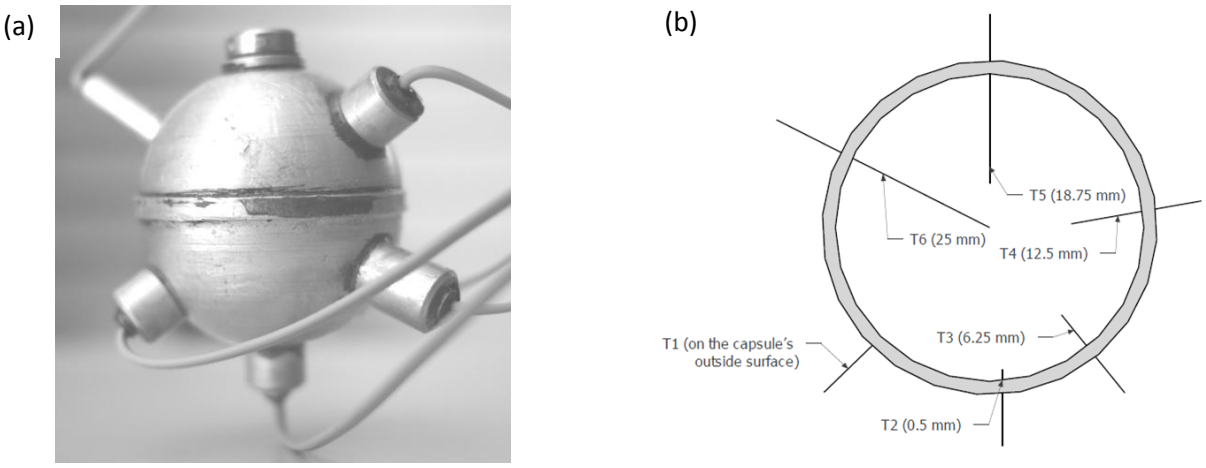

Fig. 5.3. (a) A photograph of one of the aluminum capsules (b) A cross-section of the aluminum capsule showing the positions of the thermocouples.

Thermocouple wires from the capsules and the storage tank were connected to the data acquisition unit. The data acquisition rate was set at 10 seconds. The masses of acetanilide, meso-erythritol and the In-Sn in the capsules were determined to be 10.596 g, 44.526 g and 377.896 g respectively (± 0.001 g for each). It should be noted that the capsules also contained air voids, after the PCMs cooled down, which allowed for volume expansion of the PCMs during melting. To investigate the influence of the HTF flow rate during the charging of the EPCMs, the maximum heater temperature was set at 150 ^{o}C while the average HTF flow rates used were 3 ml/s, 6 ml/s, 9 ml/s and 12 ml/s. The influence of the charging temperature was investigated by charging the EPCMs simultaneously at a flow rate of 9 ml/s, with the maximum heater temperature set at 140 ^{o}C, 150 ^{o}C and 160 ^{o}C. The discharging experiments were performed with HTF flow rates set at 3 ml/s, 6 ml/s 9 ml/s and 12 ml/s respectively.

5.4.3. Method of analysis

The temperature of the PCM in each of the capsule was taken as the average of the temperatures at the five radial nodes (T2, T3, T4, T5, T6). The ranges of the mean absolute deviations of the radial temperatures from the average temperature of the EPCMs at each data point during charging and discharging experiments are given in Table 5.2 below.

Table 5.2. The ranges of the mean absolute deviation of the radial temperatures inside the EPCMs from their average temperatures.

MODE	EPCM	3 ml/s	6 ml/s	9 ml/s	12 ml/s
CHARGING	Acetanilide	0.02 - 0.88 ^{o}C	0.02 - 1.42 ^{o}C	0.01 - 1.31 ^{o}C	0.01 - 1.36 ^{o}C
	Meso-erythritol	0.04 - 1.28 ^{o}C	0.06 - 1.51 ^{o}C	0.04 - 1.71 ^{o}C	0.04 - 1.71 ^{o}C
	In-Sn alloy	0.03 - 0.63 ^{o}C	0.02 - 1.17 ^{o}C	0.02 - 1.31 ^{o}C	0.05 - 1.35 ^{o}C
DISCHARGING	Acetanilide	0.07 - 1.29 ^{o}C	0.09 - 1.77 ^{o}C	0.09 - 1.95 ^{o}C	0.09 - 2.14 ^{o}C
	Meso-erythritol	0.12 - 3.32 ^{o}C	0.16 - 4.41 ^{o}C	0.15 - 4.23 ^{o}C	0.13 - 5.58 ^{o}C
	In-Sn alloy	0.03 - 1.10 ^{o}C	0.02 - 1.42 ^{o}C	0.02 - 1.66 ^{o}C	0.03 - 1.83 ^{o}C

Larger deviations from the average temperatures can be observed with increasing HTF flow rate and also during the discharging cycles. These were caused by the larger thermal gradient across each EPCM due to the faster heat transfer rate to or from the PCM layer closest to the capsule under these conditions. The largest mean absolute deviations were also observed for the average temperatures of meso-erythritol. Though the instantaneous thermal energies calculated may have associated uncertainties, the total energies stored by each PCM should be more accurate thus the relative energies stored by the PCMs should be adequate for the purpose of comparison. The cumulative quantity of heat stored by the PCM in each capsule during charging, at the different stages, was calculated using the following expressions:

Sensible heating before melting commenced,

$$Q_{cum} = m_{PCM} c_S (T_{av} - T_{ini}) \tag{5.1}$$

where m_{PCM} is the mass of the PCM in the capsule, c_S is the specific heat capacity of the solid PCM, T_{av} is the average temperature of the PCM and T_{ini} is the initial average temperature of the PCM at the start of the experiment. During melting,

$$Q_{cum} = m_{PCM} c_S (T_{m1} - T_{ini}) + f m_{PCM} H + f m_{PCM} c_L (T_{av} - T_{m1}) \tag{5.2}$$

where $T_{m1}$is the melting onset temperature, H is the enthalpy of melting, c_L is the specific heat capacity of the liquid PCM and f is the liquid fraction of the PCM in the capsule.

Sensible heating after melting,

$$Q_{cum} = m_{PCM} c_S (T_{m1} - T_{ini}) + m_{PCM} H + m_{PCM} c_L (T_{av} - T_{m2}) \quad (5.3)$$

where $T_{m2}$is the peak melting temperature of the PCM at which melting is completed. T_{m1} and T_{m2} for each PCM were the melting onset and melting peak temperatures obtained from its DSC thermogram (Table 1). The cumulative quantity of thermal energy discharged by the PCM in each capsule was determined, at each stage, by the following equations:

During the discharging of sensible heat until the solidification/nucleation temperature,

$$Q_{cum,dis} = m_{PCM} c_L (T_{Hot} - T_{av}) \quad (5.4)$$

where T_{Hot} is the initial elevated average temperature of the PCM before the commencement of discharging. During solidification,

$$Q_{cum,dis} = m_{PCM} c_L (T_{Hot} - T_{S2}) + f_s m_{PCM} H + (1 - f_s) m_{PCM} c_S (T_{av} - T_{S1}) \quad (5.5)$$

where T_{S1} is the solidification onset temperature as observed from the average temperature history of the PCM, H is the enthalpy of melting of the PCM from Table 1 and f_s is the solid fraction.

During the discharging of sensible heat after the solidification/nucleation temperature,

$$Q_{cum,dis} = m_{PCM} c_L (T_{Hot} - T_{S1}) + m_{PCM} H + m_{PCM} c_S (T_{S2} - T_{av}) \quad (5.6)$$

where T_{S2} is the peak solidification temperature as is observed from the average temperature history of the PCM.

5.5. Results and discussion

5.5.1. Radial thermal distribution in the PCM capsules

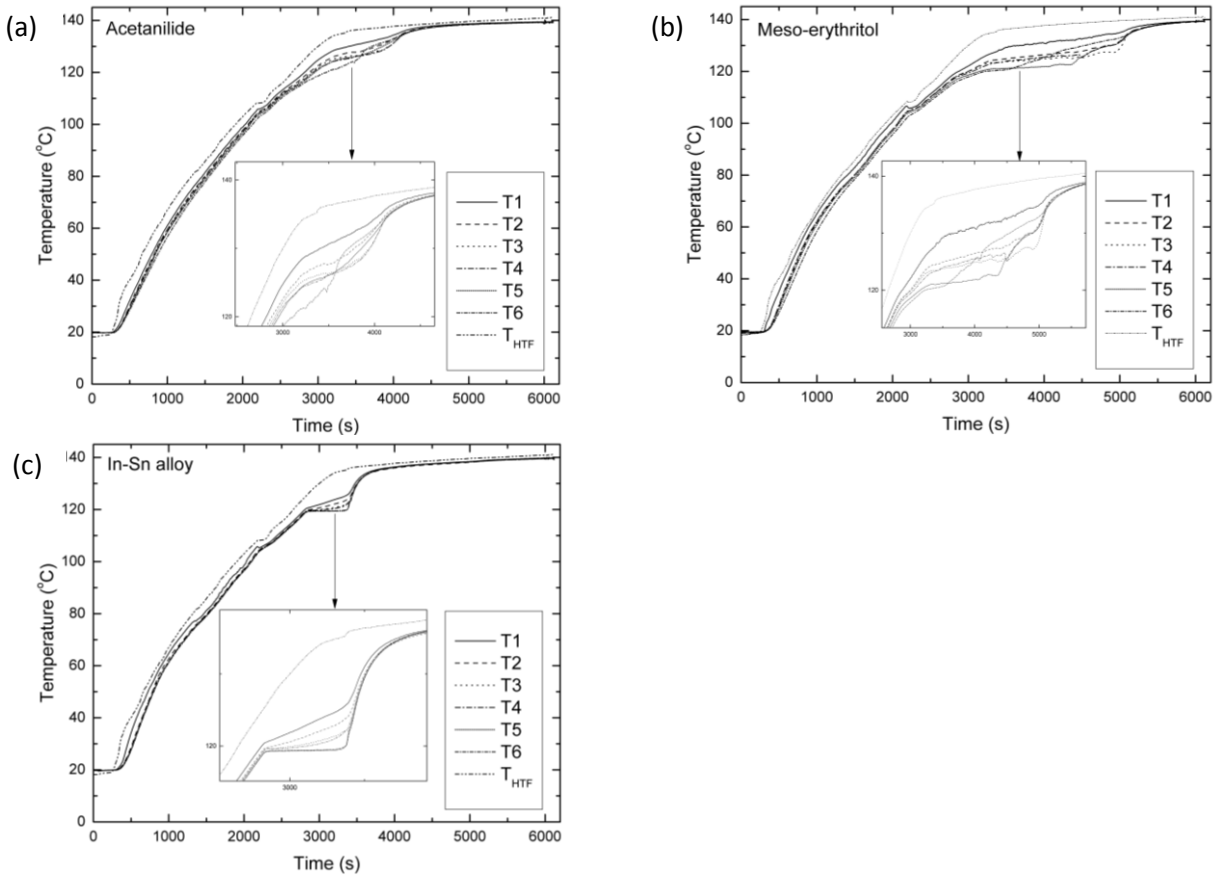

Fig. 5.4. Temperature histories of the HTF, capsules and radial temperatures in the PCM while charging at a flow rate of 9 ml/s with the maximum heater temperature set at 150 ^{o}C for (a) Acetanilide, (b) Erythritol and (c) In-Sn alloy.

To illustrate the temperature distribution across the EPCMs during charging, we consider their temperature histories with the HTF flow rate at 9 ml/s and the heater maximum temperature set at 150 ^{o}C shown in Fig 5.4 (a) - (c). The temperature differential between the HTF and the interior of each of the three EPCMs is dependent on the charging rate of the EPCM. Very minimal radial thermal gradients exist in each of the EPCM due to the size of the capsules which is observable from the closeness of the radial temperatures. Larger thermal gradients in the capsules were only observed during melting of each of the PCM at all the charging flow rates considered even during melting. All the EPCMs melt congruently with the phase change process progressing from the node closest to the capsule wall, to that at the center of the sphere. In both acetanilide and meso-erythritol, the temperature at the central node (T6) is observed to overshoot that of the radial node preceding it (T5) during the phase change (insets).

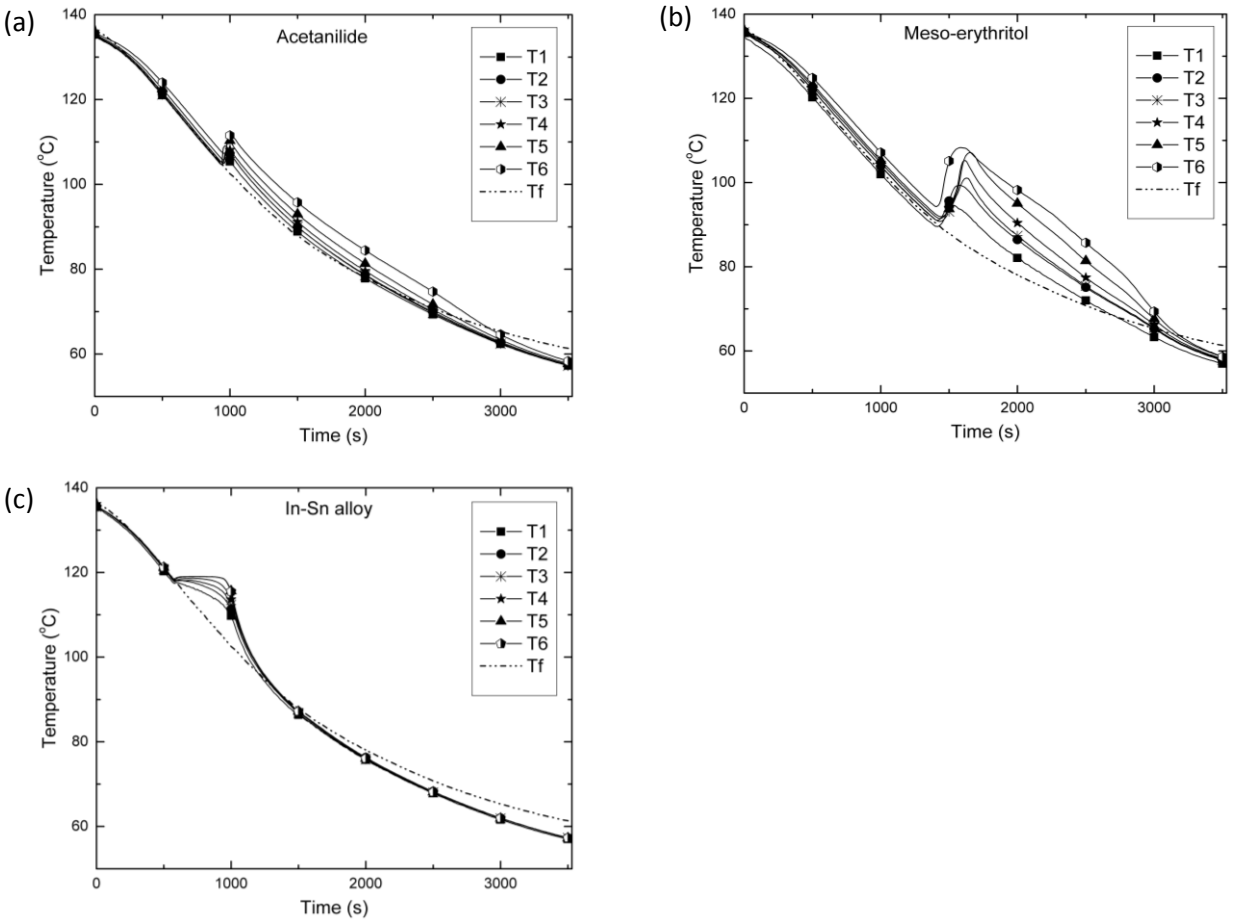

Fig. 5.5. Temperature histories of the HTF, capsules and radial temperatures in the PCM while discharging at flow rate of 9 ml/s for (a) Acetanilide, (b) Erythritol and (c) In-Sn alloy.

This is considered to be due to convection currents set up as a result of buoyancy effects during melting, as a stream of liquid PCM at higher temperature rises to the upper part of the capsule while the solid PCM sinks to the bottom. This is not observed in the curves for the In-Sn alloy indicating that conduction still remains the mode of heat transfer in the alloy. The temperature histories of the HTF, the capsules and the radial temperatures of the PCMs while discharging at an HTF flow rate of 9 ml/s, shown in Fig. 5.5 (a) - (c), can also be used to illustrate the discharging process in each of the PCMs. Meso-erythritol can be observed to possess greater thermal gradients followed by acetanilide and then the In-Sn alloy. The thermal gradients widen during solidification in all the PCMs and gradually thin out as the discharging progressed. The phase change in all the PCMs can be observed to progress from the layer closest to the capsule towards the center of the capsule. The large degrees of subcooling were exhibited in meso-erythritol and then in acetanilide, while very small degrees of subcooling can be noticed from all the nodal temperature histories of the In-Sn alloy. This indicates that the amount of energy required to rearrange the molecules of meso-

erythritol in its solid crystalline structure is the highest followed by that required for acetanilide and finally that for the In-Sn alloy.

5.5.2. Influence of HTF flow rate during charging

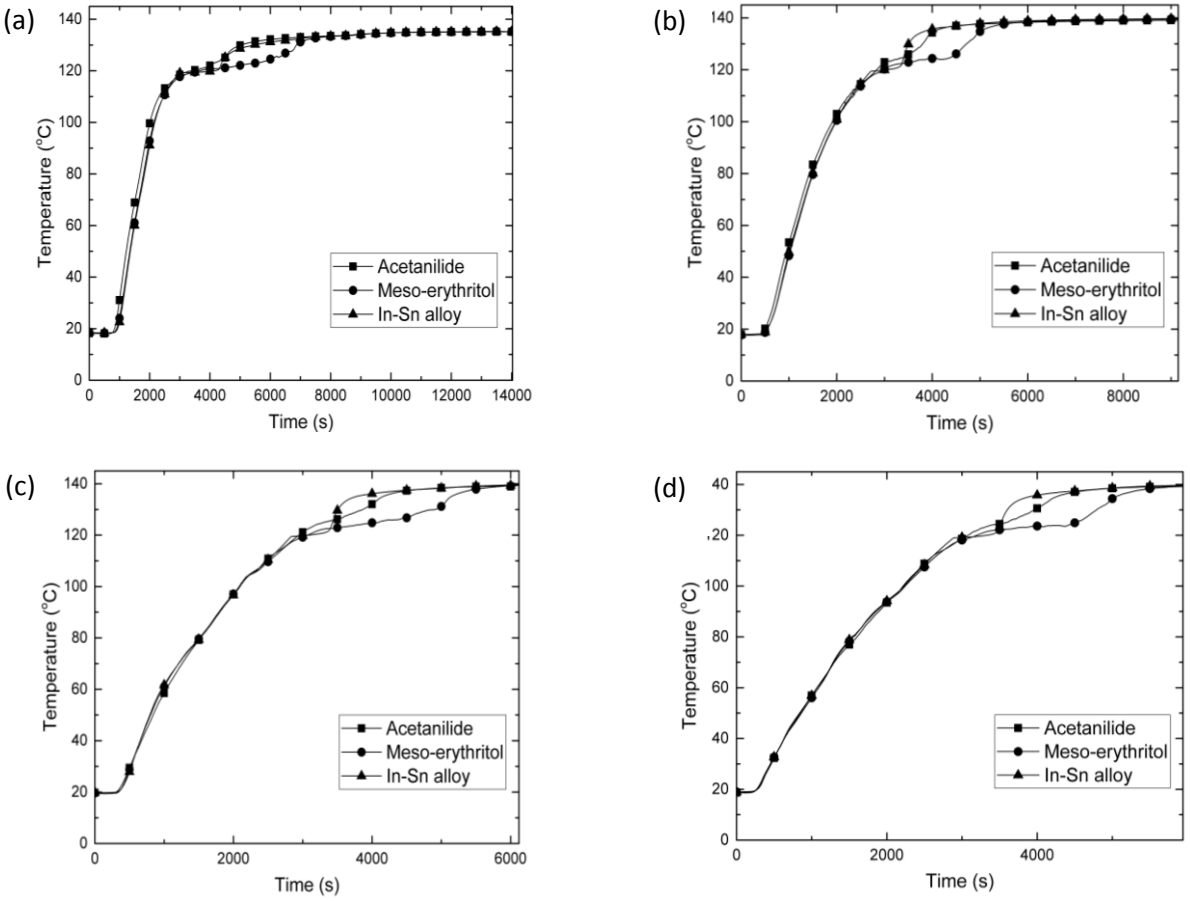

Fig. 5.6. Average temperature histories of the EPCMs while charging with HTF flow rate of (a) 3 ml/s, (b) 6 ml/s, (c) 9 ml/s and (d) 12 ml/s.

The average temperature histories of the EPCMs are shown in Fig. 5.6 (a) - (d) with the heater temperature set to a maximum of 150 ^{o}C and at HTF flow rates of 3 ml/s, 6 ml/s, 9 ml/s and 12 ml/s respectively. The temperature responses of the EPCMs showed almost similar behaviours from the beginning of charging until around their phase change states. Then after the phase change, the In-Sn alloy showed a faster temperature response due to its small enthalpy of melting, high thermal conductivity and narrow melting range. The temperature response of the alloy is then followed by acetanilide because of its low thermal conductivity and low thermal capacity. Meso-erythritol shows the slowest temperature response during the phase change due to the large melting enthalpy required and its wide melting range. Though the In-Sn alloy presented the largest thermal mass, it possesses the highest thermal diffusivity of the three PCMs. Acetanilide has the lowest thermal diffusivity

but also the lowest thermal capacity, thus it had a quicker temperature response. A comparison of thermal storage rates will give a clearer understanding of the thermal performances of the EPCMs.

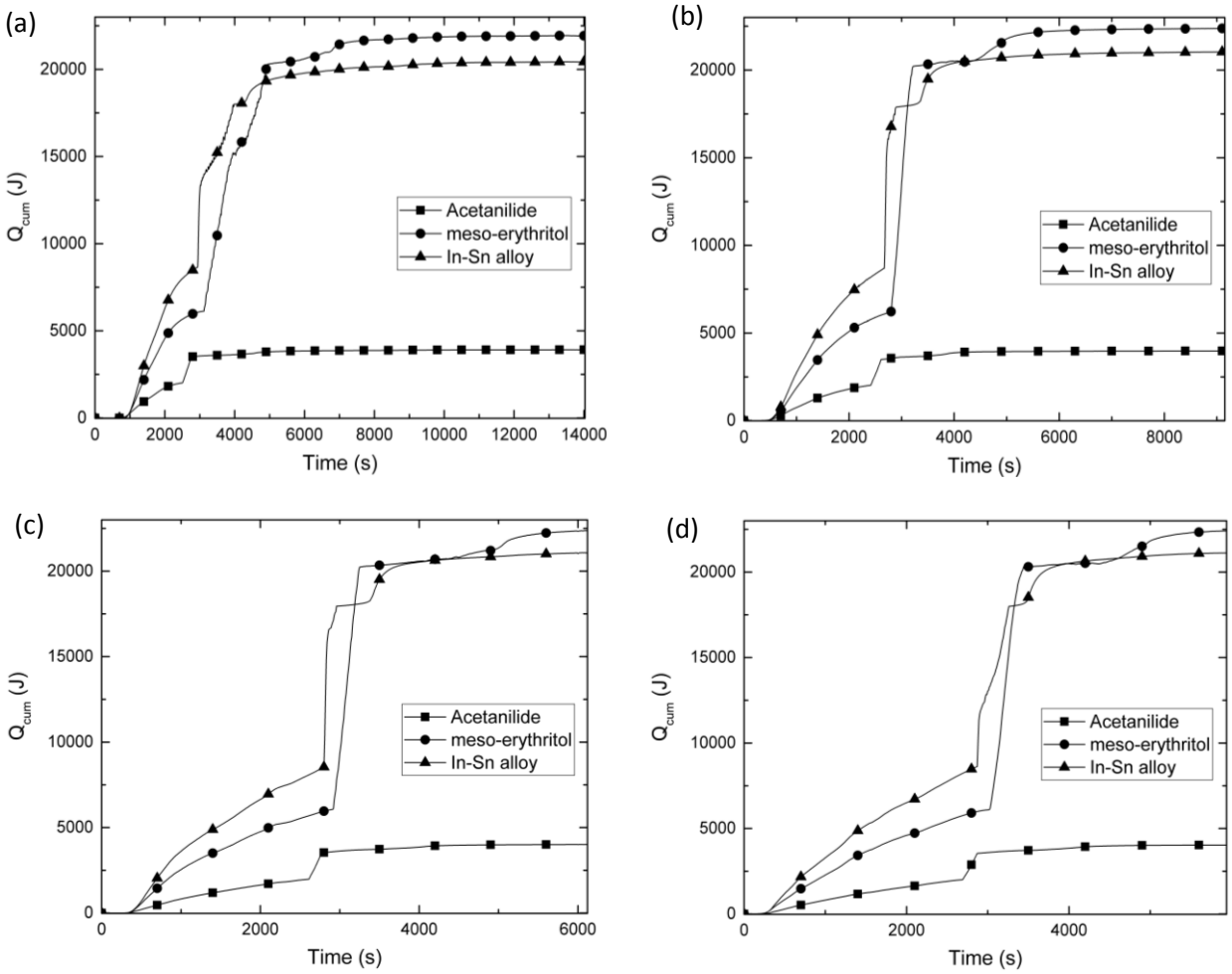

Fig. 5.7. Cumulative energies stored by the EPCM while charging at HTF flow rate of (a) 3 ml/s, (b) 6 ml/s, (c) 9 ml/s and (d) 12 ml/s.

Fig. 5.7 (a) - (d) shows the cumulative energy stored by the three encapsulated PCMs (EPCMs) while charging simultaneously at different HTF flow rates. It can be observed that at all HTF flow rates, the In-Sn alloy initially showed the fastest rates of charging followed by meso-erythritol and lastly by acetanilide. This is due to the fact that there was rapid heat transfer in the In-Sn alloy capsule compared to the others, due to its high thermal diffusivity. The large mass of the In-Sn alloy in the capsule also resulted in a large thermal energy storage density. However, due to the large enthalpy of melting of meso-erythritol, the cumulative quantity of heat stored by meso-erythritol overshot that stored by the In-Sn alloy towards the end of melting at all the flow rates. The almost-vertical parts in all the graphs indicate thermal energy accumulation during the melting of the PCM. Due to the small

thermal mass presented by acetanilide in its capsule, the least quantity of thermal energy was stored by this PCM. The charging rates of each of the EPCMs, at each of the HTF charging flow rate considered, are listed in Table 5.3. Meso-erythritol showed the highest rates of thermal energy accumulation at all flow rates, followed by the In-Sn alloy and lastly by acetanilide. It can also be observed that the average charging rate of each of the EPCM increased with an increase in the HTF flow rate thus, implying a decrease in the charging times.

Table 5.3. Average charging rates of the encapsulated PCM at the different HTF charging flow rates.

EPCM	Average charging rate (J/s) at different HTF flow rates			
	3 ml/s	**6 ml/s**	**9 ml/s**	**12 ml/s**
Acetanilide	0.28	0.44	0.66	0.68
Meso-erythritol	1.56	2.45	3.66	3.77
In-Sn alloy	1.46	2.30	3.44	3.56

5.5.3. Influence of the charging temperature

The implication of the set maximum temperature of the heater is the temperature attained by the HTF, which also determines the amount of thermal energy available for transfer into the PCM capsules. Fig. 5.8 (a) - (c) shows the temperature and cumulative energy histories of the EPCMs while charging at a flow rate of 9 ml/s with the maximum heater temperature set at 140 ^{o}C, 150 ^{o}C and 160 ^{o}C respectively, for 6120 s. The three EPCMs showed almost similar temperature responses from the beginning of the experiment until about 121 ^{o}C when the In-Sn alloy, being more thermally diffusive, showed a faster temperature response. Acetanilide showed a lower temperature response compared to the alloy due to its lower thermal diffusivity. Meso-erythritol at this point is still in its phase transition and can be observed to be storing more thermal energy than the alloy. The same pattern is observed for all the charging temperatures considered. The cumulative energy stored at all the heater's set temperatures showed the In-Sn alloy with highest charging rate from the beginning of the experiment due to its large thermal diffusivity and large thermal mass.

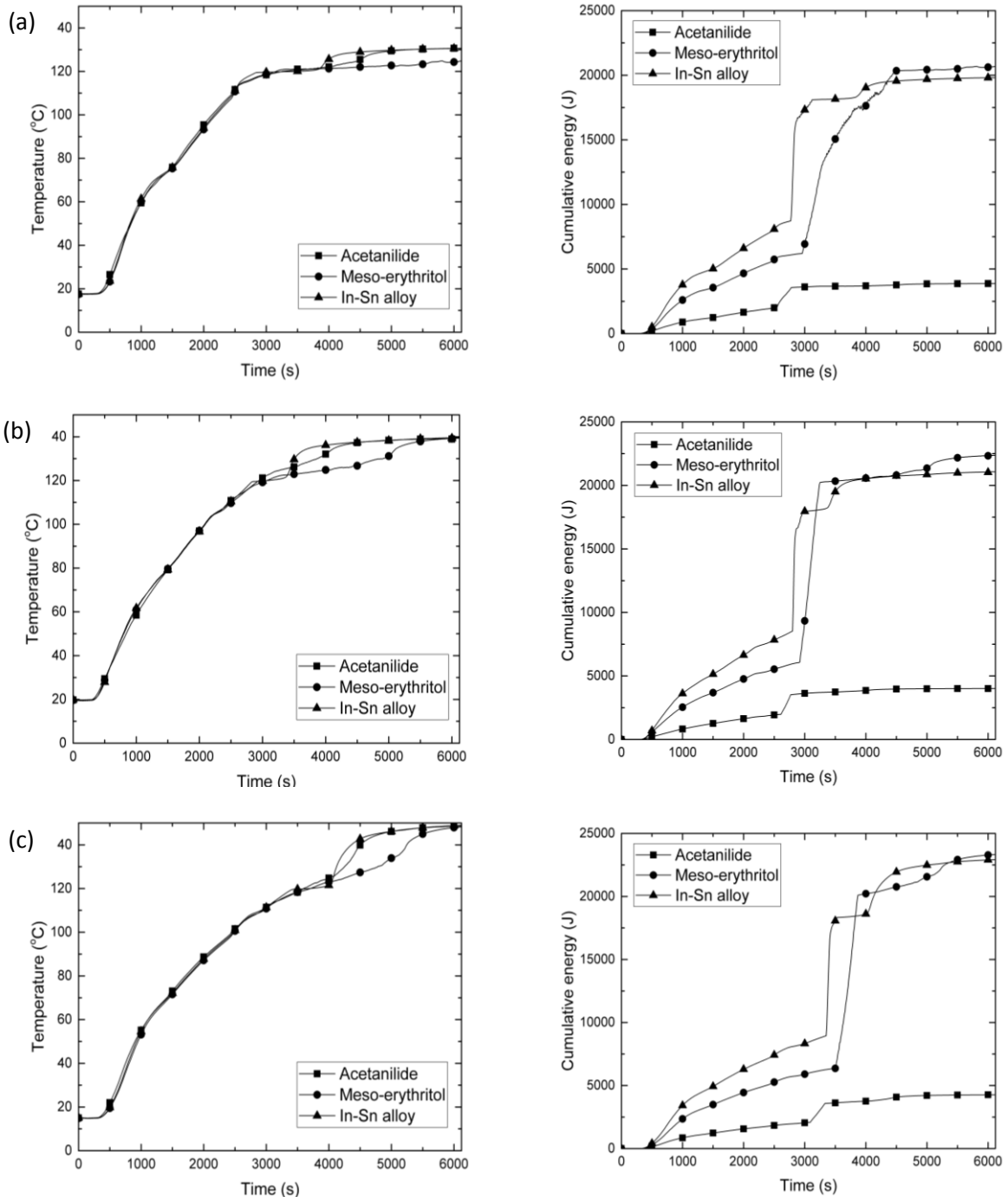

Fig. 5.8. Temperature histories and the corresponding cumulative energy stored by the EPCMs with HTF flow rate of 9 ml/s while charging for 6120 s with heater maximum temperature set at (a) 140 ^{o}C, (b) 150 ^{o}C and (d) 160 ^{o}C.

However, meso-erythritol eventually achieved a higher rate of energy accumulation than the alloy at the end of the charging experiments due to its large melting enthalpy. The lowest charging rates were exhibited by acetanilide due to its small mass in the capsule. The obvious influence of the charging temperatures is on the final temperature attained by the EPCMs and also on the charging rate. An increase in the charging temperature led to an increase in the maximum temperature attained by the EPCMs and also to an increase in the charging rate due

to a larger thermal gradient between the HTF and the EPCM. The results are summarized in Table 5.4 and it shows that meso-erythritol has the highest charging rates followed closely by the In-Sn alloy and then by acetanilide.

Table 5.4. The average charging rate of the EPCMs when charged with HTF flow rate of 9 ml/s and at different set heater temperatures.

EPCM	Average charging rate (J/s)		
	140 ^{o}C	**150 ^{o}C**	**160 ^{o}C**
Acetanilide	0.63	0.66	0.70
Meso-erythritol	3.38	3.66	3.81
In-Sn alloy	3.24	3.44	3.75

When the heater temperature changed from 140 ^{o}C to 150 ^{o}C, the percentage increase in the average charging rate for acetanilide was 4.76 %, for meso-erythritol it was 8.28 % and for the In-Sn alloy it was 6.17 %. When the temperature increased from 150 ^{o}C to 160 ^{o}C, the percentage increase in the average charging rate was 6.06 % for acetanilide, 4.10 % for meso-erythritol and 9.01 % for the In-Sn alloy. The greater thermal gradients between the HTF and the EPCMs, with an increase in the HTF temperature, obviously increased the rate of heat transfer into each of the EPCMs.

5.5.4. Influence of HTF flow rate during discharging

Fig. 5.9 (a) - (d) shows the average temperature histories of the EPCMs while discharging with the HTF flow rates at 3 ml/s, 6 ml/s, 9 ml/s and 12 ml/s respectively. The discharging times can be observed to reduce with an increase in the HTF flow rate which is shown by the increasing discharging rate. The In-Sn alloy shows very little degrees of subcooling at all the flow rates while acetanilide and meso-erythritol show varying degrees of subcooling. The rates of thermal energy discharged from the EPCMs at the different flow rates can be seen in Fig. 5.10 with the observed phase transition temperatures for each EPCM indicated in each case. Meso-erythritol showed a slightly higher discharging rate from the beginning of discharging at all the flow rates but it was overtaken at about 118 ^{o}C, in each case, by the In-Sn alloy which began releasing its solidification enthalpy.

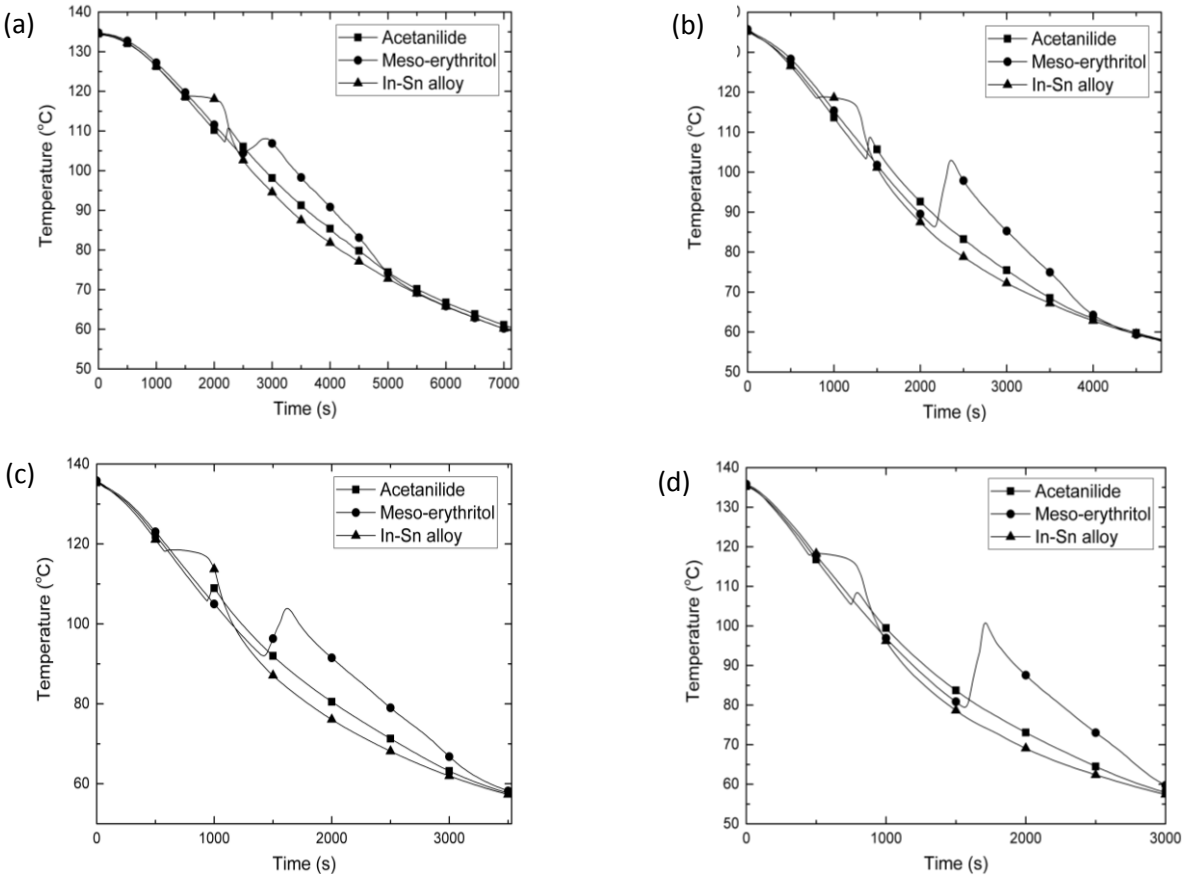

Fig. 5.9. Average temperature histories of the EPCMs while discharging with HTF flow rates at (a) 3 ml/s, (b) 6 ml/s, (c) 9 ml/s and (d) 12 ml/s.

Meso-erythritol later emerged with higher discharging rates during its phase transition due to the release of its large solidification enthalpy. Acetanilide, due to its small thermal mass in the capsule, showed the least rate of discharging at all the flow rates. Meso-erythritol, at each flow rate, showed the highest rate of discharging followed closely by the In-Sn alloy. The largest degree of subcooling, at each flow rate, was exhibited by meso-erythritol followed by acetanilide and lastly by the In-Sn alloy. The implication of subcooling in a PCM is that the melting enthalpy that is most sought after, is released at a lower temperature than the melting temperature. Also, part of the released latent heat is used to heat up the PCM (peaks observed on the acetanilide and the meso-erythritol discharging temperature curves).

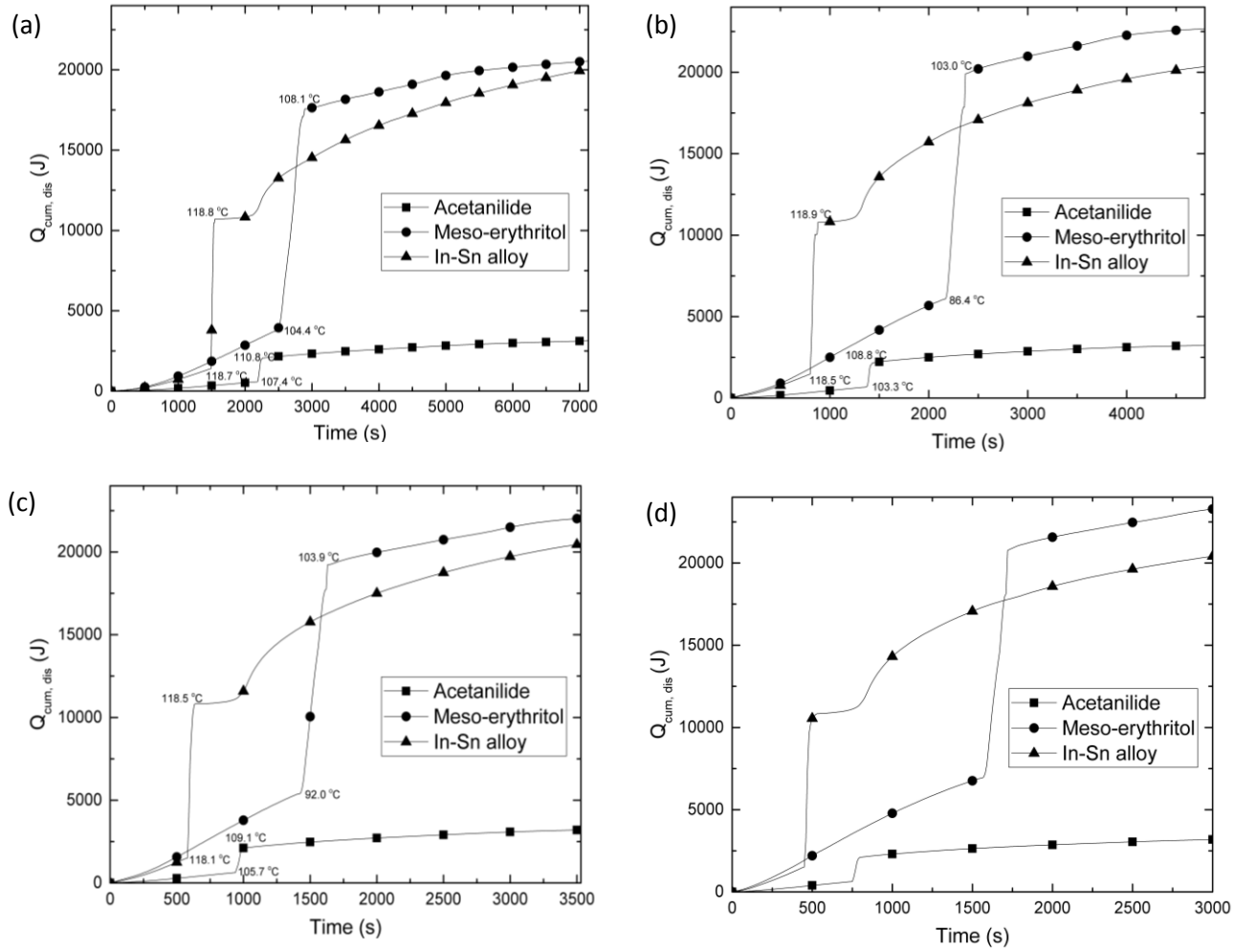

Fig. 5.10. Cumulative energies discharged by the EPCMs while discharging charging with HTF flow rate at (a) 3 ml/s, (b) 6 ml/s, (c) 9 ml/s and (d) 12 ml/s.

The summary of the discharging experiments are presented on Table 5.4. Meso-erythritol, due to its large heat capacity and large enthalpy of melting, is observed to have discharged the largest quantity of total thermal energy at each flow rate. It is followed by the In-Sn alloy and lastly by acetanilide. But of more interest is the quality of the thermal energy discharged by the EPCMs, that is, the temperature at which the energies were discharged. Since the EPCMs were being investigated for use in temperature applications between 110 ^{o}C and 120 ^{o}C, the quantity of thermal energy discharged at temperatures 110 ^{o}C and above shall be considered as the useful energy discharged. The In-Sn alloy can be observed to have discharged more useful energy at all the flow rates, nearly four times than that which was discharged by meso-erythritol and almost twenty times than that discharged by acetanilide at all the flow rates. The In-Sn alloy suffers very little subcooling and its solidification enthalpy was released, in each case, at temperatures above 110 ^{o}C.

Table 5.5. A summary of the discharging performances the EPCMs at the different HTF flow rates.

PCM	HTF flow rate	Total energy (J)	Discharging rate (J/s)	Degree of subcooling (^{o}C)	Useful energy discharged (J)	% Useful energy discharged
Acetanilide	**3 ml/s**	3123.16	0.44	8.83	756.17	24.2
	6 ml/s	3231.32	0.68	12.90	532.68	16.5
	9 ml/s	3203.71	0.91	10.48	537.23	16.8
	12 ml/s	3183.40	1.06	10.79	530.51	16.7
Meso-erythritol	**3 ml/s**	20545.22	2.88	17.63	3036.83	14.8
	6 ml/s	22676.75	4.73	35.68	3135.90	13.8
	9 ml/s	22034.53	6.24	30.01	3135.85	14.2
	12 ml/s	23278.78	7.76	42.58	3163.36	13.6
In-Sn alloy	**3 ml/s**	20031.51	2.81	1.07	12055.86	60.2
	6 ml/s	20358.04	4.25	1.20	12041.18	59.2
	9 ml/s	20482.29	5.80	1.59	12087.11	59.0
	12 ml/s	20405.65	6.80	1.82	12065.75	59.1

5.6. Conclusions

The performances of acetanilide, meso-erythritol and an Indium-Tin alloy during charging and discharging, inside three similar separate spherical capsules, have been compared quantitatively as EPCMs for medium temperature applications. The 50 mm capsules were made from aluminum and sunflower oil was used as the heat transfer fluid to and from the EPCMs. Meso-erythritol showed the greatest charging rates at all the HTF flow rates considered followed very closely by the In-Sn alloy and then acetanilide, which seriously lagged behind due to its low energy storage density. Similar patterns were also observed when the charging temperature was varied. All the EPCMs showed increasing charging rates with an increase in the HTF flow rate and in the HTF charging temperature. Investigation of the discharging of the EPCMs at different HTF flow rates revealed that meso-erythritol also possessed the highest discharging rates followed closely by the In-Sn alloy while acetanilide had the least. However, varying degrees of subcooling were exhibited by PCMs with meso-erythritol showing the largest degrees (17.63 - 42.58 ^{o}C) at all the flow rates followed by acetanilide (8.83 - 12.90 ^{o}C) and lastly, by the In-Sn alloy (1.07 - 1.82). The degree of subcooling is indicative of the magnitude of the potential barrier that needs to be overcome in order to rearrange the molecules of PCM in a stable solid state [31]. The large degrees of subcooling exhibited by both acetanilide and meso-erythritol impacted heavily on the qualities of thermal energies they discharged at all the flow rates. This is because much of the

solidification enthalpy was discharged at temperatures lower 110 ^{o}C which is the intended temperature for application. The measure of the quality of the heat discharged by the EPCMs was determined by considering the quantities of heat discharged with the temperatures of the EPCMs at 110 ^{o}C and above. Due to the small degrees of subcooling exhibited by the In-Sn alloy, it discharged the greatest quantities of useful thermal energy at all the flow rates. Though meso-erythritol was observed to have discharged greater amounts of useful energy than acetanilide, acetanilide was observed to have discharged greater percentages of useful energy due to its smaller degrees of subcooling at all the flow rates. The small density of acetanilide however, gives it a very low thermal energy storage capacity compared to the other two PCMs while subcooling also robs it of the quality of thermal energy during discharging. Though meso-erythritol possesses a very large thermal capacity, this is marred by its large degrees of subcooling during discharging. For greater efficiency, means of reducing the subcooling of meso-erythritol need to be investigated. Although the In-Sn alloy possessed the smallest melting enthalpy of the three PCMs, its large density presented it with a good thermal capacity. The alloy has showed very good potential as a PCM when encapsulated in the spherical capsules for use in a packed bed thermal energy storage system for medium temperature applications. In a separate study carried out by the authors, the In-Sn alloy was found to also possess very good thermal and cycling stability. The high cost of the In-Sn alloy however, might discourage its use as a PCM for medium temperature applications. Since the solder performed better than the other EPCMs, cheaper lead-free solders need to be investigated in the near future for possible applications as PCMs. There is also a necessity in the future to investigate on a suitable nucleating agent that may be added to meso-erythritol in the capsules in order to reduce the degree of subcooling.

Acknowledgements

The authors wish to acknowledge the support provided by the Material Science Innovation and Modeling (MaSIM) research focus area, Faculty of Agriculture, Science and Technology, Northwest University, South Africa. The authors also wish to acknowledge the National Research Foundation, South Africa, through the Research Development Grants for Y-rated Researchers (RDYR-Grant number: 95574) and the Incentive Funding for Rated Researchers (IFRR-Grant number: 90638) schemes.

References

[1] Nomura T, Tsubota M, Oya T, Okinaka N, Akiyama T. Heat transfer release performance of direct-contact heat exchanger with erythritol as phase change material. Appl Energy 2013; 61: 28-35.

[2] Farid M, Khudhair AM, Razack SAK, Al-Hallaj S. A review on phase change energy storage materials and applications. Energ Convers Manage 2004; 45: 1597-615.

[3] Liu M, Saman W, Bruno F. Review on storage materials and thermal performance enhancement techniques for high temperature phase change thermal storage systems. Renew Sust Energ Rev 2012; 16: 2118-32.

[4] Zhao W, Neti S, Oztekin A. Heat transfer analysis of encapsulated phase change materials. Appl Therm Eng 2013; 50: 143-51.

[5] Agyenim F, Hewitt N, Eames P, Smyth M. A review of materials, heat transfer and phase change formulation for latent heat thermal energy storage systems. Renew Sust Energ Rev 2010; 14: 615-28.

[6] Hasnain SM. Review on sustainable thermal energy storage technologies, Part I: Heat storage materials and Techniques. Energ Convers Manage 1998; 39(11): 1127-38.

[7] Xia L, Zhang P, Wang RZ. Numerical heat transfer analysis of the packed bed latent heat storage system based on an effective packed bed model. Energy 2010; 35: 2022-32.

[8] Wei J, Kawaguchi Y, Hirano S, Takeuchi H. Study on a PCM heat storage for rapid heat transfer. Appl Therm Eng 2005; 25: 2903-20.

[9] ElGhnam RI, Abdelaziz RA, Sakr MH, Abdelrhman HE. An experimental study of freezing and melting of water inside capsules used in thermal energy storage systems. Ain Shams Engineering Journal 2012; 3: 33-48.

[10] Tan FL, Hosseinizadeh SF, Khodadadi JM, Fan L. Experimental and computational study of constrained melting of phase change materials inside a spherical capsule. Int J Heat Mass Tran 2009; 52: 3464-72.

[11] Akiyama T, Ashizawa Y, Yagi J. Storage and release of heat in a single capsule containing phase-change material with high melting point. Heat transfer - Japanese research 1992; 21: 199-217.

[12] Amin NAM, Bruno F, Belusko M. Effective thermal conductivity for melting in PCM encapsulated in a sphere. Appl Energy 2014; 122: 280-7.

[13] Sharma SD, Iwata T, Kitano H, Sagara K. Thermal performance of a solar cooker based on an evacuated tube collector with a PCM storage unit. Sol Energy 2005; 78: 416-26.

[14] Kaizawa A, Marouka N, Kawai A, Kamano H, Jozuka T, Senda T, Akiyama T. Thermophysical and transfer properties of phase change material candidate for waste heat transportation system. Heat Mass Transfer 2008; 44: 763-9.

[15] Wang Y, Wang L, Xie N, Lin X, Chen H. Experimental study on the melting and solidification behavior of erythritol in a vertical shell-and tube latent heat thermal storage unit. Int J Heat Mass Tran 2016; 99: 770-81.

[16] Sharma A, Tyagi VV, Chen CR, Buddhi D. Review on thermal energy storage with phase change materials and application. Renew Sust Energ Rev 2009; 13: 318-45.

[17] Choudhari KS, Shende MD. Solar Cooker using PCM material. Journal of Basic and Applied Engineering Research 2015; 2: 1449-53.

[18] Sharma SD, Sagara K. Latent heat storage materials and systems: a review. Int J Green Energy 2005; 2: 1-56.

[19] Buddhi D, Sharma SD, Sharma A. Thermal performance evaluation of a latent heat storage unit for late evening cooking in a solar cooker having three reflectors. Energ Convers Manage 2003; 44(6): 809-17.

[20] Risueño E, Faik A, Rodriguez-Aseguinolaza J, Blanco-Rodriguez P, Gil A, Tello M, D'Aguanno B. Mg-Zn-Al eutectic alloys as phase change material for latent heat thermal energy storage. Energy Procedia 2015; 69: 1006-13.

[21] Myers B, Chauhuri A, Burns J. (2003/08/21). Thermally-capacitive phase change encapsulant for electronic devices. Google Patents, US20030157342. http://www.google.is/patents/US20030157342 (accessed June 2016).

[22] Meso-Erythritol specification sheet, https://www.jk-scientific.com/Download/SPEC/13201112289642.pdf (accessed July 2016).

[23] Acetanilide specification sheet, https://www.alfa.com/en/prodspec/A14361 (accessed July 2016).

[24] Indalloy - Indium with Tin, Lead or Silver safety data sheet, http://www.indium.com/technical-documents/safety-data-sheets/ (accessed July 2016).

[25] Mawire A, Phori A, Taole S. Performance of thermal energy storage oils for solar cookers during charging. Appl Therm Eng 2014; 73: 1321-9.

[26] Kutz M. Handbook of Materials selection, New York: John Wiley & Sons; 2002.

[27] Kenisarin M, Mahkamov K, Solar energy storage using phase change materials, Renew. Sust. Energ. Rev. 11 (2007) 1913-65.

[28] Kaikuchi H, Yamazaki M, Yabe M, Chihara S, Terunuma T, Sakata Y, Usami T. A study of erythritol as phase change material. IEA Annex 10-PCMs and chemical reactions for thermal storage, second workshop, 11-13, November 1998, Sofia, Bulgaria.

[29] Sharma SD, Sagara K. Latent heat storage materials and systems: A review. Int J Green Energy 2005; 2: 1-56.

[30] Yaws CL. Handbook of Thermal Conductivity, Organic Compounds C_8 to C_{28}, vol. 3, Texas, Gulf Publishing Company; 1995.

[31] Jankowski NR. Electrical supercooling mitigation in erythritol. In: Proceedings of The International Heat Transfer Conference, IHTC14, 8 - 13 August 2010, Washington, USA.

CHAPTER SIX: PACKED BED THERMAL ENERGY STORAGE SYSTEM

6.1 An Overview

The main objective of this research work is to design and construct a laboratory-scale oil/packed bed thermal energy storage system with encapsulated phase change material for cooking application and investigate its thermal performances during charging and discharging cycles as stated in chapter one. From the studies in the previous chapters, meso-erythritol possesses a large volumetric heat storage capacity and a fair cycling stability. It is very cheap, available and is a food-grade material therefore a very good PCM candidate in a TES system for cooking applications. Hence meso-erythritol has been chosen as the PCM to be used in the TES fabricated in this study. The spherical capsule to contain meso-erythritol had also shown (Chapter Three) to be mechanically stable within the intended range of temperature application for this study. Aluminum, the capsule material, also showed chemical compatibility with both meso-erythritol (PCM) and sunflower oil (HTF). From the understanding gathered from previous chapters, an oil/packed bed thermal energy storage system has been designed and fabricated. Photographs of the fabricated system can be seen in Appendices A-E. The performances of the fabricated system during charging and discharging cycles has been studied and this research work is contained in research paper 5 attached. This manuscript has been submitted for publication in the Renewable Energy journal and it is currently under review.

Elsevier Editorial System(tm) for Renewable Energy

Manuscript Draft

Manuscript Number: RENE-D-16-02943

Title: EXPERIMENTAL INVESTIGATION OF A PACKED BED LATENT HEAT THERMAL ENERGY STORAGE SYSTEM FOR DOMESTIC USE

Article Type: Research Paper

Keywords: Erythritol; latent heat thermal energy storage; packed bed; encapsulation; sunflower oil.

Corresponding Author: Mr. ADEDAMOLA BABAJIDE SHOBO, M.Sc.

Corresponding Author's Institution: NORTHWEST UNIVERSITY

First Author: ADEDAMOLA BABAJIDE SHOBO, M.Sc.

Order of Authors: ADEDAMOLA BABAJIDE SHOBO, M.Sc.; ASHMORE MAWIRE, PHD

6.2. Research paper 5:

EXPERIMENTAL INVESTIGATION OF A PACKED BED LATENT HEAT THERMAL ENERGY STORAGE SYSTEM FOR DOMESTIC USE

SHOBO A. B.[a] MAWIRE A.[a]

[a] Department of Physics and Electronics, Northwest University, Private Bag X2046, Mmabatho 2745, South Africa.

Abstract

The performance of a thermal energy storage system consisting of a packed bed, latent heat thermal energy storage unit, for domestic use, is investigated in this paper. The primary storage unit consisted of an insulated cylinder packed randomly with meso-erythritol macro-capsules. The capsule material was aluminum and the heat transfer fluid (HTF) used was sunflower oil. Water inside a cylindrical tank was used as a secondary thermal storage medium in the system while heat was supplied using an electric heater. The influences of the HTF's flow rate and HTF inlet temperature on the charging performance of the system is investigated as well as the influence of the HTF's flow rate on the discharging performance of the system. Results showed that the average cumulative charging rate of the storage system varied directly as the HTF's flow rate. Higher charging rates were obtained for the packed bed at higher HTF inlet temperatures while the charging rates of the secondary storage were lower. The average rate of energy delivery by the packed bed increased with an increase in the HTF flow rate during the discharging cycles.

Keywords: Meso-erythritol; latent heat thermal energy storage; packed bed; encapsulation; sunflower oil.

6.3. Introduction

Cooking, water heating and space heating account for about 76 % of energy consumption in the residential sector [1]. Studies indicate that there is still heavy reliance on solid biomass to meet these domestic heating demands in developing countries [2-4]. Combustion of solid biomass for heating needs has been reported to produce high levels of both indoor and outdoor pollution, which has been traced to have severe health impacts [5-6]. The combustion of solid biomass to meet heating needs is also reported to contribute greatly towards environmental degradation, gender/social inequality and economic wastages [7].

It is therefore important to pursue cleaner, safer, environment-friendly and sustainable alternatives to meet domestic heating demands particularly for the developing countries.

Latent heat thermal energy storage systems have been reported to possess large thermal energy storage densities capable of being used for the storage of solar thermal energy [8]. The choice of the phase change material (PCM) to utilize in a latent heat storage system, for a particular application depends on a number of properties of the PCM. These properties include: the solidification temperature being around the desired heating temperature, high density, low thermal expansion, small or zero degree of supercooling, chemical stability after several melting/solidification cycles, compatibility with containment materials, abundance/availability, low cost and a low degree of health hazard [9-10].

Erythritol has been identified by several studies to be a promising PCM for heat storage applications [11-15]. Erythritol is a sugar alcohol that naturally occurs in various fruits, fermented foods as well as in body fluids of humans and animals [16]. The solidification temperature, high enthalpy of phase change, good cycling stability and the non-toxic nature of erythritol makes it attractive for domestic heating applications [12, 15]. Sharma et al. [17] utilized erythritol as a PCM for solar thermal energy storage in a solar cooker based on an evacuated tube solar collector. Wang et al. [18] used erythritol as a PCM in a mobilized thermal energy storage system for recovery and utilization of industrial waste heat. Nomura et al. [19] also studied the heat storage performance of a direct-contact latent heat exchanger using erythritol as a PCM in a vertical heat storage vessel. The discouraging factors in the use of erythritol as a PCM in thermal energy storage systems are its low thermal conductivity and its exhibition of supercooling. Packed bed configurations in thermal energy storage systems have been reported to possess high heat transfer effectiveness between the heat transfer fluid (HTF) and the solid fillers [20]. An investigation of micro-encapsulation of erythritol by Hayashi et al. [21] reported that supercooling of erythritol can be reduced by increasing the capsule diameter since the phenomenon is strongly dependent on the volume of the PCM. Therefore, macro-encapsulation of erythritol might be preferable to reduce the supercooling problem. Spherical encapsulation has been reported to give a greater heat transfer rate than some other geometries of encapsulation [22]. Additionally, spherical capsules were reported to give a high packing density in a thermal energy storage tank [23].

Several experimental studies have investigated the performance of erythritol as a PCM for thermal storage applications in configurations such as a direct-contact bed [18-19], a

horizontal shell and tube [24-25] and a vertical shell and tube [26]. However, no experimental study of a packed bed of spherically encapsulated erythritol for thermal energy storage has been found in literature. In this work, the performance of a thermal energy storage system incorporated with a packed bed of spherically encapsulated erythritol for the provision of domestic heating needs is experimentally investigated with sunflower oil as the HTF. The novelty of the thermal storage system considered in this study stems from the fact that it is a combination of separate latent heat thermal storage and sensible heat thermal storage units. The authors earlier investigated the encapsulation of meso-erythritol in an aluminum spherical capsule [27]. The aluminum alloy used as the capsule material showed compatibility with both the PCM (meso-erythritol) and sunflower oil. The 50 mm diameter spherical capsule fabricated with a wall thickness of 1 mm and filled with meso-erythritol also showed mechanical stability when subjected to temperatures above the melting point of the PCM.

Nomenclature

Symbols	***Description***		
$c_{aluminum}$	Specific heat capacity of aluminum, J/kg ^oC	T_{din}	Temperature of HTF entering the discharging unit, ^oC
c_{HTF}	Specific heat capacity of the HTF, J/kg ^oC		
c_l	Specific heat capacity of solid PCM, J/kg ^oC	T_{dout}	Temperature of HTF exiting the discharging unit, ^oC
c_m	Average specific heat capacity of PCM, J/kg ^oC		
c_s	Specific heat capacity of solid PCM, J/kg ^oC	T_{in}	Temperature of HTF entering the packed bed, ^oC
H_f	Melting enthalpy, J/kg		
HTF	Heat transfer fluid	T_l	Melting onset temperature of PCM, ^oC
$m_{capsule\ wall}$	Mass of capsule wall, kg		
m_{HTF}	Mass of HTF, kg	T_{out}	Temperature of HTF exiting the packed bed, ^oC
m_{pcm}	Mass of PCM, kg		
m_{water}	Mass of water, kg	T_{PCM}	Temperature of PCM, ^oC
PCM	Phase change material	T_{ref}	Reference temperature, ^oC
$Q_{Capsule\ wall}$	Quantity of heat stored in the capsule wall, J	T_s	Melting peak temperature of PCM, ^oC
$Q_{delivered}$	Quantity of heat delivered by HTF to packed bed, J		
Q_{HTF}	Quantity of heat stored by HTF, J	$\dot{V}$	Volumetric flow rate, m^3/s
Q_{PCM}	Quantity of heat stored by PCM, J	***Greek letters***	***Description***
Q_{water}	Quantity of heat stored by water, J	ΔT	Change in temperature, ^oC
T_{in}	Temperature of HTF entering the packed bed, ^oC	ρ	Density, kg/m^3

6.4. Materials and methods

6.4.1. Materials

Commercial grade meso-erythritol (purity 98%) used as the PCM was purchased from J&K Scientific, China. The melting onset, melting peak and melting enthalpy of the PCM was determined using a differential scanning calorimeter (SDT Q600, TA Instruments). Fig. 6.1 shows the DSC thermogram of meso-erythritol obtained with a heating rate of 10 ^{o}C/min, under a constant nitrogen flow of 25 ml/min. The melting onset of meso-erythritol was 118.35 ^{o}C, the melting peak was 122.03 ^{o}C and the melting enthalpy was 312.7 J/kg.

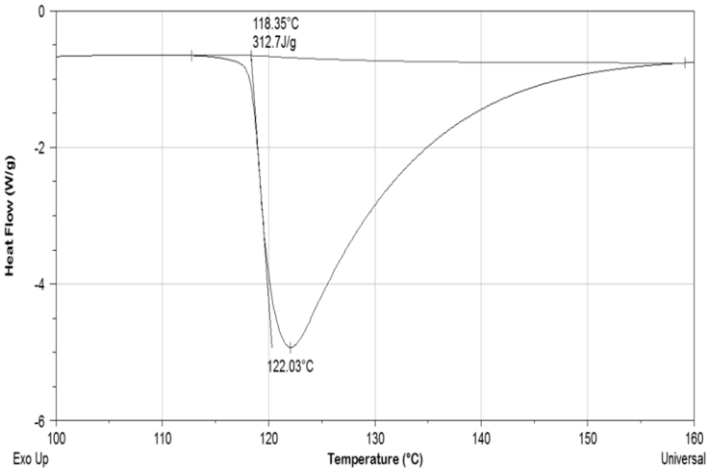

Fig. 6.1. DSC thermogram of meso-erythritol during melting.

The values of the density and the specific heat capacity found in literature were used and are listed in Table 6.1. A commercial brand of refined sunflower oil, Excella (manufactured by Wilmar Continental in South Africa), was used as the heat transfer fluid (HTF). Mawire et al. [29] reported that sunflower oil possesses good heat transfer and heat storage properties.

Table 6.1. Density and specific heat capacity of erythritol [28].

PROPERTY	PHASE	VALUE
Density (kg/m^3)	Solid (20 ^{o}C)	1480
	Liquid (140 ^{o}C)	1300
Specific heat capacity (J/kg K)	Solid	1383
	Liquid	2765

The variation of the density of the sunflower oil with temperature was determined by using a Stabinger Viscometer SVM 3000 (Anton Paar GmbH, Austria). Equation (6.1) gives the

correlation obtained from the temperature-density plot. The correlation between the specific heat capacity of sunflower oil with temperature was obtained from literature [29] and is given in equation (6.2).

$$\rho = 932.37 - 0.66 * T(℃) \quad (6.1)$$

$$c = 2115.00 + 3.13 * T(℃) \quad (6.2)$$

6.4.2. Description of the experimental set-up

Fig. 6.2 shows a schematic diagram of the experimental set-up. It consists of an insulated packed bed thermal storage tank (a), an electric heating unit (g), a secondary sensible thermal storage (e) and a discharging unit (d). The packed bed storage tank is a stainless steel cylinder of a diameter of 0.128 m and a height of 0.69 m, insulated with rock wool of thickness 0.05 m and placed in a stainless steel, hexagonal casing.

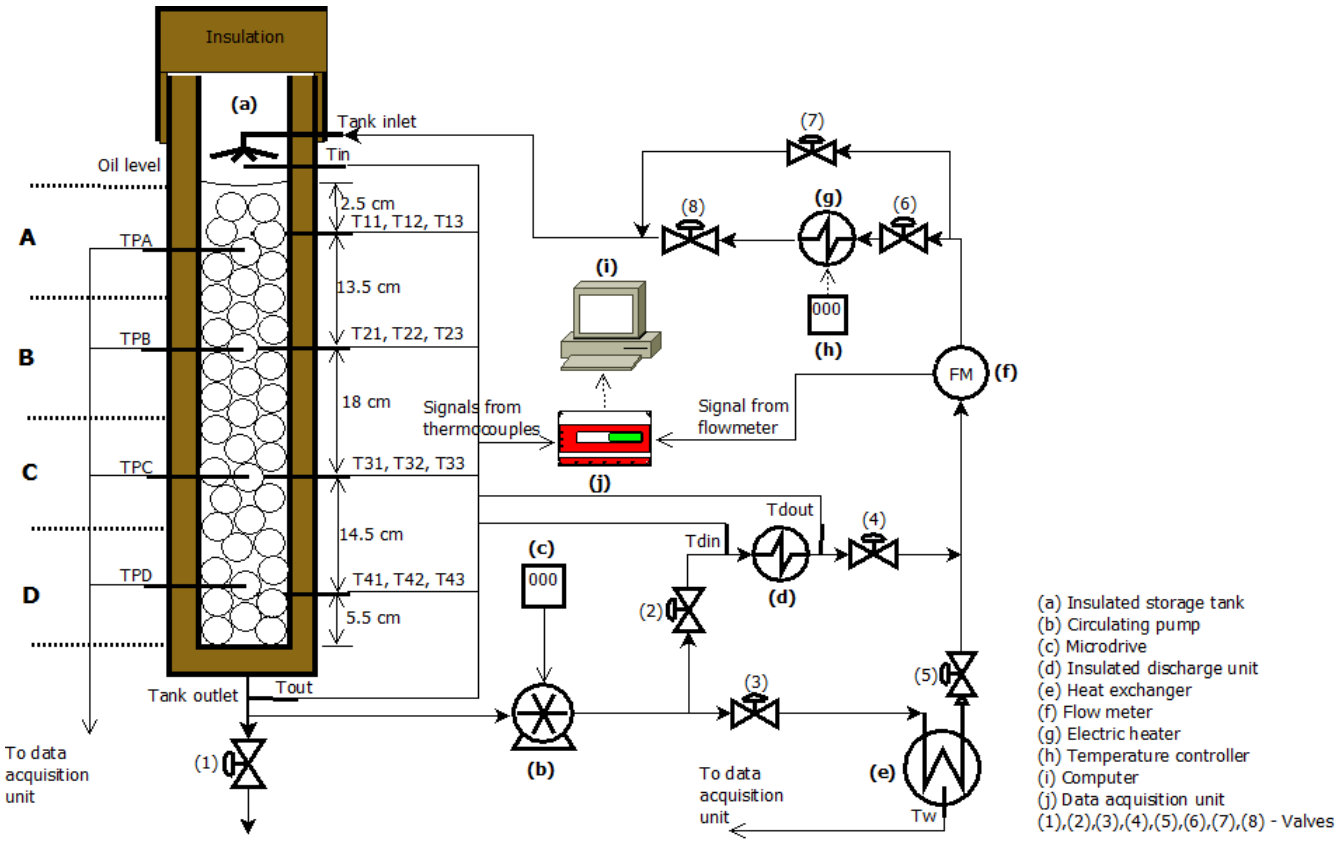

Fig. 6.2. A schematic diagram of the experimental set-up.

Three K-type (accuracy: ± 2.2 ^{o}C) thermocouples each of lengths 0.013 m, 0.038 m and 0.064 m are fixed at four axial distances (5.5 cm, 20.0 cm, 38.0 cm and 51.5 cm) from the bottom of the tank in order to determine the radial temperatures of the HTF at each axial position.

The PCM spherical capsules with outside diameters of about 0.05 m were made from an aluminum alloy 1050-H14 plate with a thickness of 0.001 m. Meso-erythritol was heated to a temperature of about 140 ^{o}C, then the liquid PCM was poured into the capsules and allowed to cool under a flow of dry air. The actual outside volume of the PCM capsules were determined by measuring the volume of one PCM capsule through a volume displacement method. 40 PCM capsules were stacked randomly in the storage tank such that one PCM sphere with an inserted thermocouple (Fig. 6.3), lies at about the same axial level with the thermocouples in the storage tank measuring the HTF temperatures (as shown in Fig. 6.2). The storage tank was then filled with sunflower oil until the oil level was 0.54 m measured from the bottom of the tank. The storage tank was then covered with an insulated lid. The porosity of the packed bed was calculated to be 0.4893. One K-type thermocouple was placed at the HTF inlet into the bed and another in the outlet pipe from the tank respectively, to measure the temperatures of the HTF entering and leaving the bed. A sliding vane, magnetic drive pump (Packaged Metering and Pumping solutions, Benoni, South Africa) whose frequency was controlled by a VLT Micro drive FC 51 (Danfoss A/S, Graasten, Denmark. Maximum error: 0.8 % of full scale), was used to circulate the HTF around the flow line. Thermal energy was supplied by an electric heating unit that is composed of a heating element and a copper coil through which the HTF flowed.

Fig. 6.3. (a) PCM capsule with inserted thermocouple (b) PCM capsule with no thermocouple.

The maximum heater temperature was pre-set by a TZN4S temperature controller (Autonics, Illinois, USA. Display accuracy: ± 0.3 %). The secondary storage unit is a stainless steel cylinder with a diameter of 0.27 m and with a height of 0.25 m inside which a copper spiral coil is placed through which the HTF flowed. The secondary storage was filled with water for

provision of hot water for immediate use after charging and a K-type of thermocouple (T_w) was used to measure the average water temperature. The secondary storage also helped to limit the temperature of the HTF that flowed through the flowmeter so that the maximum operating temperature of 120 ^oC for the flowmeter was not exceeded. Thus, the need to use a more expensive flowmeter with a higher operational temperature was avoided. The discharging unit consisted of an insulated stainless steel cylinder with a diameter of 0.25 m and with a height of 0.14 m, inside which a copper coil was attached, through which the HTF flows. The flow rate of the HTF through the flow line was measured by a positive displacement flowmeter M1SSP (Macnaught Pty. Ltd., Sydney, Australia. Accuracy: ± 1 %). K-type of thermocouples measured the inlet temperature of the HTF into (T_{din}) and out of (T_{dout}) the discharging unit respectively. Temperature measurements from all the thermocouples and flow rate measurements by the flowmeter were acquired every 10 s, by a data acquisition unit (Agilent 34970A, Keysight Technologies, California, USA). The accuracy of the thermocouple measurements acquired by the unit is ± [1 + accuracy of the K-type of thermocouple] and the acquired data was recorded on a personal computer. The connecting pipes between all components in the experimental set-up were insulated with closed-cell foam rubber insulation. During charging cycles, valves 3, 5, 6 and 8 were kept opened while valves 1, 2, 4 and 7 were closed. During discharging cycles, valves 2, 4 and 7 were opened while valves 1, 3, 5, 6 and 8 were kept closed. The HTF flow direction during both charging and discharging cycles, through the packed bed, was from the top to the bottom.

6.4.3. Procedure of the experiment

Charging experiments were performed at flow rates of 3 ml/s, 6 ml/s, 9 ml/s and 12 ml/s with the maximum heater temperature set at 150 ^oC to investigate the influence of the HTF flow rate on the charging performance of the system. The charging experiments were stopped in each case when the thermocouple T43 indicated a temperature of 139.5 ^oC. The influence of the charging temperature was investigated by setting the maximum heater temperature at 140 ^oC, 150 ^oC and 160 ^oC with the HTF flow rate at 9 ml/s for a charging time of 14400 s in each case. The discharging experiments were conducted 5-10 mins after each charging experiment with the same HTF flow rate used for charging in order to investigate the effect of the HTF flow rate on the discharging performance of the system. The condition used for the end of the discharging experiment was when T_{din} was equal to T_{dout}.

6.4.4. Method of analysis

Some assumptions were made during the analyses of the results. The assumptions are given as follows:

1) The temperature of the HTF in each axial section of the tank (TFA, TFB, TFC and TFD) was given by the average of the radial temperatures measured by the three thermocouples in that section.
2) The PCM capsules were perfect spheres, identical and contained the same amounts of PCM.
3) The PCM capsules were initially filled to 90 % of their volume with meso-erythritol.
4) There were no temperature gradients in the PCM capsules.
5) Each axial section of the tank contained 10 PCM capsules each and all the PCM capsules in the same axial section were at the same temperature.

The cumulative quantity of thermal energy stored in the packed bed during charging is made up of heat that is stored by the HTF and the PCM capsules. The cumulative quantity of thermal energy delivered by the HTF to the packed bed is calculated by:

$$Q_{delivered} = \int_0^t \dot{V} \rho_{HTF} c_{HTF} (T_{in} - T_{out}) dt \tag{6.3}$$

where $\dot{V}$ is the HTF's volumetric flow rate (in m^3/s), ρ_{HTF} and c_{HTF} are the density and specific heat capacity of the HTF evaluated at an average temperature of $(T_{in}+T_{out})/2$.

The quantity of heat stored in the PCM capsule wall was calculated by:

$$Q_{Capsule\ wall} = m_{Capsule\ wall} c_{\ aluminum} \Delta T \tag{6.4}$$

The quantity of thermal energy stored in the PCM was determined by expressing the enthalpy of the PCM as a function of temperature [30]:

$$Q_{PCM} = \begin{cases} m_{PCM} c_s (T_{PCM} - T_{ref}) & (T_{pcm} < T_s) \\ m_{PCM} \left(\left(c_m + \frac{H_f}{\Delta T} \right) (T_{PCM} - T_s) + c_s (T_s - T_{ref}) \right) & (T_s \le T_{pcm} < T_l) \\ m_{PCM} \left(c_l (T_{pcm} - T_l) + c_s (T_{PCM} - T_{ref}) + c_m \Delta T + H_f \right) & (T_{pcm} > T_l) \end{cases} \tag{6.5}$$

where T_{pcm}, T_s, T_l are the PCM's temperature, the melting onset temperature of PCM and the melting peak temperature of the PCM respectively. m_{pcm} is the mass of the PCM, c_s and c_l are

the specific heat capacity of the PCM in the solid state and liquid state respectively, c_m is given by $(c_s + c_l)/2$. T_{ref} is the reference temperature.

The quantity of heat stored by the HTF in the storage tank was calculated by:

$$Q_{HTF} = m_{HTF} c_{HTF} \left(T_{HTF} - T_{ref}\right) \tag{6.6}$$

The quantity of heat stored by the water in both the secondary storage during charging and in the discharge unit during discharging was calculated by:

$$Q_{water} = m_{water} c_{water} (\Delta T) \tag{6.7}$$

The cumulative quantity of heat delivered by the packed bed during discharging was calculated by:

$$Q_{delivered} = \int_0^t \dot{V} \rho_{HTF} c_{HTF} (T_{out} - T_{in}) dt \tag{6.8}$$

6.5. Results and discussion

6.5.1. The influence of the HTF flow rate on the charging performance

Fig. 6.4 (a) - (d) shows the temperature profiles of the packed bed while charging at HTF flow rates of 3 ml/s, 6 ml/s, 9 ml/s and 12 ml/s, with the maximum heater temperature set at 150 ^{o}C. TFA, TFB, TFC and TFD are the average HTF temperatures at axial positions A, B, C and D respectively while TPA, TPB, TPC and TPD are the PCM temperature at axial positions A, B, C and D. At an HTF flow rate of 3 ml/s, the packed bed takes a long time (25440 s) to get charged as there are large thermal losses through the flow lines and from the walls of the storage due to the low HTF flow rate. The charging time at 6 ml/s is 11460 s, at 9 ml/s it is 11640 s while at 12 ml/s it is 11360 s.

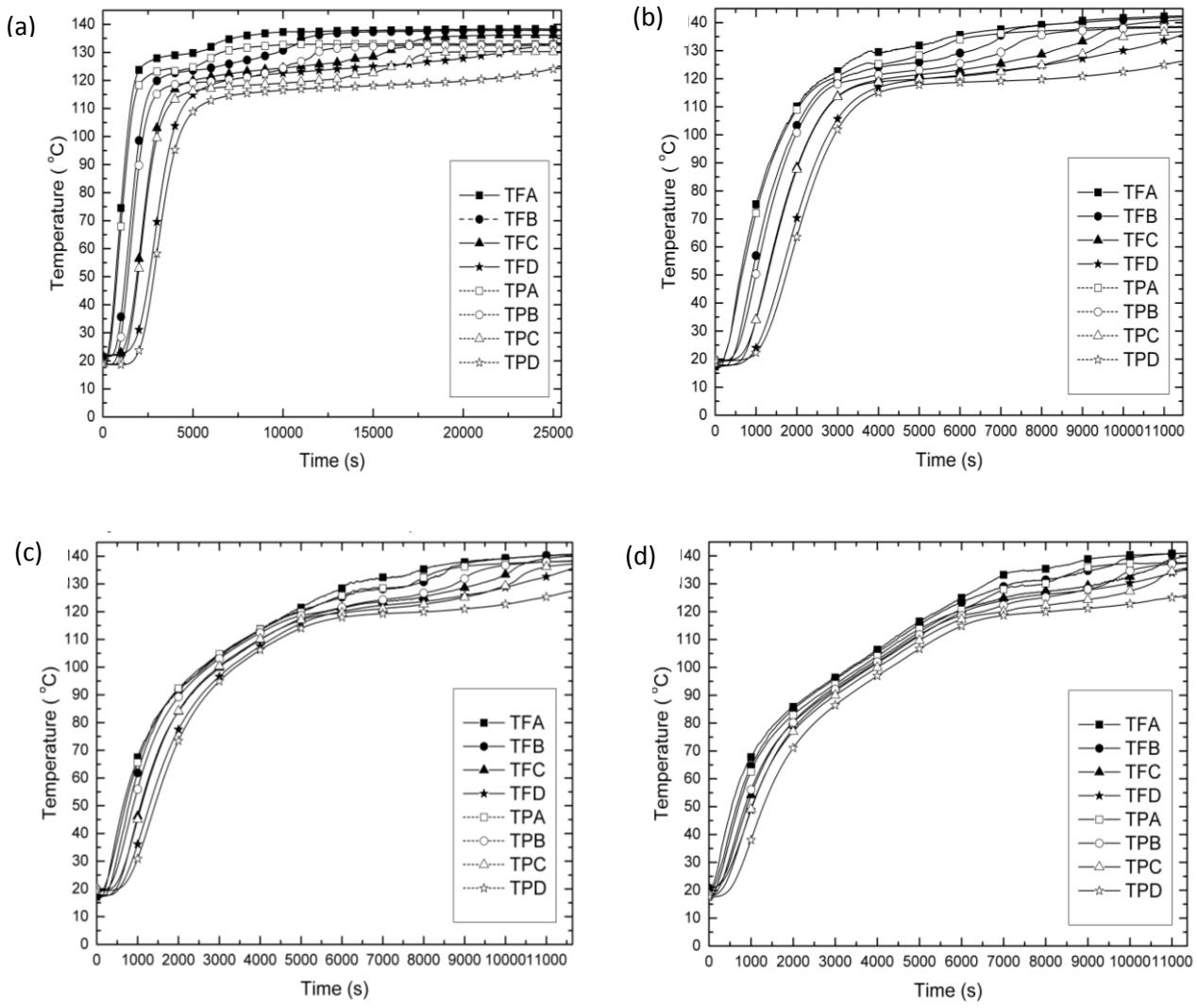

Fig. 6.4. Temperature profile of the packed bed while charging at flow rate of (a) 3 ml/s, (b) 6 ml/s, (c) 9 ml/s and (d) 12 ml/s, with the maximum heater temperature set at 150 ^{o}C.

It can also be observed from Fig. 6.4 (a) - (d) that temperature stratification in the tank reduced with increasing HTF flow rate because thermal energy is transported to lower parts of the tank more rapidly. It can be observed from Fig. 6.5 (a) - (d) that the HTF inlet temperature into the packed bed (T_{in}) increased very rapidly at lower flow rates than at higher flow rates. This is due to the fact that at a low HTF flow rate, the HTF resided longer in the heater while the heater temperature rose rapidly as there was a low rate of thermal energy transportation away from the heater. This gave rise to a large thermal gradient between the HTF entering the packed bed and the components of the packed bed. Therefore heat transfer to the HTF and the PCM capsules initially occurred rapidly. Thermal losses through the walls of the storage tank to the ambient also increased due to the sudden large thermal gradient between the packed bed and the ambient.

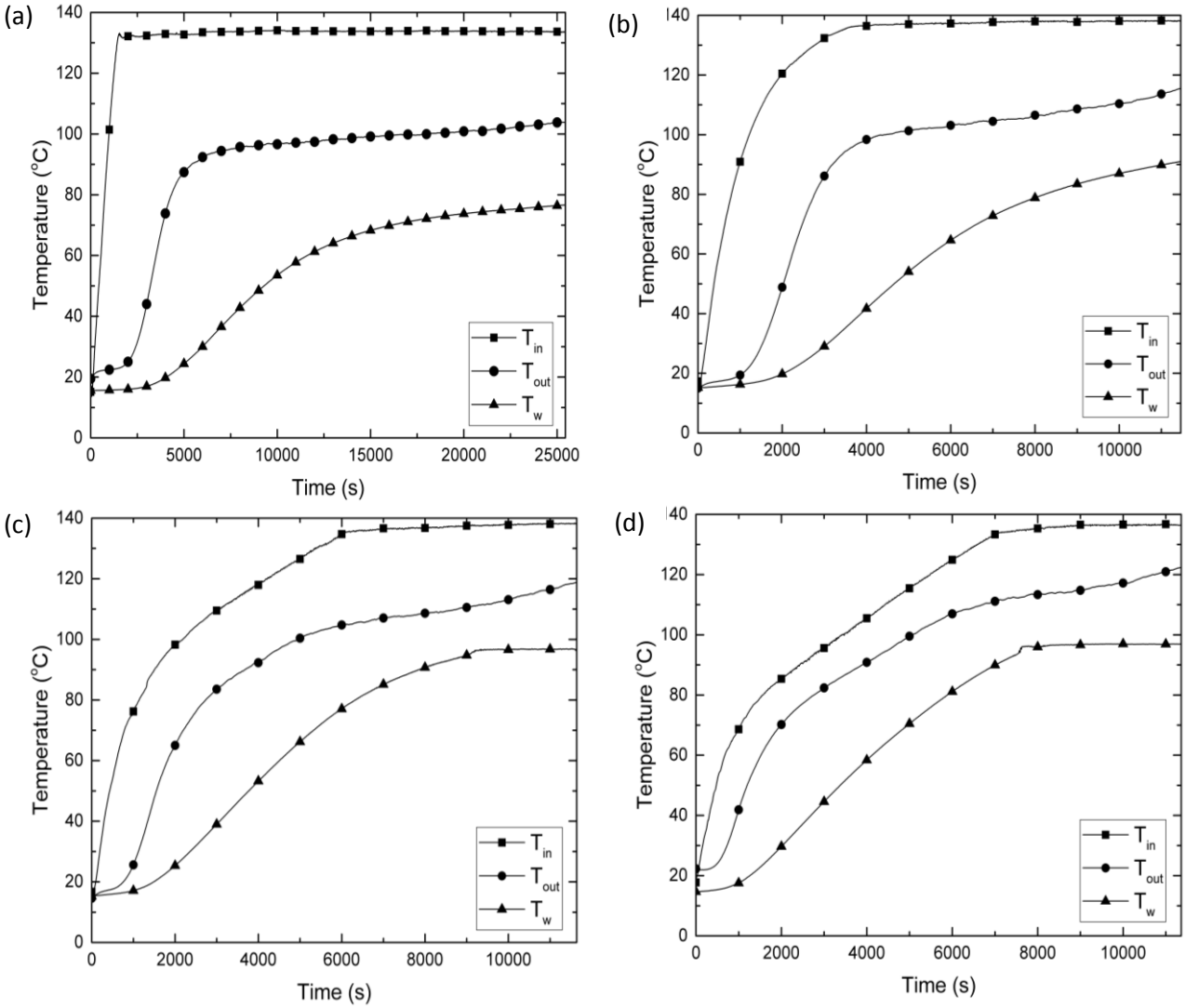

Fig. 6.5. Temperature histories of the HTF at storage tank's inlet, outlet and water in secondary storage while charging at flow rate of (a) 3 ml/s, (b) 6 ml/s, (c) 9 ml/s and (d) 12 ml/s, with the maximum heater temperature set at 150 °C.

The values of T_{out} can be observed to get closer to the values of T_{in} as the HTF flow rate increased while more thermal energy was transferred to the water in the secondary storage as can be observed in Fig. 6.5 (a) - (d). The dynamics of the charging cycles may be better understood by analyzing the system in terms of energy. Fig. 6.6 (a) - (d) shows the temporal variations of the cumulative energy delivered to the packed bed, cumulative energy stored in the packed bed and cumulative energy stored in the secondary storage at all the HTF flow rates considered. At lower HTF flow rates, the cumulative energy delivered to the packed bed was initially very close to cumulative energy stored in the packed bed than at higher flow rates. However towards the end of charging, the difference between cumulative energy stored in the packed bed and the cumulative energy delivered to the packed bed widened at the low HTF flow rate. The energy storage efficiency of the packed bed was 35.9 % for flow rate of 3 ml/s, 43.7 % for 6 ml/s, 39.6 % for 9 ml/s and 46.7 % for 12 ml/s.

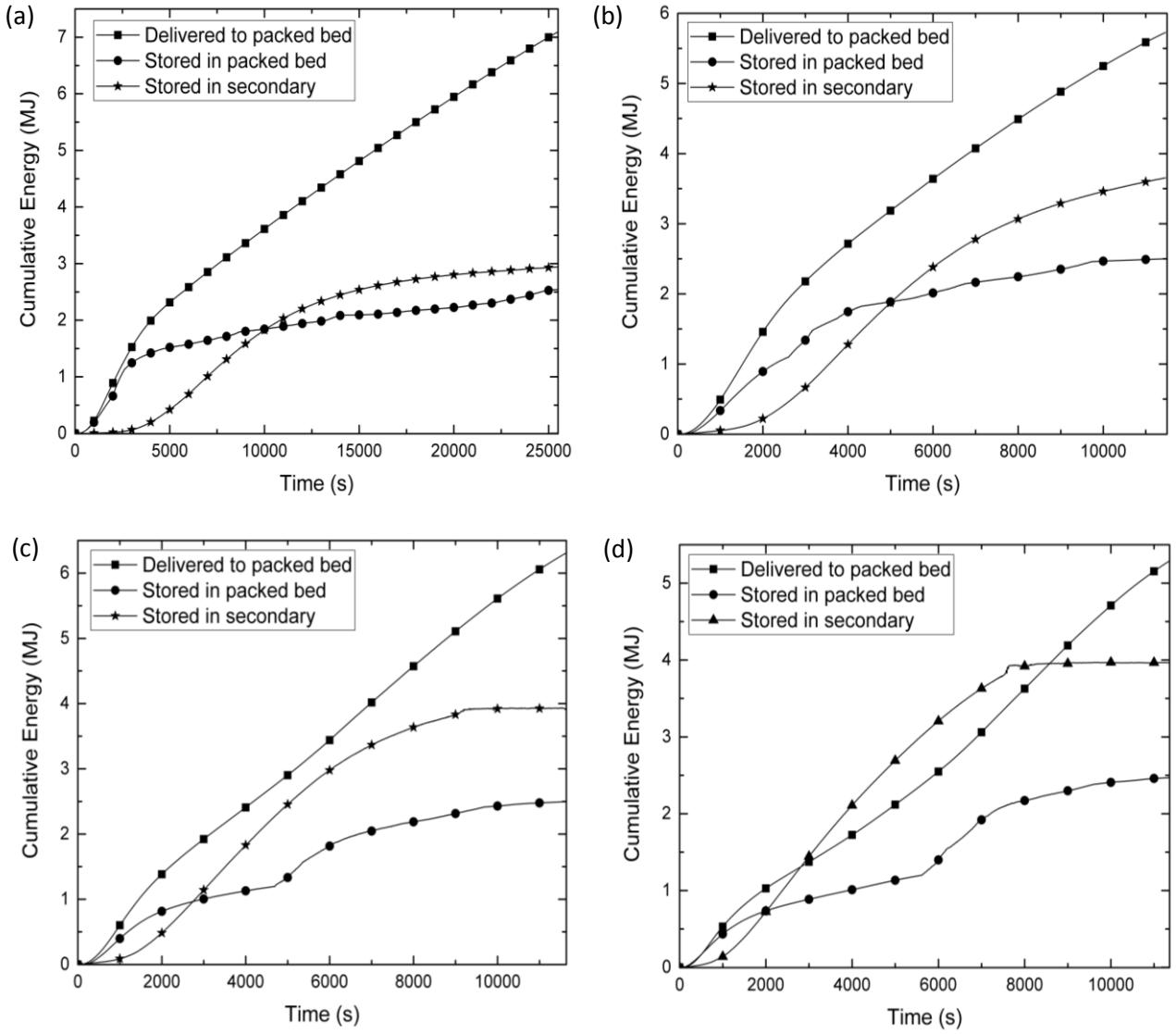

Fig. 6.6. Temporal variation of the cumulative energy delivered to the packed bed, stored in the packed bed and stored in the secondary storage while charging at flow rates of (a) 3 ml/s, (b) 6 ml/s, (c) 9 ml/s and (d) 12 ml/s, with the maximum heater temperature set at 150 ^{o}C.

Ideally, the charging time of the packed bed should reduce with increasing HTF flow rate and the charging efficiency should increase with increasing HTF flow rate. However, it was observed that the charging time at 9 ml/s was higher than that at 6 ml/s and also the charging efficiency is lower than that at 6 ml/s. This anomaly may be attributed to fluctuations of the ambient temperature in the laboratory caused by changes in the weather condition because the interior of the laboratory was not totally isolated from effects of the weather conditions.

Fig. 6.7 shows the ambient temperatures in the laboratory during the charging experiments. Since it is impossible to have 100 % perfect thermal insulation, conduction of thermal energy occurs through the walls of the storage tank and the insulation, to the ambient.

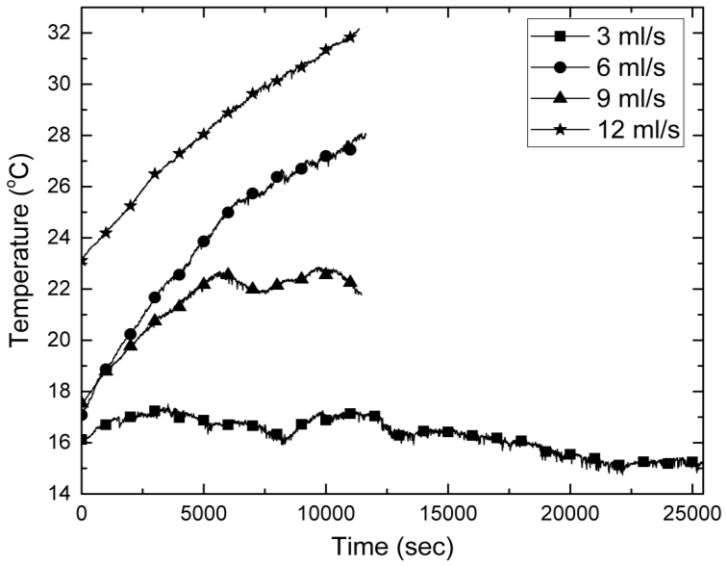

Fig. 6.7. Temporal variation of the ambient temperature during charging at the different flow rates.

The rate at which thermal energy is lost to the ambient depends largely on the thermal gradient between the packed bed and the ambient. From Fig. 6.7, it can be observed that the ambient temperatures during charging at an HTF flow rate of 3 ml/s were very low (between 14.75 ^{o}C and 17.51 ^{o}C) as compared to those at other flow rates. High rate of thermal losses from the storage tank are therefore expected as the temperature of the packed bed increased thus contributing to the unusually long charging time at a flow rate of 3 ml/s. A sudden fall in the ambient temperature can also be observed in Fig. 6.7 during charging at 9 ml/s at a time of about 5700 s. This contributed to more thermal losses from the storage tank and hence, a longer charging time as compared to the flow rate of 6 ml/s. The average rate of energy storage cumulatively in both the packed bed and in the secondary storage was 116.4 J/s for HTF flow rates of 3 ml/s, 537.0 J/s for 6 ml/s, 551.7 J/s for 9 ml/s and 566.5 J/s for 12 ml/s. The average cumulative charging rate of the whole system consequently increased with an increase in the HTF flow rate. It can be observed that thermal energy is more rapidly delivered to the secondary storage at high HTF flow rates and maximum energy was delivered to the secondary storage with a HTF flow rate of 12 ml/s.

6.5.2. The influence of the charging temperature on the charging performance

Fig. 6.8 shows the cumulative heat stored in the packed bed with the maximum heater temperature set at 140 ^{o}C, 150 ^{o}C and 160 ^{o}C while the charging flow rate was kept at an average of 9 ml/s with the charging time of 14400 s in each case.

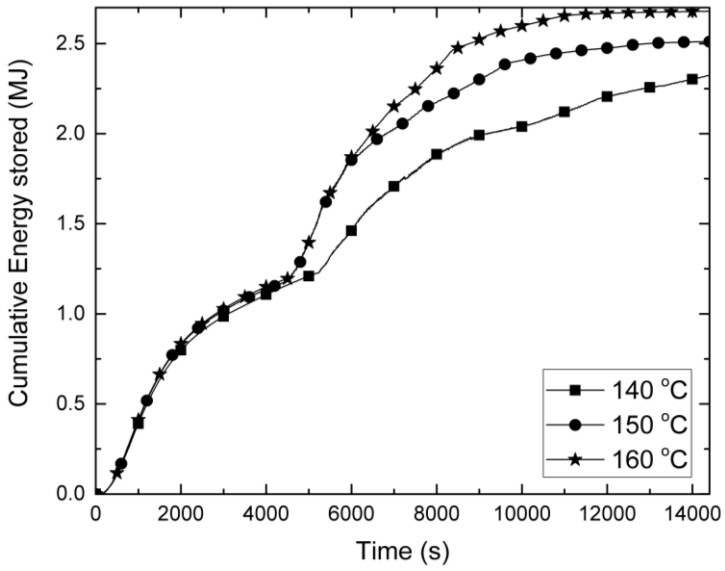

Fig. 6.8. Cumulative energy stored in the packed bed with the maximum heater temperature set at 140 °C, 150 °C and 160 °C while charging at 9 ml/s for 14400 s.

The rate of charging at all temperatures was be observed to be very comparable from the onset of charging until about 1200 s when rate of charging for 140 °C shows a lower rate than that at the other temperatures. At about 6000 s, the rate of energy accumulation for 160 °C can be observed to be more rapid than that for 150 °C. The direct influence of charging temperature is that at higher charging temperatures, the thermal gradient between the HTF and the packed bed is increased thus, greater heat transfer and higher packed bed temperatures. Fig.6. 9 shows the cumulative heat stored in the secondary storage during the charging at different maximum set temperatures of the heater.

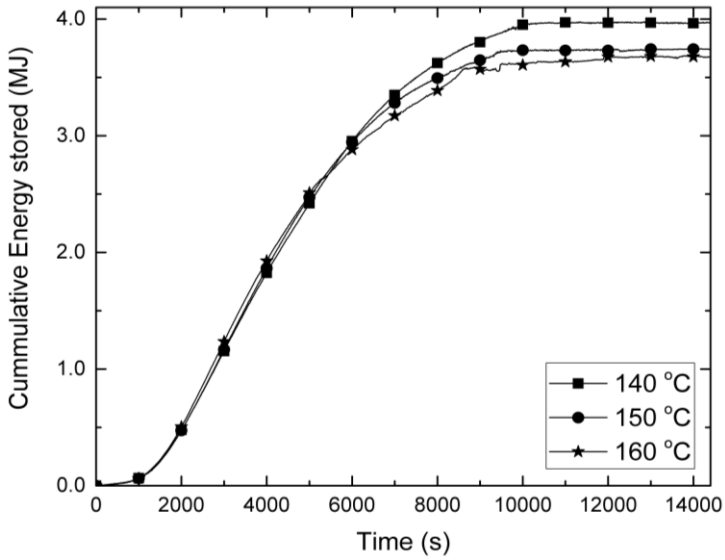

Fig. 6.9. Cumulative energy stored in the secondary storage with the maximum heater temperature set at 140°C, 150 °C and 160 °C while charging at 9 ml/s for 14400 s.

The rate of heat storage in the secondary storage appears to be independent of the set temperatures until about 2000 s when the rate of heat storage for the set temperature of 160 ^{o}C began to rise more rapidly, followed by 150 ^{o}C and then 140 ^{o}C. The implication of this is that greater thermal energy is available from the HTF exiting the packed bed initially at higher charging temperatures than at lower temperatures. At about 5500 s, the trend became reversed where the rate of thermal storage in the secondary for 140 ^{o}C rose higher followed by 150 ^{o}C and then 160 ^{o}C. Greatest quantity of thermal energy was stored in the secondary with heater set temperature at 140 ^{o}C followed by 150 ^{o}C and then 160 ^{o}C. The implication is that at higher set temperatures of the heater, higher thermal gradients attained between the HTF and the packed bed favored higher rates of thermal energy storage in the packed bed while less thermal energy is available for storage in the secondary storage. While with a lower HTF temperature, the thermal gradient between the HTF and the packed bed is reduced leading to a lower charging rate of the packed bed and thus, availability of more thermal energy for storage in the secondary storage.

6.5.3. The influence of the HTF flow rate on the discharging performance

Fig. 6.10 (a) - (d) shows the temperature profile of the packed bed while discharging at HTF flow rates of 3 ml/s, 6 ml/s, 9 ml/s and 12 ml/s respectively. At low HTF flow rates, heat exchange between the packed bed and the HTF occurs slowly and progressively as the HTF flows down the storage tank. Thus, greater axial thermal stratification can be observed in the packed bed at lower HTF flow rates than at higher flow rates. At higher HTF flow rates, rapid heat exchange occurs between the HTF at the top of the storage tank (A) and as the HTF flows down the storage tank, the thermal gradient between the HTF and the PCM capsules towards the bottom of the tank reduces. This led to lower rates of heat transfer at lower axial positions in the storage tank and hence, higher temperatures at the bottom than at the top of the packed bed. The discharging time of the packed bed can also be observed to reduce with an increase in the HTF flow rate. The degree of supercooling of the PCM can be observed to increase with increase in the HTF flow rate which is due to the higher rate of heat extraction from the PCM.

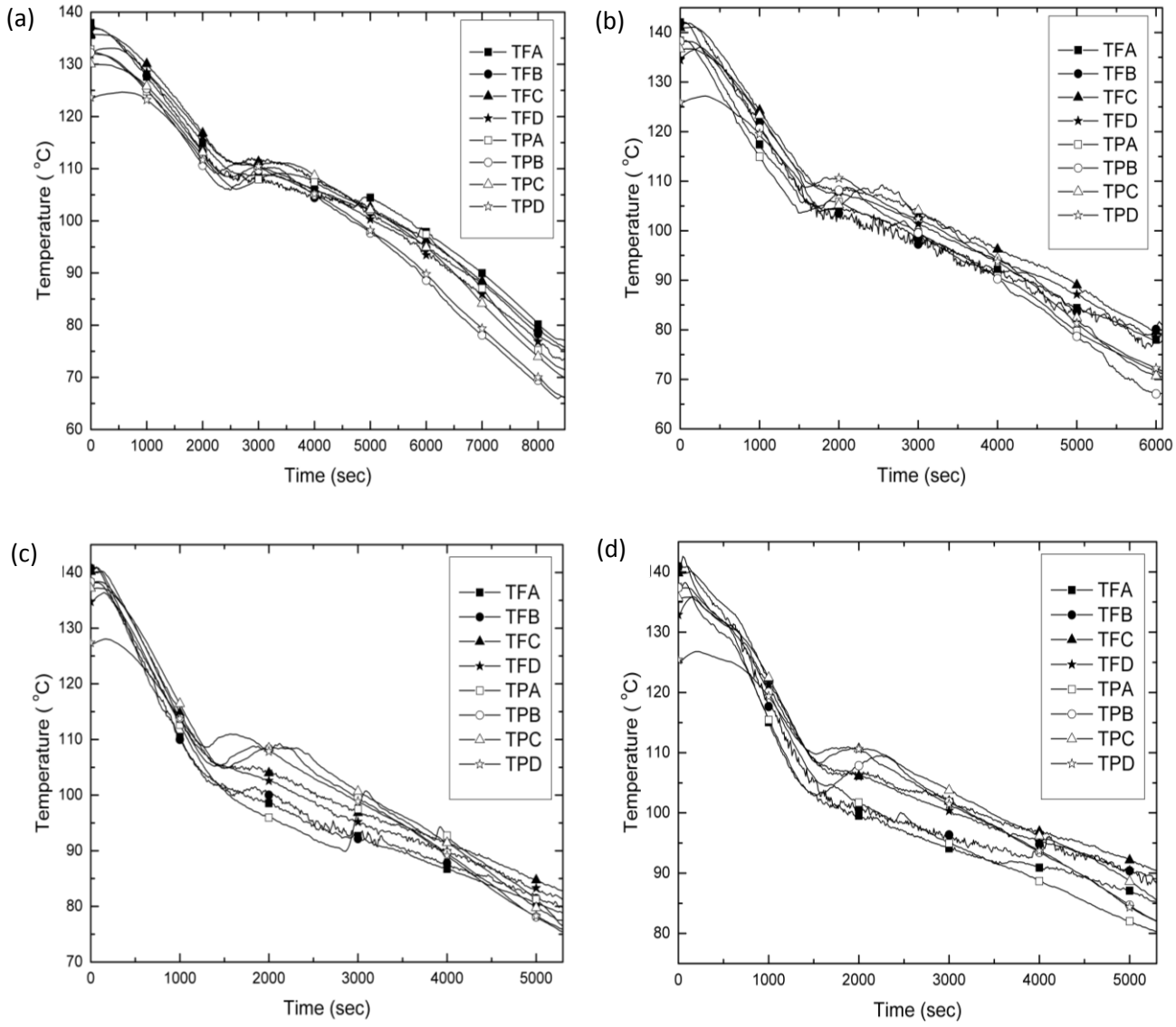

Fig. 6.10. The temperature profile of the packed bed while discharging at flow rate of (a) 3 ml/s, (b) 6 ml/s, (c) 9 ml/s and (d) 12 ml/s.

Fig. 6.11 (a) - (d) show the temperature histories of the packed bed inlet and outlet, discharging unit inlet and outlet, and the water in the discharging unit while discharging at different HTF flow rates. It can be observed that greater thermal losses were experienced in the flow pipes at low flow rates which are evident in the larger deviation of T_{din} from T_{out}. The final temperature attained by the water (T_{dw}) in the discharging unit increased with increasing HTF flow rate. Fig. 6.12 shows the temporal variation of the quantity of heat delivered by the packed bed at the different flow rates during discharging cycles. The HTF entering into the packed bed at the onset of discharging (T_{in}), at all the flow rates, is at an elevated temperature compared to the temperature of the HTF (T_{out}) exiting the packed bed.

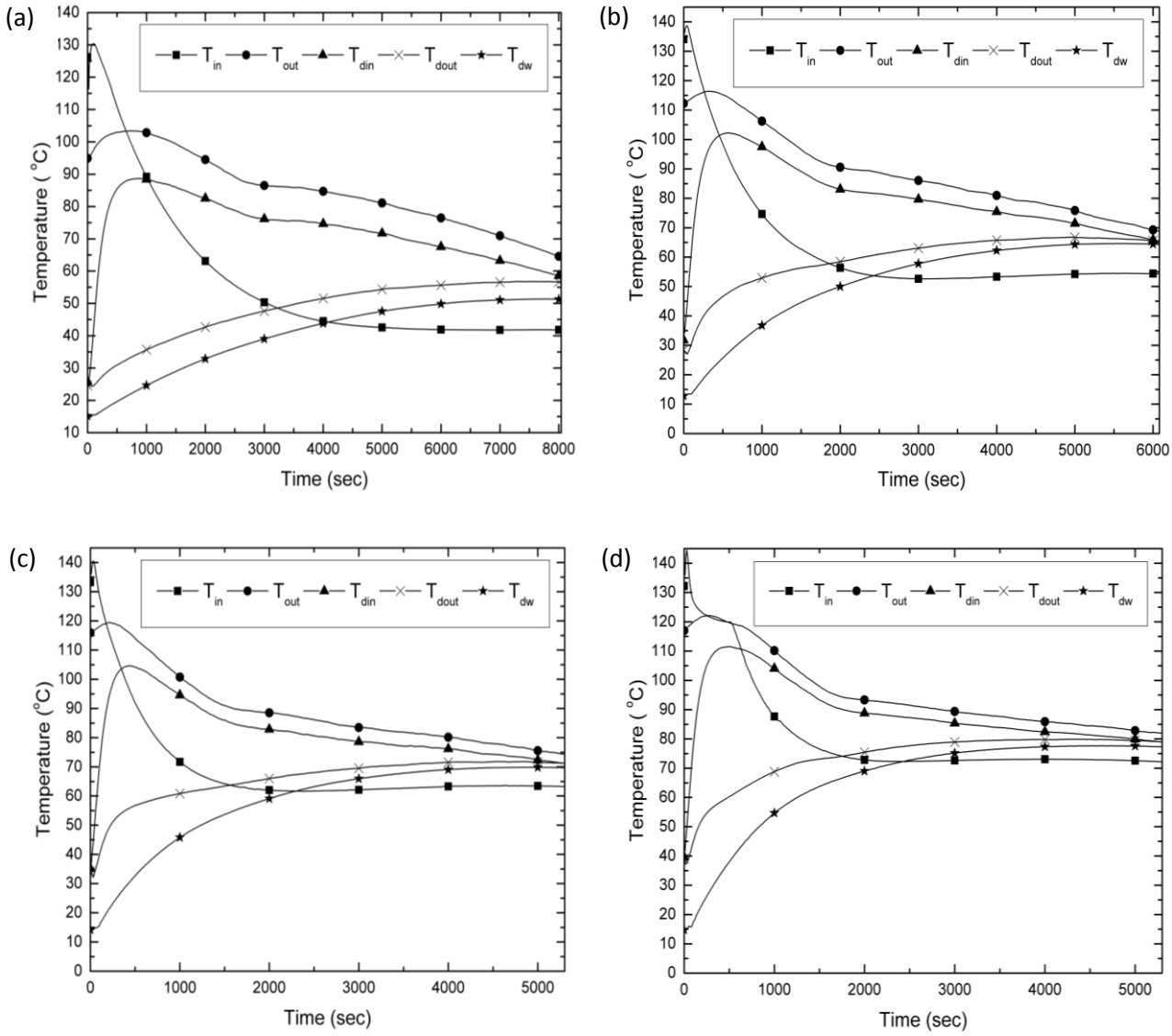

Fig. 6.11. The temperature histories of the packed bed inlet and outlet; discharge inlet and outlet; and water in the discharge unit during discharging cycle at HTF flow rate of (a) 3 ml/s, (b) 6 ml/s, (c) 9 ml/s and (d) 12 ml/s.

This is due to the fact that hot HTF that resided in the heating unit and in the pipe leading from the heating unit to the packed bed was initially pumped into the bed. Thus initially at the beginning of all the discharging cycles, the packed bed was storing more heat until the temperature of the inlet HTF (T_{in}) fell below the temperature of the packed bed. Discharging started effectively when such condition was attained for discharging at each HTF flow rate considered. This period of initial charging of the packed bed can be observed to extend longer for the HTF flow rate of 12 ml/s. from the heating unit to the packed bed was initially pumped into the bed. Thus at the beginning of all the discharging cycles, the packed bed was storing more heat until the temperature of the inlet HTF (T_{in}) fell below the temperature of the packed bed. Discharging started effectively when such condition was

attained for discharging at each HTF flow rate considered. This period of initial charging of the packed bed can be observed to extend longer for the HTF flow rate of 12 ml/s.At about 483 s, the packed bed began to effectively deliver heat at the flow rate of 12 ml/s with a peak heat delivery of about 5673.0 J at about 1190 s, which is the highest energy delivery as compared to other flow rates. The average rate of thermal energy discharged by the packed bed was 172.7 J/s at flow rate of 3 ml/s, 317.1 J/s at 6 ml/s, 367.5 J/s at 9 ml/s and 350.1 J/s at 12 ml/s. The rate of heat delivery from the packed bed can be observed to increase with an increase in the HTF flow rate.

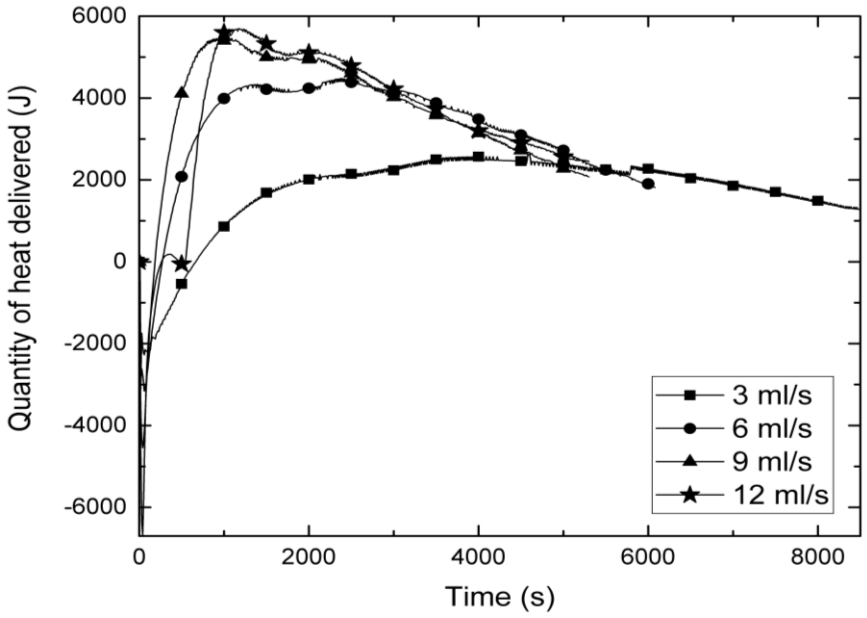

Fig. 6.12. Temporal variations of the quantity of heat delivered by the packed bed during discharging cycles at different HTF flow rates.

The discharging characteristics of the packed bed storage system may be further investigated by examining the cumulative quantity of heat discharged to the water in the discharging unit. As seen in Fig. 6.13, the rate of discharging of heat clearly increased with an increase in the HTF flow rate. The average rate of heat discharge to the water was 111.3 J/s at 3 ml/s, 222.4 J/s at 6 ml/s, 275.0 J/s at 9 ml/s and 309.5 J/s at 12 ml/s. The discharging effectiveness of the storage thus increased with an increase in the HTF flow rate. The total quantity of heat discharged to the water in the discharging unit was 0.944 MJ for an HTF flow rate of 3 ml/s, 1.352 MJ for 6 ml/s, 1.457 MJ for 9 ml/s and 1.641 MJ for 12 ml/s. Thus, the total quantity of heat delivered increased with an increase in the HTF flow rate during discharge.

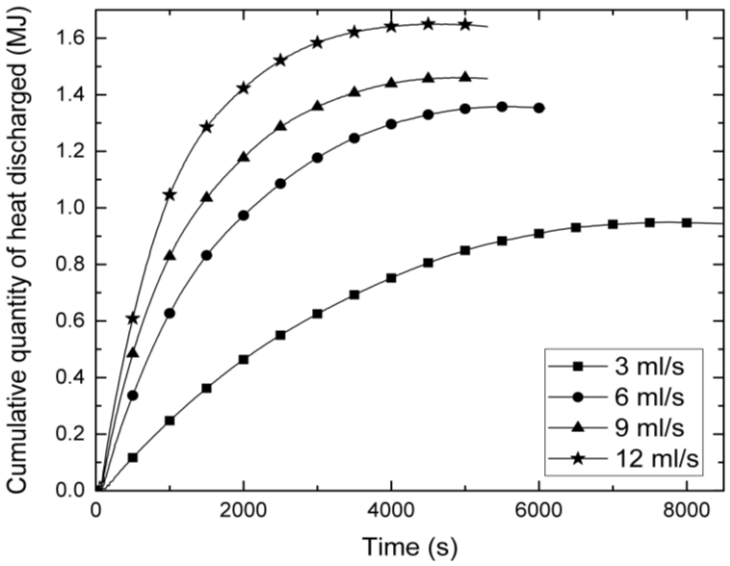

Fig. 6.13. Temporal variations of the cumulative quantity of heat discharged to the water in the discharge unit at different flow rates.

6.6. Conclusions

This paper has presented an experimental investigation of the performance of a thermal energy storage system incorporated with a packed bed of spherically encapsulated PCM. The primary thermal storage was made up of a packed bed of spherically encapsulated erythritol while the secondary thermal storage was done with water. The average rates of energy storage in both the packed bed and in the secondary storage were observed to increase with increasing HTF flow rates during the charging cycles. Thermal losses to the ambient through the walls of the packed bed storage were observed to be of great significance. As the set maximum charging temperature was increased, greater quantity of thermal energy was stored in the packed bed while the quantity of thermal energy stored in the secondary storage decreased. Therefore, high temperature (below the degradation temperature of the PCM) and high HTF flow rate will be desirable for effective thermal energy storage in the storage system. During the discharging cycles, it was observed that the average rate of thermal energy delivery by the packed bed increased with an increase in the HTF flow rate. Care must be taken however, on increasing the HTF's flow rate during discharging as the degree of supercooling of erythritol increases as well with an increase in the rate of thermal energy extraction from the erythritol capsules. The designed thermal energy storage system may be charged with solar energy if the electric heating unit is replaced with a solar collector. The system may be used for the provision of hot water as with the configuration in this experimental setup. However, if the secondary storage and the discharging units are replaced with radiators, the system may be used to provide space heating. Also, if the storage is sized

with a larger volume compared to the discharging unit, there is a potential that cooking of food may be done in the discharging unit with the stored thermal energy in the packed bed while hot water provision will be made available by the secondary storage.

Efforts will be made in the future to improve on the insulation of the system in order to reduce thermal losses. Further experiments will also be conducted by charging the system with solar energy by replacing the electric heating unit with a suitable solar collector.

Acknowledgements

The authors wish to acknowledge the support provided by the Material Science Innovation and Modeling (MaSIM) research focus area, Faculty of Agriculture, Science and Technology, Northwest University, South Africa. The authors also wish to acknowledge the National Research Foundation, South Africa, through the Research Development Grants for Y-rated Researchers (RDYR-Grant number: 95574) and the Incentive Funding for Rated Researchers (IFRR-Grant number: 90638) schemes.

References

[1] IEA energy indicators database 2014. International Energy Agency, Paris. Available at: https://www.iea.org/newsroomandevents/graphics/2014-07-22-what-drives-energy-consumption-in-households.html (accessed 25/08/16).

[2] Nakagami H, Murakoshi C, Iwafune Y. International comparison of household energy consumption and its indicator. In: Proceeding of ACEEE Summer Study on Energy Efficiency in Buildings, California, USA, 2008.

[3] International Energy Outlook 2016. U.S. Energy Information Administration, Washington, DC. Available at: www.eia.gov/forecasts/ieo/world.cfm (accessed 27/08/16).

[4] International Energy Agency (IEA) and the World Bank, 2015. "Sustainable Energy for All 2015 - Progress Towards Sustainable Energy" (June), World Bank, Washington DC. Doi: 10.1596/978-1-4648-0690-2. License: Creative Commons Attribution CC BY 3.0 IGO.

[5] Rehfuess E. Fuel for life: household energy and health. World Health Organisation, Geneva 2006. Available at: www.who.int/indoorair/publications/fuelforlife.pdf?ua=1

[6] Arbex MA, Cançado JED, Pereira LAA, Braga ALF, Saldiva PHD. Biomass burning and its effects on health. Journal Brasileiro de Pneumologia 2004; 30(2): 158-75. Available at: https://dx.doi.org.10.1590/S1806-37132004000200015 (accessed 27/09/16).

[7] Putti VR, Tsan M, Mehta S, Kammila S. The state of the clean and improved cooking sector. In: Technical report 007/15 for Energy Sector Management Program, Global Alliance for Clean Cook stoves, The World Bank 2015.

[8] Sharma SD, Sagara K. Latent heat storage materials and systems: A review. International Journal of Green Energy 2005; 2: 1-56.

[9] Farid MM, Khudhair AM, Razack SAK, Al-Hallaj S. A review on phase change energy storage: materials and applications. Energy Conversion and Management 2004; 45:1597-615.

[10] Miro L, Barreneche C, Ferrer G, Solé A, Martorell I, Cabeza LF. Health hazard, cycling and thermal stability as key parameters when selecting a suitable phase change material. Thermochimica Acta 2016; 627-29: 39-47.

[11] Kakiuchi H, Yamazaki M, Yabe M, Chihara S, Terunuma Y, Sakata Y, Usami T. A study of Erythritol as phase change material. IEA Annex 10-PCMs and chemical reactions for thermal energy storage, Second workshop, Sofia, Bulgaria 1998.

[12] Kaizawa A, Maruoka N, Kawai A, Kamano H, Jozuka T, Senda T, Akiyama T. Thermophysical and heat transfer properties of phase change material candidate for waste heat transportation system. Heat and Mass Transfer 2008; 44:763-9.

[13] Gunasekara SN, Pan R, Chiu JN, Martin V. Polyols as phase change materials for low-grade excess heat storage. Energy Procedia 2014; 61:664-9.

[14] Kenisarin M, Mahkamov K. Solar energy storage using phase change materials. Renewable and Sustainable Energy Reviews 2007; 11:1913-65.

[15] Shukla A, Buddhi D, Sawhney RL. Thermal cycling test of few selected inorganic and organic phase change materials. Renewable energy 2008; 33(12): 2606-14.

[16] Jesus AJL, Nunes SCC, Silva MR, Beja AM, Redinha JS. Erythritol: Crystal growth from the melt. International Journal of Pharmaceutics 2010; 388:129-35.

[17] Sharma SD, Iwata T, Kitano H, Sagara K. Thermal performance of a solar cooker based on an evacuated tube solar collector with a PCM storage unit. Solar Energy 2005; 78:416-26.

[18] Wang W, Guo S, Li H, Yan J, Zhao J, Li X, Ding J. Experimental study on the direct/indirect contact energy storage container in mobilized thermal energy system (M-TES). Applied Energy 2014; 119:181-9.

[19] Nomura T, Tsubota M, Oya T, Okinaka N, Akiyama T. Heat storage in direct-contact heat exchanger with phase change material. Applied Thermal Engineering 2013; 50:26-34.

[20] Bindra H, Bueno P, Morris JF, Shinnar R. Thermal analysis and exergy evaluation of packed bed storage systems. Applied Thermal Engineering 2013; 52:255-63.

[21] Hayashi Y, Fuchigami K, Taguchi Y, Tanaka M. Preparation of microcapsules containing Erythritol with interfacial polycondensation reaction by using the (w/o) emulsion. Journal of Encapsulation and Adsorption Sciences 2014; 4: 132-41.

[22] Wei J, Kawaguchi Y, Hirano S, Takeuchi H. Study on a PCM heat storage system for rapid heat supply. Applied Thermal Engineering 2005; 25: 2903-20.

[23] Xia L, Zhang P, Wang RZ. Numerical heat transfer analysis of the packed bed latent heat storage system based on an effective packed bed model. Energy 2010; 35(5): 2022-32.

[24] Agyenim F, Eames P, Smyth M. Heat transfer enhancement in medium temperature thermal energy storage system using a multitube heat transfer array. Renewable Energy 2010; 35(1): 198-207.

[25] Agyenim F, Eames P, Smyth M. Experimental study on the melting and solidification behaviour of a medium temperature phase change storage material Erythritol system augmented with fins to power a LiBr H_2O absorption cooling system. Renewable Energy 2011; 36(1): 108-117.

[26] Wang Y, Wang L, Xie N, Lin X, Chen H. Experimental study on the melting and solidification behaviour of Erythritol in a vertical shell-and-tube latent heat thermal storage unit. International Journal of Heat and Mass Transfer 2016; 99:770-81.

[27] Shobo AB, Mawire A. Investigation of aluminum encapsulation of a pcm for domestic cooking. In: Proceedings of the twenty-fourth conference on the domestic use of energy, cape peninsula university of technology, Cape town, South Africa 2016.

[28] Agyenim F, Rhodes M, Knight I. The use of phase change material (PCM) to improve the coefficient of performance of a chiller for meeting domestic cooling in Wales. In: Proceedings of the 2nd PALENC Conference and 28th AIVC Conference on Building Low Energy Cooling and Advanced Ventilation Technologies in the 21st Century, Crete island, Greece, 2007.

[29] Mawire A, Phori A, Taole S. Performance comparison of thermal energy storage oils for solar cookers during charging. Applied Thermal Engineering 2014; 73: 1321-9.

[30] Galione P, Pérez-Segarra C, Rodriguéz I, Lehmkuhl O, Rigola J. A new thermocline-PCM thermal storage concept for CSP plants. Numerical analysis and perspectives. Energy Procedia 2014; 49:790-9.

APPENDIX A: The front view of the oil/packed bed thermal energy storage system.

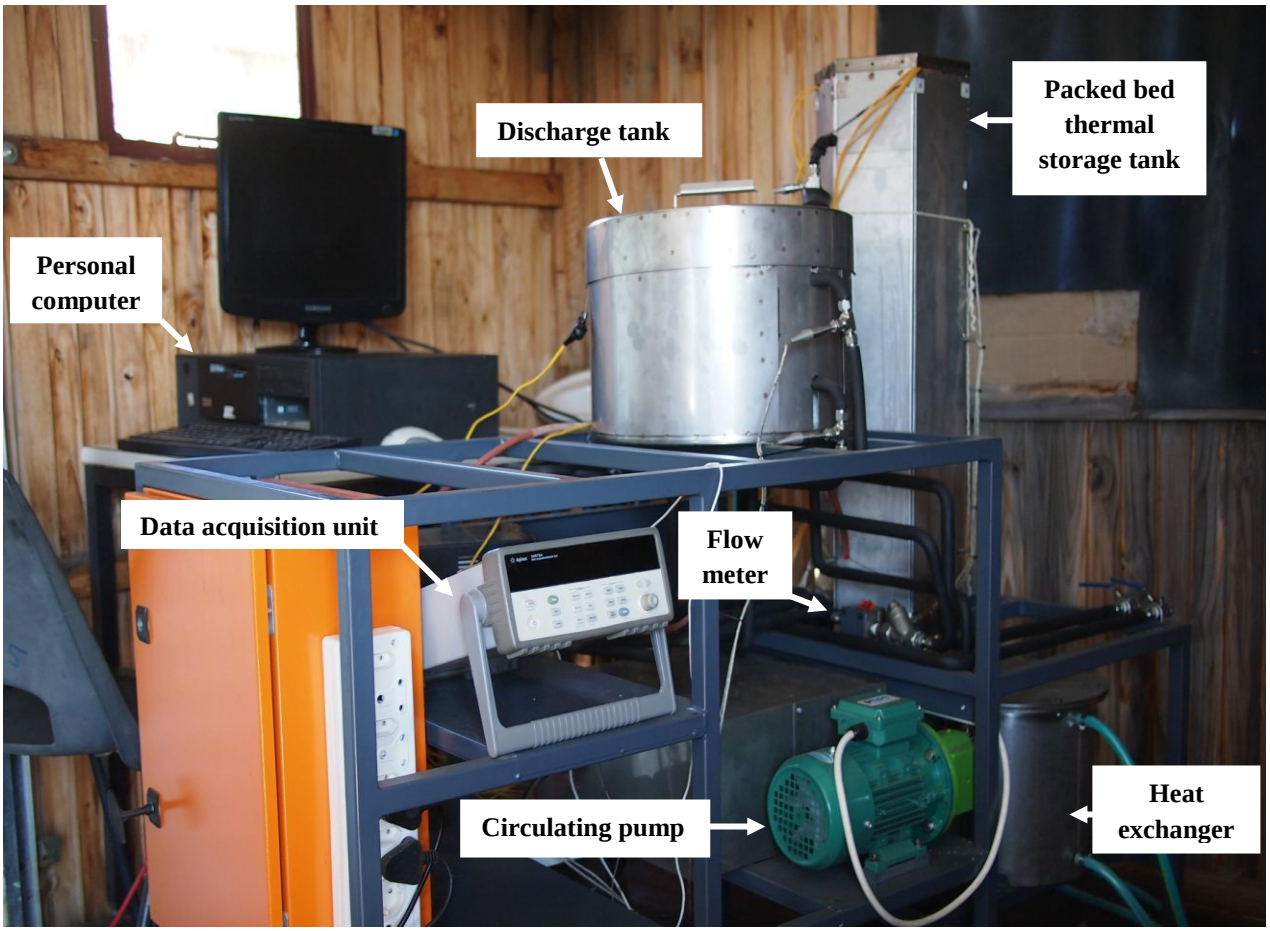

APPENDIX B: The rear view of the oil/packed bed thermal energy storage system.

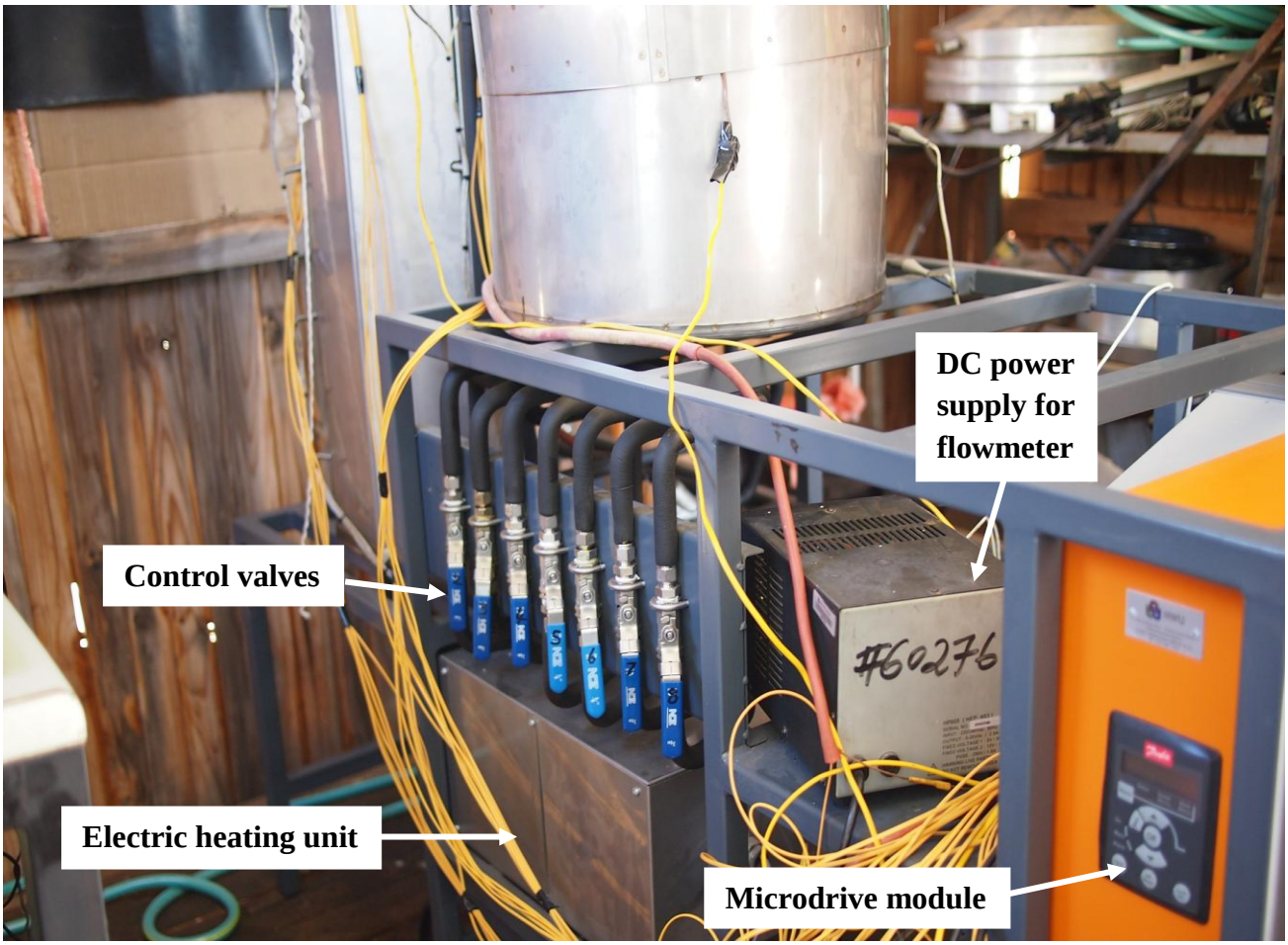

APPENDIX C: The interior of the partially filled packed bed storage tank.

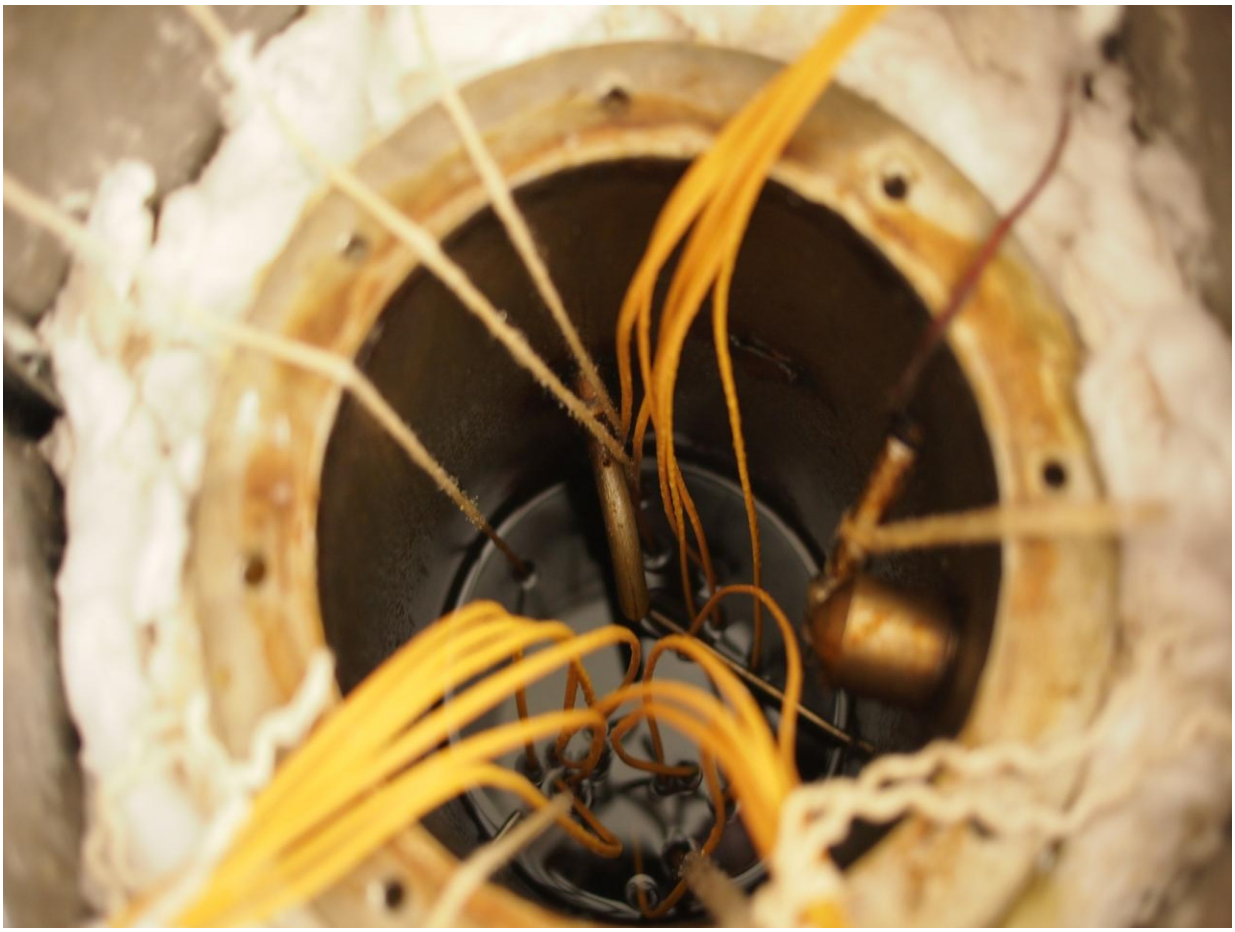

APPENDIX D: The interior of the discharging tank.

APPENDIX E: The interior of the heat exchanger (secondary storage tank).

CHAPTER SEVEN: CONCLUSIONS AND RECOMMENDATIONS

7.1. Conclusions

An investigation of an oil/packed bed thermal energy storage system for domestic cooking has been carried out in this research work. The desired phase change material was meso-erythritol while the desired heat transfer fluid was sunflower oil. A preliminary numerical study of the oil/packed bed TES indicated that spherically encapsulated erythritol possess immense thermal energy storage potential in the packed bed. The inlet temperature of the HTF into the packed bed had more significant impact on the quantity of heat stored in the packed bed than the HTF flow velocity. Both the HTF inlet temperature and the HTF flow velocity had significant impact on the charging time of the charged bed.

Aluminum encapsulation was found to be chemically compatible with both meso-erythritol and sunflower oil. For the 50 mm diameter spherical capsule desired for the packed bed, a wall thickness of 1 mm was found to be adequate for the capsule to be mechanically stable during charging and discharging cycles.

An investigation of the thermal stability of meso-erythritol revealed that the charging temperature of should be kept lower than 177.0 ^{o}C as the PCM begins to degrade around this temperature thus reducing the thermal storage capacity of the TES in which it is applied. On comparison with acetanilide and an Indium-Tin alloy (PCMs of comparable melting point) meso-erythritol can operate at higher temperatures than acetanilide but lower temperatures than the Indium-Tin alloy. A fast thermal cycling of meso-erythritol indicated a shift of its melting temperature from an initial value of about 119.2 ^{o}C to about 105.4 ^{o}C which is caused by the fast cooling of the PCM leaving it in a metastable state. There were only slight variations in the solidification temperature and solidification enthalpies. Meso-erythritol also showed some significant weight loss during the thermal cycling. This needs to be factored in to the projections of the productivity of a thermal energy storage system in which this PCM is utilized. When compared with acetanilide and the In-Sn alloy, meso-erythritol showed better cycling stability than acetanilide but less superior stability when compared to the In-Sn alloy. However, meso-erythritol presents less health hazards as compared to the other two PCMs and this should be given serious considerations particularly when the proposed application of the PCM is domestic. The three PCMs showed good chemical stability after 20 fast cycles but the fast rate of degrading of acetanilide will be a discouraging factor for its use in a TES system.

The charging and discharging performances of acetanilide, meso-erythritol and the In-Sn alloy was investigated simultaneously in similar spherical aluminum capsules. Meso-erythritol gave the highest charging and discharging rates while acetanilide gave the least due to its low density which gave it a small thermal storage capacity. However, the quality of thermal energy discharged by the encapsulated meso-erythritol is seriously affected by the large degrees of supercooling exhibited by the PCM. The In-Sn alloy discharged a greater quantity of heat that was useful for cooking applications but the cost of the alloy is a discouraging factor for its use.

A packed bed of spherically encapsulated meso-erythritol was included in a TES that was fabricated. The performances of the TES system during its charging and discharging cycles, using sunflower oil as the HTF was investigated. High HTF inlet temperatures and large HTF flow rates were conditions for achieving high charging rates of the system. Moreover, very large thermal losses were observed at a low HTF flow rate of 3 ml/s from the thermal storage tanks and the flow pipes. Significant supercooling was observed during the discharging cycles and this impacted negatively on the quantity and the quality of thermal energy discharged by the packed bed TES system. The quantity of thermal energy discharged by the packed bed generally increased with an increase in the HTF flow rate. The design of the TES system is such that thermal energy might be utilized (secondary storage) as well as stored (primary storage) during the charging cycles. The highest temperature attained by the water in the discharging unit was about 77.3 ^{o}C while discharging with an HTF flow rate of 12 ml/s. This can only be used for cooking some vegetables which do not require high temperatures. However, with appropriate matching of the size of the discharging unit to that of the packed bed storage, temperatures of 100 ^{o}C and above may be achieved in the discharging unit in order to cook foods that require boiling. The heat exchanger, which is a secondary thermal energy storage, can be used to provide hot water while the packed bed is being charged.

The packed bed TES system of the spherically encapsulated meso-erythritol has shown a good potential of providing sufficient thermal energy storage useful for cooking applications. To improve the performance as obtained from this study, some further studies will be necessary.

7.2. Recommendations for future work

Further investigations to find a suitable nucleating agent for meso-erythritol are very necessary in order to drastically reduce the degree of supercooling exhibited by the PCM. This is because meso-erythritol has shown immense thermal energy storage capabilities. It is cheap, readily available and it constitutes no serious hazard to health if used as a TES material for a domestic application. The mixture of different encapsulated PCMs, with different melting points, in the packed bed storage needs to be investigated for possible improvement on the thermal performances of the TES system. Thermal energy losses in the TES system developed are quite considerable, therefore a means of achieving a more effective insulation should be pursued. There is a need to investigate the use of locally available materials that may be used as effective thermal insulators in the present system and in other thermal energy storages generally. A further investigation of the charging performance of the fabricated system is necessary when thermal energy is provided by a solar collector instead of using the electric heating unit. Stratification analyses of the packed bed need to be carried out in order to optimize the performance of the system. The configuration of the flow of the HTF packed bed during discharging also need to be reconfigured to operate from the bottom to the upward direction in order to reduce thermal losses from the bed. The In-Sn alloy has shown very good promise of being used as a metallic PCM but because of its high cost, it is therefore necessary to further investigate other lead-free solders as PCM candidates for thermal energy storage applications. Concerted efforts also need to be made to develop a mathematical model that will correctly describe the operation of the TES system in order to optimize its performance numerically. The fabricated TES system has shown a good potential to be used for the provision of hot water as well for storage of thermal energy for cooking if properly sized.